Personalized Medicine in Surgical Treatments Combining Tracking Systems, Augmented Reality and 3D Printing

by

Rafael Moreta Martínez

A dissertation submitted in partial fulfillment of the requirements for the degree of Doctor of Philosophy in

Biomedical Science and Technology

Universidad Carlos III de Madrid

Advisor:

Javier Pascau González-Garzón

Tutor:

Javier Pascau González-Garzón

October 2021

"There are no two words in the English language more harmful than ***good job***."

— Damien Chazelle, Whiplash.

AGRADECIMIENTOS

Realizar una tesis significa sacrificio, trabajo y dedicación por parte de uno mismo, pero, en mi opinión, esta tesis no hubiera salido adelante sin el apoyo, ayuda y cariño de todos aquellos que han formado parte de ella, en mayor y menor medida. Gracias a todos de corazón.

Me gustaría empezar agradeciendo a mi tutor, **Javi**, por confiar en mi desde el principio y haberme dado la oportunidad de trabajar a su lado. Gracias por tu apoyo, por ser siempre justo, por tu dedicación al trabajo, por no tirar la toalla corrigiendo mis papers (sé que ha sido duro), por respaldarme cuando lo he necesitado, y por tu forma de ser. Javi, creo que no he podido tener mejor mentor que tú, y sé que gracias a ti he podido crecer como investigador y como persona.

A **Raúl**, por haber creído en mí potencial y ofrecerme la oportunidad de formar parte de sus proyectos de investigación en Boston. Creo que eres una grandísima persona, con un talento increíble, y me siento muy afortunado de haber podido evolucionar en muchos aspectos, científicos y personales, gracias a todo lo aprendido de tus conocimientos. Gracias por haberme acogido con tanta amabilidad y haberme hecho sentir como de tu familia, justo cuando no tenía la mía cerca.

A los mejores compañeros que uno puede tener. Al **Deivid**, por su honradez, su sinceridad, por luchar por lo que es justo, por su confianza, por su productividad, por ponerle música a la investigación, por saber reaccionar en momentos críticos, por su ayuda con mis proyectos, por sus bromas en el despacho, por soportar mis tonterías, por ser el mejor copiloto, por meterme en la música Indie, por ser un poeta de la ciencia y un virtuoso de la palabra. A **Moni**, por su amabilidad, por saber escuchar, por saber comprender, por su humildad, su generosidad, por nuestros viajes compartiendo coche al LIM y a la uni, por esos momentos de brainstorming, por nuestras conversaciones de 5 minutos y acaban siendo de horas, por nuestras partidas a la Wii. Trabajar a vuestro lado ha sido el mayor lujo que he podido tener durante estos 5 años. Vosotros habéis sido el impulso que necesitaba cada día para seguir con la tesis y haber podido llegar a acabarla. Gracias por todos esos experimentos, por todas esas cirugías, por todos esos viajes a congresos o para hacer teambuilding (Toronto, Barcelona, Bilbao, Nuremberg, Berlín, Favignana, Granada, Washington, Boston, Londres, Gran Canaria, …), por haberme aficionado a ir a festivales y conciertos (todo empezó con Sunset and Sons), por ir plantando semillas, por detectar todas mis erratsa, por reíros cuando me invento nombres (que majo es Maxilopoulus), por soportarme cuando me quejo demasiado, por estar ahí siempre. Todo esto ha hecho que esta etapa haya sido la mejor de mi vida. Por todo esto, y por todo lo que queda por venir, gracias. Solo me queda deciros… ¿Calibramos?

A todo el equipo de Cirugía Ortopédica y Traumatología del Hospital General Universitario Gregorio Marañón. En especial, al **Dr. José Calvo** por su tiempo, por su dedicación a la investigación, por su confianza, por su paciencia en las cirugías, por saber ponerse en el lado de un ingeniero y por esas reuniones que intentaban sacar la tesis adelante. También agradecerle al **Dr. Rubén Pérez**, por su soltura a la hora de vender lo que hacemos, por su dedicación a querer ser pionero, por su habilidad de entender lo que se necesita para crecer. Sin vuestras ganas de querer seguir innovando, de no rendiros ante las adversidades encontradas, y de vuestra

involucración, nada de esto habría sido posible. Gracias a la **Dra. Lydia Mediavilla**, por ser otra cirujana más en querer seguir innovando, dando su tiempo a la investigación. También agradecer a todas las personas dentro del Marañón que han formado parte de todo esto. En especial, al **Dr. Santiago Ochandiano**. La pasión que transmites por realizar tu trabajo lo mejor posible y tu dedicación hace que me despierte cada mañana orgulloso de desarrollar soluciones que puedan mejorar la cirugía. Ha sido un placer haber podido trabajar contigo. Y por supuesto, agradecer a todos aquellos que han formado parte de todas las cirugías que hemos hecho, por vuestra paciencia, profesionalidad y por estar siempre dispuestos a ayudar.

Al equipo de Cirugía General del Hospital La Paz. En especial a la **Dra. Inés Rubio**, por creer y apostar en mi proyecto, por tu dedicación y tiempo como profesional a la investigación y por tu involucración total al trabajo. Creo que eres una médico excepcional, que hace que trabajar a tu lado sea todo más fácil. También agradecer a todos los participantes en el experimento de raíces sacras, muchas gracias por vuestro tiempo y paciencia en querer formar parte de esto.

A **Anita**. Por haber estado ahí cuando te he necesitado, por haberme ayudado a tomar las decisiones correctas, por entenderme, por haberme esperado, por apostar por mí, por ser un ejemplo de querer luchar por lo que uno cree, por haber sufrido a mi lado, por esos abrazos que te transportan a otro mundo, por lo increíble que eres, por esos paseos por el retiro, por todos esos viajes, por todos esos pequeños momentos que hacen que me saquen una sonrisa, por tu cariño. Por todo eso, y mucho más, han hecho que mi camino hasta aquí haya sido mucho más fácil.

A **mis padres**, por vuestro apoyo incondicional, cariño, dedicación, por ser un ejemplo a seguir, por mostrarme vuestra fuerza y valentía a lo largo de todos estos años, por vuestros sacrificios, por creer en mí, por hacerme sentir afortunado, por haber cuidado tan bien de mí, por vuestros consejos, por ayudarme a encontrar mi camino y por quererme. Porque os merecéis mucho más que estas palabras. A mis hermanas pequeñas. A **Paola**, por su dulzura, por sus pequeños detalles, por lo justa que es, por preguntarme siempre que tal estoy, por escucharme, por ser tan valiente, y por ayudarme a querer siempre ser mejor hermano. A **Sofi**, por sus abrazos espontáneos, por su risa, por tener siempre una sonrisa en la cara, por su sensibilidad, por seguir mis consejos, por mirarme siempre con orgullo, por nuestros momentos viendo pelis en el sofá, por hacerme sentir muy querido y por dejarme ser tu hermano mayor. Gracias a las dos por haberme hecho sentir tan orgulloso de vosotras, por haberme soportado todos mis días malos, y aun así haberme entendido y haber seguido a mi lado. Ha sido un lujo disfrutar de vuestra compañía al llegar a casa. Sois increíbles.

Al resto de mi familia. A mis hermanos mayores y cuñadas, **Guille** e **Inés**, **Miki** y **Lucía**, **Dani** y **Ana**, por todos esos momentos en familia, ya sea una comida un domingo o un viaje a Asturias, que hace que uno se sienta querido, arropado y agradecido de teneros. Y por supuesto, por haber traído al mundo a unos sobris maravillosos, **Miguelito**, **Carmencita**, **Danielito** y **Martina**, que te alegran los malos días con sus sonrisas y viendo como crecen cada día. A mi abuela **Juana**, por desearme siempre lo mejor, por sus historias, por su valentía, su cariño y su fortaleza innata a darlo todo por los demás. A mi abuela **Asún**, por su amabilidad, su preocupación y su afecto que siempre he recibido. A mis tíos **Nines** y **Sebastian**, **Merce** y **Juanma**, por hacerme sentir que lo que hago es importante, por no parar de preguntar cuando iba a terminar, por apoyarme tanto. Al resto de tíos y primos, por estar ahí cuando se os necesita. También me gustaría

darle las gracias de una forma muy especial a mi **abuelo Ángel**, por haber creído siempre en mí y en mis capacidades, en desearme siempre lo mejor, por sus chistes, su generosidad y su sabiduría. Sé que estarías orgulloso de ver lo que he conseguido.

A todos los compañeros del equipo IGT. A **Vero**, por ser una gran mentora, por sus ganas infinitas de ayudar y de enseñar, por nunca poner mala cara, y por haberme introducido en el campo de la cirugía guiada. A **Ro**, por lo divertida que eres, por sus locuras y por haber sido una gran compañera. A **Bego**, por su apoyo constante y por poner siempre buena cara. A **Alicia**, por haberme sentido orgulloso como docente, sus ganas de aprender, y por haber seguido los caminos de la navegación. A **Laura**, por su trabajo excepcional, eficacia y ayudarme cuando te lo he pedido. A todos los demás, **Eu**, **Manu**, **Maite**, **Lucía**, **Estela**, y **Anxela**, por haber sido unos compañeros excepcionales.

A todos mis compañeros del Laboratorio de Imagen Médica y del Departamento de Bioingeniería e Ingeniería Aeroespacial con los que he tenido la oportunidad de coincidir todos estos años. En especial a **Mario**, **Álvaro**, **Cristóbal**, **Claudia**, **Nerea**, **Inés**, **Alba**, **Asier**, **Estibaliz**, **Laura Nicolás**, **Blanca**, **Dani**, **Rigo**, **Pedro**, **David**, **Ana**, **Roberto**, **Juanjo**, **Arrate**, **Jorge**, **Mónica**, **Manolo**, **Ramón**, **Marta**, **Esther**, **María de la Jara**, **Patricio**, **Nico**, **Trajana**, **Elena**, **Marisa**, **Joaquín**, **Alessandro**, **Nik**, **Leo**, **Josu**, **Carlos**, **Claire**, **Alberto**. Ha sido un placer haber podido trabajar con todos y cada uno de vosotros.

A mis mejores amigas de la carrera. A **Irene**, por ser siempre tan alegre, por su cariño, por estar siempre ahí cuando la he necesitado y por ser una muy buena amiga. A **Marina**, por enseñarme a ver la vida de otra manera y saber escuchar. **José** por nunca darte por vencido, por lo currante y buena persona que eres. A **Patricia**, por su sonrisa, su personalidad, y sus infinitas ganas ayudar. **María**, por saber entender a los demás, por enseñarme a valorar lo que tenemos, por ser un amor de persona. A **Noelia**, por ser un claro ejemplo de superación y enseñarme a ver que no hay límites en la vida. Gracias por todos esos viajes y momentos vividos, porque, aunque pase tiempo sin vernos, nuestra amistad siga siendo intocable. Gracias por vuestro apoyo y sabios consejos que me habéis ofrecido a lo largo de esta etapa. Siempre he querido ser como vosotras de mayor. Sois las mejores.

A mis amigos de toda la vida. A **Sink**, **Gongo**, **Negro**, **Miry**, **Melenas**, **Cris**, **Pablo**, **Llerllio**, **Burgui**, **Chechu**, **Pili**, **María**, **Javi** y **Toni**. Por todo el desquicie vivido, por todas esas tardes de cerveceo, por esas barbacoas, por esos viajes, por vuestros consejos, por criticarnos con cariño, por estar ahí siempre que lo he necesitado, por nuestros partidos de pádel, por ahorrarnos unos segundos, por el muro (RIP Mou), por quererme aun con mis locuras, por hacerme creer que el tiempo no ha pasado y que seguimos estando en el parque de los altos de cuando éramos pequeños. A **Rojas**, por todas esas conversaciones frikis, por sus consejos, por preocuparte por mí y por ayudarme siempre que te lo he pedido. A **Barrio**, por ser siempre un amigo leal y por decir que si siempre a cualquier plan. Todos y cada uno de vosotros habéis hecho que mi vida sea más feliz.

A todos mis compañeros de ACIL (Boston). A **Rubén**, por ser el mejor compañero de piso, por sus guisos (y pulled pork), por su sabiduría popular, por echarme una mano con los pepinos (y muchas más cosas), por ser un gran tipo en todos los aspectos. A **Jorge**, por su paciencia infinita, por intentar enseñarme a programar de verdad, y por su disposición a ayudar siempre que

te lo he pedido. A **Pietro**, por ser un gran compañero, una gran persona, y mejor investigador. A **Gonzalo**, por su sabiduría, por ayudarme a ver la investigación de otra manera y por nuestras conversaciones de cine y de cubos de Rubik. A **Mónica**, por su sonrisa de cada mañana, por los buenos ratos y risas mientras luchábamos por las GPUs. Gracias a todos vosotros por todas esas sobremesas en la sala de reuniones, por las cervezas de después del trabajo, por las pequeñas escapadas, por haberme acogido con tanto cariño. Habéis hecho que mi estancia en Boston fuese muy especial. También me gustaría agradecer a los Doctores **Stephanie**, **Alejandro** y **George**, por haber podido formar parte de vuestros proyectos de investigación dentro del Brigham and Women's Hospital. Vuestra contribución a la ciencia es excelente y un ejemplo a seguir.

PUBLISHED AND SUBMITTED CONTENT

Journal Articles:

[1] **R. Moreta-Martinez**, A. Pose-Díez-de-la-Lastra, J. A. Calvo-Haro, L. Mediavilla-Santos, R. Pérez-Mañanes, and J. Pascau, "Combining Augmented Reality and 3D Printing to Improve Surgical Workflows in Orthopedic Oncology: Smartphone Application and Clinical Evaluation," Sensors, vol. 21, no. 4. 2021, *https://doi.org/10.3390/s21041370* [Impact Factor: 3.275; Q1]

Author contributions: Rafael Moreta Martinez was responsible for software development, data acquisition, data analysis and writing the paper. All authors were responsible for conceptualizing the framework, writing, editing, and reviewing the paper.

Contributions completely included in Chapter 6. Figures from this paper have been reprinted with permission from the copyright holder. This is an open access article distributed under the Creative Commons Attribution License.

[2] **R. Moreta-Martinez**, J. A. Calvo-Haro, R. Pérez-Mañanes, M. García-Sevilla, L. Mediavilla-Santos, and J. Pascau, "Desktop 3D Printing: Key for Surgical Navigation in Acral Tumors?," Appl. Sci., vol. 10, no. 24, p. 8984, Dec. 2020, *https://doi.org/10.3390/app10248984* [Impact Factor: 2.474; Q2]

Author contributions: Rafael Moreta Martinez was responsible for software development, data acquisition, data analysis and writing the paper. All authors were responsible for conceptualizing the framework, writing, editing, and reviewing the paper.

Contributions completely included in Chapter 3. Figures from this paper have been reprinted with permission from the copyright holder. This is an open access article distributed under the Creative Commons Attribution License.

[3] **R. Moreta-Martinez**, D. García-Mato, M. García-Sevilla, R. Pérez-Mañanes, J. A. Calvo-Haro, and J. Pascau, "Combining Augmented Reality and 3D Printing to Display Patient Models on a Smartphone," J. Vis. Exp., no. 155, 2020, *https://dx.doi.org/10.3791/60618* [Impact Factor: 1.163; Q3]

Author contributions: Rafael Moreta Martinez was responsible for software development, data acquisition, data analysis and writing the paper. All authors were responsible for conceptualizing the framework, writing, editing, and reviewing the paper.

Contributions partially included in Chapter 5.

[4] **R. Moreta-Martinez**, D. García-Mato, M. García-Sevilla, R. Pérez-Mañanes, J. Calvo-Haro, and J. Pascau, "Augmented reality in computer-assisted interventions based on patient-specific 3D printed reference," *Healthc. Technol. Lett.*, vol. 5, no. 5, pp. 162–166, 2018, https://doi.org/10.1049/htl.2018.5072

Author contributions: Rafael Moreta Martinez was responsible for data acquisition, data analysis and writing the paper. All authors were responsible for conceptualizing the framework, writing, editing, and reviewing the paper.

Contributions completely included in Chapter 4. Figures from this paper have been reprinted with permission from the copyright holder. This is an open access article published by the IET under the Creative Commons Attribution-NonCommercial-NoDerivs License.

[5] **R. Moreta-Martínez**, I. Rubio-Pérez, M. García-Sevilla, L. García-Elcano, and J. Pascau, "Proposal and comparison of two alternatives for needle navigation in sacral nerve stimulation," *Computer Methods and Programs in Biomedicine* [Impact factor: 5.428; Q1] (submitted)

Author contributions: Rafael Moreta Martinez was responsible for software development, data acquisition, data analysis and writing the paper. All authors were responsible for conceptualizing the framework, writing, editing, and reviewing the paper.

Contributions completely included in Chapter 7.

[6] **R. Moreta-Martínez**, G. Vegas Sánchez-Ferrero, L. Andresen, J. Qvortrup Holsting, and R. San José Estépar, "Multi-cavity Heart Segmentation in Non-contrast Non-ECG Gated CT Scans with F-CNN," *Thoracic Image Analysis*, 2020, pp. 14–23, https://doi.org/10.1007/978-3-030-62469-9_2

Author contributions: Rafael Moreta Martinez was responsible for data acquisition, data analysis and writing the paper. All authors were responsible for conceptualizing the framework, writing, editing, and reviewing the paper.

Contributions partially included in Chapter 10. Figures from this paper have been reprinted with permission from the copyright holder.

[7] **R. Moreta-Martínez**, S. Mason, J. Onieva-Onieva, J. Pascau, and R. San José Estepar, "End-to-End Body Composition Assessment in Thoracic CT scans with Deep Learning," *Radiology AI*. (In preparation)

Author contributions: Rafael Moreta Martinez was responsible for data acquisition, data analysis and writing the paper. All authors were responsible for conceptualizing the framework, writing, editing, and reviewing the paper.

Contributions partially included in Chapter 10.

Conference Proceedings:

[1] **R. Moreta-Martinez**, M. García-Sevilla, D. García-Mato, A. Pose-Díez-de-la-Lastra, I. Rubio-Pérez, and J. Pascau. "Smartphone-based augmented reality system for needle insertion guidance in sacral nerve stimulation". *In: CARS 2021 - Computer Assisted Radiology and Surgery Proceedings of the 35th International Congress and Exhibition, Munich, Germany, June 21–25, 2021. Int J CARS 16, 1–119 (2021)* https://doi.org/10.1007/s11548-021-02375-4

Author contributions: Rafael Moreta Martinez was responsible for software development, data acquisition, data analysis and writing the paper. All authors were responsible for conceptualizing the framework, writing, editing, and reviewing the paper.

Contributions partially included in Chapter 7.

[2] **R. Moreta-Martinez**, J. Onieva-Onieva, J. Pascau, and R. San Jose Estepar. "Pectoralis muscle and subcutaneous adipose tissue segmentation on CT images based on convolutional networks". *In: CARS 2017 - Computer Assisted Radiology and Surgery Proceedings of the 31st International Congress and Exhibition, Barcelona, Spain, June 20-24, 2017. Int J CARS 12, 1–286 (2017)* https://doi.org/10.1007/s11548-017-1588-3

Author contributions: Rafael Moreta Martinez was responsible for data acquisition, data analysis and writing the paper. All authors were responsible for conceptualizing the framework, writing, editing, and reviewing the paper.

Contributions partially included in Chapter 10.

TABLE OF CONTENT

ABSTRACT

In the last twenty years, a new way of practicing medicine has been focusing on the problems and needs of each patient as an individual thanks to the significant advances in healthcare technology, the so-called personalized medicine. In surgical treatments, personalization has been possible thanks to key technologies adapted to the specific anatomy of each patient and the needs of the physicians. Tracking systems, augmented reality (AR), three-dimensional (3D) printing and artificial intelligence (AI) have previously supported this individualized medicine in many ways. However, their independent contributions show several limitations in terms of patient-to-image registration, lack of flexibility to adapt to the requirements of each case, large preoperative planning times, and navigation complexity.

The main objective of this thesis is to increase patient personalization in surgical treatments by combining these technologies to bring surgical navigation to new complex cases by developing new patient registration methods, designing patient-specific tools, facilitating access to augmented reality by the medical community, and automating surgical workflows.

In the first part of this dissertation, we present a novel framework for acral tumor resection combining intraoperative open-source navigation software, based on an optical tracking system, and desktop 3D printing. We used additive manufacturing to create a patient-specific mold that maintained the same position of the distal extremity during image-guided surgery as in the preoperative images. The feasibility of the proposed workflow was evaluated in two clinical cases (soft-tissue sarcomas in hand and foot). We achieved an overall accuracy of the system of 1.88 mm evaluated on the patient-specific 3D printed phantoms. Surgical navigation was feasible during both surgeries, allowing surgeons to verify the tumor resection margin.

Then, we propose and augmented reality navigation system that uses 3D printed surgical guides with a tracking pattern enabling automatic patient-to-image registration in orthopedic oncology. This specific tool fits on the patient only in a pre-designed location, in this case bone tissue. This solution has been developed as a software application running on Microsoft HoloLens. The workflow was validated on a 3D printed phantom replicating the anatomy of a patient presenting an extraosseous Ewing's sarcoma, and then tested during the actual surgical intervention. The results showed that the surgical guide with the reference marker can be placed precisely with an accuracy of 2 mm and a visualization error lower than

3 mm. The application allowed physicians to visualize the skin, bone, tumor and medical images overlaid on the phantom and patient.

To enable the use of AR and 3D printing by inexperienced users without broad technical knowledge, we designed a step-by-step methodology. The proposed protocol describes how to develop an AR smartphone application that allows superimposing any patient-based 3D model onto a real-world environment using a 3D printed marker tracked by the smartphone camera. Our solution brings AR solutions closer to the final clinical user, combining free and open-source software with an open-access protocol. The proposed guide is already helping to accelerate the adoption of these technologies by medical professionals and researchers.

In the next section of the thesis, we wanted to show the benefits of combining these technologies during different stages of the surgical workflow in orthopedic oncology. We designed a novel AR-based smartphone application that can display the patient's anatomy and the tumor's location. A 3D printed reference marker, designed to fit in a unique position of the affected bone tissue, enables automatic registration. The system has been evaluated in terms of visualization accuracy and usability during the whole surgical workflow on six realistic phantoms achieving a visualization error below 3 mm. The AR system was tested in two clinical cases during surgical planning, patient communication, and surgical intervention. These results and the positive feedback obtained from surgeons and patients suggest that the combination of AR and 3D printing can improve efficacy, accuracy, and patients' experience

In the final section, two surgical navigation systems have been developed and evaluated to guide electrode placement in sacral neurostimulation procedures based on optical tracking and augmented reality. Our results show that both systems could minimize patient discomfort and improve surgical outcomes by reducing needle insertion time and number of punctures. Additionally, we proposed a feasible clinical workflow for guiding SNS interventions with both navigation methodologies, including automatically creating sacral virtual 3D models for trajectory definition using artificial intelligence and intraoperative patient-to-image registration.

To conclude, in this thesis we have demonstrated that the combination of technologies such as tracking systems, augmented reality, 3D printing, and artificial intelligence overcomes many current limitations in surgical treatments. Our results encourage the medical community to combine these technologies to improve surgical workflows and outcomes in more clinical scenarios.

LIST OF FIGURES

LIST OF TABLES

LIST OF ABBREVIATIONS AND ACRONYMS

3D: Three-Dimensional

ABS: Acrylonitrile Butadiene Styrene

AI: Artificial Intelligence

AR: Augmented Reality

ASD: Average Surface Distance

ASM: Active Shape Model

BN: Batch Normalization

CAS: Computed-Aided Surgery

cMRI: cardiac MRI

CNN: Convolutional Neural Networks

COPD: Chronic Obstructive Pulmonary Disease

CT: Computed Tomography

DRR: Direct Reconstruction Radiograph

DSC: Dice Similarity Coefficient

EES: Ewing's Sarcoma

EMTS: Electromagnetic Tracking System

EtO: Ethylene Oxide

FDM: Fused Deposition Modeling

FOV: Field of View

GF: Growth Factor

HD: Harsdorf Distance

HDM: Head-Mounted Display

HU: Hounsfield Units

IGS: Image-Guided Surgery

IQR: Interquartile Ranges

ML: Machine Learning

MRI: Magnetic Resonance Imaging

NDI: Northern Digital Inc.

OR: Operating Room

OTS: Optical Tracking Systems

PET: Positron Emission Tomography

PLA: Polylactic Acid

PMA: Pectoralis Mass Area

RB: Rigid Body

ReLU: Rectified Liner Unit

RMSE: Root-Mean-Squared Error

SAT: Subcutaneous Adipose Tissue

SDK: Software Development Kit

SLA: Stereolithography

SNS: Sacral Nerve Stimulation

STL: Stereo Lithography Files

TRE: Target Registration Error

VR: Virtual Reality

VOI: Volume of Interest

1

Introduction

1.1. Personalized medicine in surgical treatments

Medicine is constantly improving thanks to advances in technology and science. New techniques and knowledge from physics, computer science, engineering, mathematics, chemistry, or biology contribute to it, but the direct application on patients is what changes the medical practice. Every day we keep discovering new detailed information about conditions, diseases, or treatments. All these new observations are improving patients' health, thanks to better diagnosis and treatment, fewer side effects, and faster recovery. In short, to achieve improved medical outcomes.

In the last twenty years, we have seen a significant increment in the advances in healthcare technology focused on the problem and needs of each patient as an individual [1]. This new way of practicing medicine is called ***personalized medicine*** [2].

Visionary scientific experts first defined this term at the beginning of the century [3], [4]. They predicted that the new advances in biological technology would bring a new medicine focused on the individual, thanks to innovative system approaches such as system biology. This discipline emerged from an increased advance in biology knowledge, the integration of new technology, and the research on multidisciplinary environments. The added value originated from understanding the modulation of biological systems and how genes, cells, organisms, and environments interact as complex systems [5]. This knowledge can also improve healthcare, enhancing efficacy, scaling, precision, monitoring, discovery, treatment, prediction, and prevention, being even more economically efficient.

Personalized medicine tries to understand each patient from the gathered data and features that characterize them, creating a specific profile to improve clinical diagnosis and treatment. This approach could be more precise and focused than present clinical medicine, enhancing patient care by boosting efficacy and reducing the number of treatment failures [6]. One of the specialties that personalized medicine has impacted the most is oncology. Cancer cells are not generic, and they depend on the genome or other features of the patient. Therefore, personalized medicine has brought a new way of thinking by looking at the patient from a genome-based perspective. The tumor is then characterized molecularly to find the most appropriate therapy [7]–[10].

Personalization in medicine implies not only genetics and molecular biology but also other areas in medicine, such as surgical treatments [11]. Computer-aided surgery (CAS) brings high-end technology and computer-based methods to surgical interventions. More than 30 years ago, this field started with key technologies during surgical planning, surgical navigation (**Figure 1.1**), and surgical robotics [12]–[18]. Preoperative medical imaging, with computed tomography (CT) or magnetic resonance imaging (MRI), has allowed designing a strategy to approach a surgical intervention by knowing the position of the affected areas. Surgical navigation has provided the surgeon real-time tool tracking with respect to the patient's anatomy. Furthermore, medical robotics has assisted with exact mechanical movements in the operating room (OR), allowing precise surgical gestures. All in all, this medical field has always tried to assist physicians in treating patients as individuals by utilizing different methodologies that adapt to their features and anatomy.

It could be said that personalization is already included in any surgical treatment [19]. However, although some surgical tools try to be personalized and specific for the patient, sometimes they are more generic than expected and not fully adapted to the patient or surgical procedure [20]. 3D printing has overcome some of these limitations fabricating patient-specific surgical guides, adapting hand-held tools for specific surgical procedures, or manufacturing implants that adjust precisely to the patient's anatomy [21]–[23]. Additionally, surgical navigation tracks instruments in real-time, allowing the surgeon to follow a personalized treatment planning performing the correct steps.

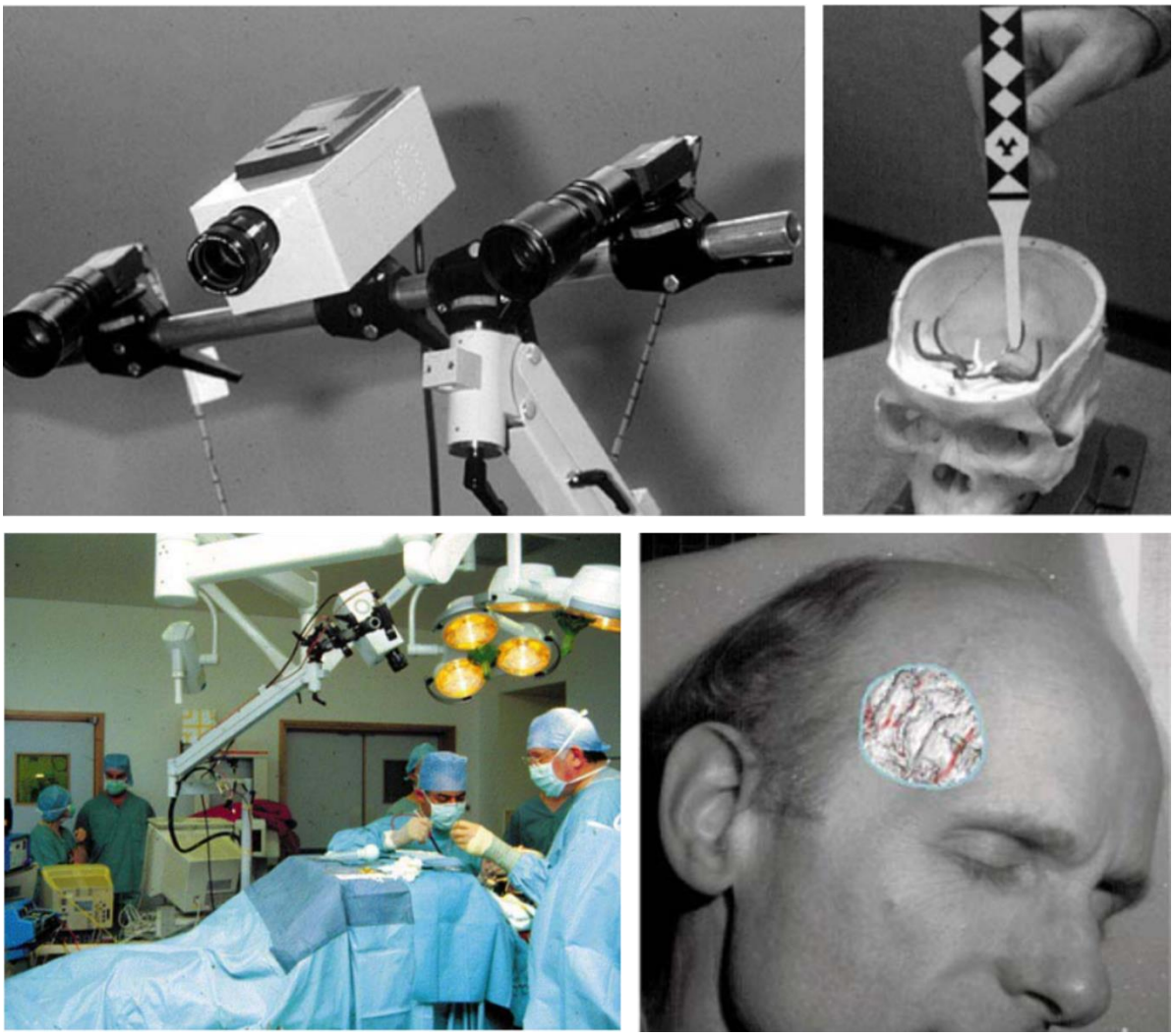

Figure 1.1. VISLAN system with pattern marked tool and image overlay on the patient. Image adapted from [24] (figure reprinted with permission of the copyright holder, Elsevier).

Currently, hospitals keep focusing on surgical treatment personalization. Nonetheless, this also implies longer preoperative times for the physicians, since they need to plan the intervention, analyzing each case in detail to customize the treatment. Therefore, there is a need to reduce processing time during specific tasks in preoperative planning, such as outcome prediction or evaluation of the patients' anatomy. During the past years, artificial intelligence (AI) has overcome this issue by using new computational power to automatically perform these cumbersome tasks, obtaining relevant information from the patients' medical images almost instantaneously [25].

Personalization in medicine also reaches the ORs, which are being customized based on surgeons' preferences and workflows to achieve a better surgical outcome. Recent

technologies provide new ways of visualizing patient information in the OR that could be essential in surgical decision-making. Augmented reality (AR), for instance, can bring science fiction to reality. AR systems allow physicians to visualize relevant virtual information on top of the patient without external screens.

We have seen how new solutions provide personalization focused on the patient. However, the use of these systems is still minimal, and the available technology still does not target every treatment that could benefit from it. Moreover, personalization requires time that surgeons do not have. Additionally, these technologies are not usually combined, limiting their potential. In the following sections, I will present the state-of-the-art of these technological advancements, focused on surgical treatments. Finally, I will report how surgical treatment could benefit if they are all combined.

1.2. Tracking systems

Tracking systems are used in CAS procedures to track the position and orientation of specific surgical instruments. These tools are tracked in real-time with respect to the patient's imaging studies during a surgical intervention improving speed, security, efficacy and, consequently, surgical outcome [26].

Tracking devices are an essential part of surgical navigation. Optical tracking systems (OTS) or electromagnetic tracking systems (EMTS) are the most common, thanks to their versatility, size, and precision. OTS provide high tracking accuracy to any tool attached to spherical reflective markers. Nonetheless, the fundamental limitation is the line-of-sight needed for tracking since, in some scenarios, it is impossible to prevent occlusions [27]. On the other hand, EMTS overcome this limitation. These devices are a good alternative when occlusions are inevitable or tracked tools are inside the patient. Nevertheless, EMTS only work in particular conditions, as precision could be degraded by the distortion of the generated electromagnetic field caused by ferromagnetic materials, commonly used inside the OR [27].

OTS and EMTS are part of most commercial navigation systems. We can find optical tracking devices, such as Polaris Vega (Northern Digital Inc., ON, Canada), in many surgical navigation stations, such as StealthStation (Medtronic Plc., Dublin, Ireland) (**Figure 1.2**) or Curve Navigation (BrainLAB AG, Munich, Germany). Other companies, such as Stryker Corporation (Kalamazoo, MI, USA), Braun Healthcare (Kronberg im Taunus, Germany), or Stereotaxis Inc. (San Luis, MO, USA), offer surgical navigation systems based on their own

tracking devices. These navigation systems are widely used in surgical treatments where rigid structures, such as bones, are involved [28], [29] because they ensure a low patient-to-image registration error. Neurosurgeries have benefited from these systems as well, given that the high tracking precision they offer is essential in these procedures [30], [31].

Figure 1.2. Spinal surgical navigation system called Medtronic StealthStation. Copyright Medtronic.

Surgical navigation systems are valuable in personalized treatments because they can be easily adapted to each patient. Nonetheless, the commercial applications are still limited. These solutions lack the flexibility necessary to adjust the approach to the requirements of each case. They are designed for specific treatments, but their software is not flexible enough in cases where more personalization is needed. For example, a navigation system for knee interventions could be used in similar body areas, such as the elbow or the ankle. However, these devices are not promoted to other locations due to their reduced market and the expenses, logistics and certification involved. Also, the high cost limits their adoption. These constraints avoid their use in specific treatments regardless of the possible benefits [20], [32].

In the past years, different open-source software proposals have reduced these limitations. *PLUS toolkit* is a good example [33], since it was implemented to provide various methods for facilitating the management of interventional tool pose and image data from a wide range of tracking and imaging devices. In order to provide live streaming of tracking information, *PLUS* uses OpenIGTLink [29], an open and simple communication protocol specifically designed for live data transfer in image-guided therapy applications. 3D Slicer, an open-source software platform for registration, interactive segmentation, and visualization of

medical images [34], supports this protocol. Moreover, this software allows specific built-in applications (named modules) to develop personalized applications for surgical treatments.

The combination of open-source software and tracking devices brings new possibilities in surgical navigation, offering extra flexibility that enables innovative solutions not available in commercial systems. García-Mato et al. proposed an intraoperative navigation solution with an OTS and customized navigation software to accurately translate preoperative surgical planning into the operating theater in craniosynostosis surgeries [35]. Ungi et al. have used EMTS to track ultrasound and surgical instruments in breast tumor excision through open-source software, significantly reducing the excised tissue compared to control procedures [36]. These systems succeed as an alternative to commercial solutions.

Nevertheless, one of the main challenges when dealing with tracking systems is the patient-to-image registration. This step is commonly solved by calculating a fiducial-based registration with anatomical landmarks that are visible during surgery. However, these landmarks are difficult to identify in some procedures, such as orthopedic oncology [37], [38], increasing the registration error. For this reason, solutions that improve patient registration on complex surgical procedures, increasing patient personalization, must be developed.

1.3. Augmented reality

Augmented reality (AR) is a technology that brings the possibility to augment the physical, real-world environment by superimposing computer-generated graphics over a user's view of the real world. While virtual reality (VR) uses computer-generated virtual elements to immerse users in a virtual environment completely, AR combines these virtual elements with the real world, allowing the user to be aware of the surroundings.

For the past 30 years, AR has provided an increasing number of applications in the medical field [39]. The interaction between virtual 3D models and the real environment has brought tangible benefits in education and training, where students and physicians can learn in a more interactive way, improving spatial vision and surgical ability [40]–[42]. Additionally, other authors have created simulators to assist surgical interventions with AR systems that provide confidence to physicians about their surgical skills [43]. AR has also enhanced interaction and collaboration between physicians by allowing long-distance real-time communication inside and outside of the OR [44].

Furthermore, AR applications have expanded to surgical treatments, trying to guide surgeons during clinical interventions in many medical fields, such as head and neck surgeries [45], maxillofacial interventions [46], orthopedic medical procedures [47], or neurosurgery [48]. It has also shown a significant impact in needle insertion treatments, thanks to direct visualization of the needle trajectory on top of the patient [49], [50]. All these examples are part of personalized medicine, since they use specific virtual models and adapt the AR application to each patient.

AR technology is mainly composed of two elements: first, a visualization device, which lets the user view the computer-generated elements; second, a combination of computers, software, and sensors that can track and understand the spatial information of the surroundings. With this in mind, two kinds of AR devices have changed the way AR was initially conceived. First, thanks to the new advances in smartphone technology, such as camera sensors and fast microprocessors, we can now use AR right from our pockets. Software development kits (SDKs) such as ARKit for iOS (Apple Inc, Santa Monica, CA, USA) or ARCore for Android (Alphabet Inc, Mountain View, CA, USA) facilitate the creation of AR applications with the cameras of our phones and a few lines of code.

The other devices that have been a game-changer for AR technology are head-mounted displays (HMD). While smartphones need to be held with one hand and the virtual elements are displayed through a screen, HMD free the user's hands. These devices have a semi-transparent glass in front of the eyes on top of which the virtual elements are projected. Then, thanks to the cameras and sensors inside, the device detects the surroundings and where the user is looking, displaying the augmented information right as if they were in the environment. These revolutionary devices were brought affordably first by Microsoft (Redmond, WA, USA) with the HoloLens (**Figure 1.3**) and later by Magic Leap (Plantation, FL, USA). Although these devices are leading the way AR should be perceived, we are still far from their everyday use in the medical field, and more possible applications need to be explored.

Besides, although AR technology has shown great potential in healthcare, the adoption by medical professionals is still limited since they require extensive knowledge of engineering and software development. We believe this technology could be applied to many more medical applications if offered more straightforwardly in terms of accessibility and complexity. For these reasons, we consider that more research is needed to spread AR through medical

professionals in surgical treatments, not only in the OR during surgical interventions, but also for surgical planning and patient communication.

Figure 1.3. Surgeon wearing Microsoft HoloLens during a surgical intervention.

1.4. 3D printing

3D printing technology, also known as rapid prototyping or additive manufacturing, has revolutionized the medical field with numerous advantages that involve a paradigm shift in healthcare [51]. Its healthcare applications have increased exponentially during the last decade, allowing anyone to easily convert 3D models created from medical imaging studies (CT, MRI…) into physical objects using a layering technique [52].

Some examples of medical applications include medical education and training [53]–[55], fabrication of medical devices [52], or bioprinting organs and tissues [56], [57]. The direct interaction with the patient's anatomy is especially important in surgery, where 3D printed patient-specific anatomical models (biomodels) improve spatial perception, enhancing the

results in preoperative planning and clinical interventions in areas such as cardiology [58], [59], urology [60], [61] or gynecology [62], [63]. Unique and specific surgical instruments can also be designed and built, reducing manufacturing time and costs, enhancing customization according to the surgeon's preference [64], [65].

More specifically, orthopedic surgery and traumatology is an area of particular interest [66]–[68] since 3D printing can offer straightforward solutions to fabricate personalized tools essential in this specialty. For example, this technology has facilitated patient-specific surgical tools used for plate pre-contouring or as cutting guides designed to fit in a unique place on the surface of the patient's bone, providing surgical guidance during the intervention [69]–[72]. Others have used rapid prototyping to design and print osteotomy guides [73], [74], contour vascularized bone flaps [75], or reconstruct ligaments [76]. Furthermore, additive manufacturing techniques allow fabricating custom-made implants that adapt specifically to each patient's anatomy in situations that require high customization [77], [78].

Several companies offer support for manufacturing 3D printed tools. Nonetheless, this technology is accessible to everyone through desktop 3D printers. This has moved hospitals towards implementing their own in-house 3D printing hubs, improving the involvement of the clinical staff in the workflow, self-acquiring knowledge for their institution, increasing productivity, and reducing both cost and delivery times of the 3D printed models [79], [80]. This new trend has a significant value in personalized medicine by giving physicians resources to create patient-specific tools (**Figure 1.4**) that could improve medical outcomes, adapting to the needs of both the patient and the physicians.

Fused deposition modeling (FDM) and stereolithography (SLA) are the most common 3D printing technologies found in hospitals. They are making a significant impact on personalizing tools in surgical treatments because of their reduced size, low cost, and flexibility. FDM allows fabricating objects at a low cost by extruding a large variety of plastic materials. Although manufacturing with this technique is straightforward, these 3D printers lack the precision that sometimes is required in surgical treatments. On the other hand, SLA printers make it possible to manufacture high precision tools in resin materials, which present adequate properties to be used inside the OR and can be biocompatible. Additionally, some of these resins can be sterilized following standard protocols without deformation.

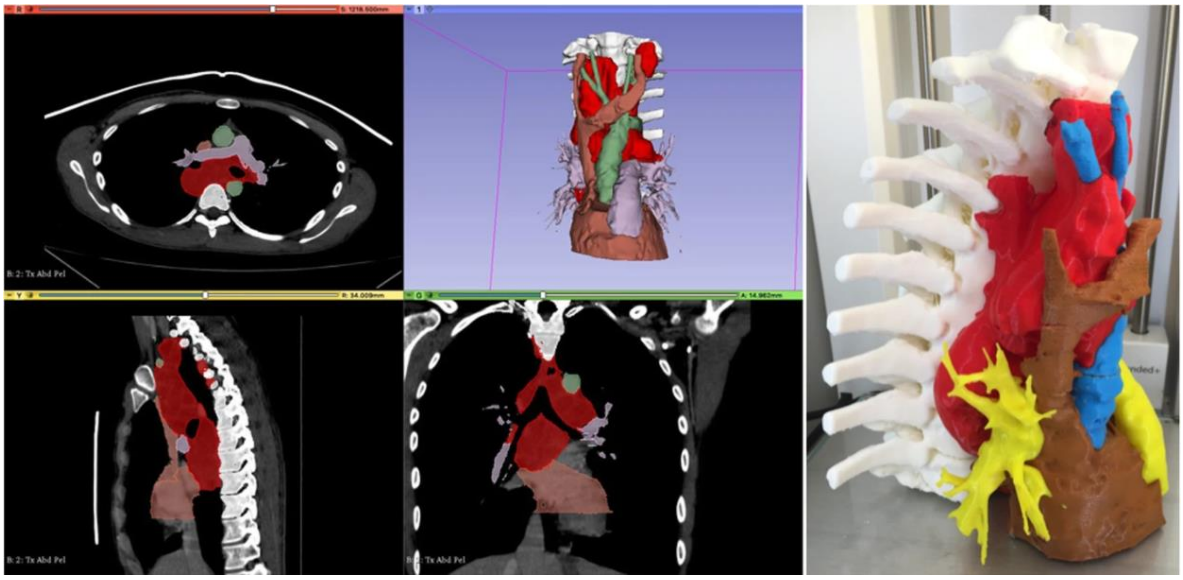

Figure 1.4. 3D printed anatomical 3D models of a complex body area. Image adapted from [80] (figure reprinted with permission of the copyright holder, Springer Nature)

There is no doubt that 3D printing has become an essential technology in everyday life in many hospitals. It gives physicians the ability to increase treatment individualization, benefiting both patient communication and surgical outcome. Their range of possibilities is yet to be explored. However, there are still some drawbacks when personalization comes to mind. Designing biomodels from medical images is time-consuming since automatic segmentation tools are still not standard in 3D printing workflows, and the printing process requires several hours, reducing the clinical translation. Therefore, more research is missing to offer alternatives that reduce the impact of these limitations.

1.5. Artificial intelligence

Artificial intelligence (AI) applies computerized algorithms to analyze and interpret large amounts of data for classification, prediction, and segmentation. Thanks to the advances in computational technology during the last decade, AI has demonstrated outstanding potential for clinical applications, boosting interpretation and automatization in disease diagnosis, personalized treatment, gene editing, or drug development [81], [82].

Machine learning (ML), a subfield of AI, has already shown an incredible increase in diagnostic performance based on medical imaging data for multiple conditions, such as cancer [83], [84], chronic obstructive pulmonary disease (COPD) [85]–[87], or diabetic retinopathy [88]. Surgical decision-making is still influenced by individual subjective judgment and

deductive reasoning, which could lead to medical errors significantly affecting the surgical outcome [89], [90]. However, the integration of AI-based tools could be a perfect alternative to support clinical decisions by, for example, proposing algorithms that could predict risks for postoperative complications [91] or mortality [92].

Other ML approaches have focused on automated identification of surgical phases and instruments and predicting adverse events during medical procedures [93], [94]. For example, Pose-Diez-de-la-Lastra et al. have proposed neural networks to automatically detect surgical instruments from video recordings, identifying the workflow phases in cranial vault remodeling [95]. In other cases, AI has enhanced soft-tissue navigation by detecting organ deformation during surgery and providing patient registration [96].

Although AI algorithms have shown to be a useful tool for improving medical care, much of the research has only been validated on local databases. It is not straightforward to spread their use to other data or domains. Products such as NVIDIA Clara (Nvidia Corporation, Santa Clara, CA, USA) have been developed to overcome these limitations and create scalable AI solutions. NVIDIA Clara is an application framework optimized for healthcare that uses built-in SDKs and reference applications, allowing researchers to develop AI tools that can easily be integrated with the healthcare system. This platform offers a simple solution for data annotation and computational model deployment to boost personalized medicine in any medical discipline [97].

Furthermore, segmentation of the patient's anatomy from medical imaging is essential for personalization in surgical treatments since it contributes to the location and quantification of healthy organs or pathological lesions. Also, the obtention of virtual 3D models of the affected anatomy could be crucial to represent important structures during surgical navigation. Nevertheless, current segmentation procedures are based on manual or semi-automatic methods, which require ample time from the users involved in this step. The need for the automatization of this process is evident. ML algorithms based on convolutional neural networks (CNNs), such as U-Net [98] or SegNET [99], can provide a binary mask for each specific region fully automatically once the computational models are trained. Automatic segmentation has shown promising results in many anatomical areas such as the thoracic cavity [100], abdominal cavity (**Figure 1.5**) [101], head and neck [102], or extremities [103]. However, although these methods show impressive segmentation results, they are usually hard

to generalize to other studies. Their performance decreases on external data not similar to the one used for training.

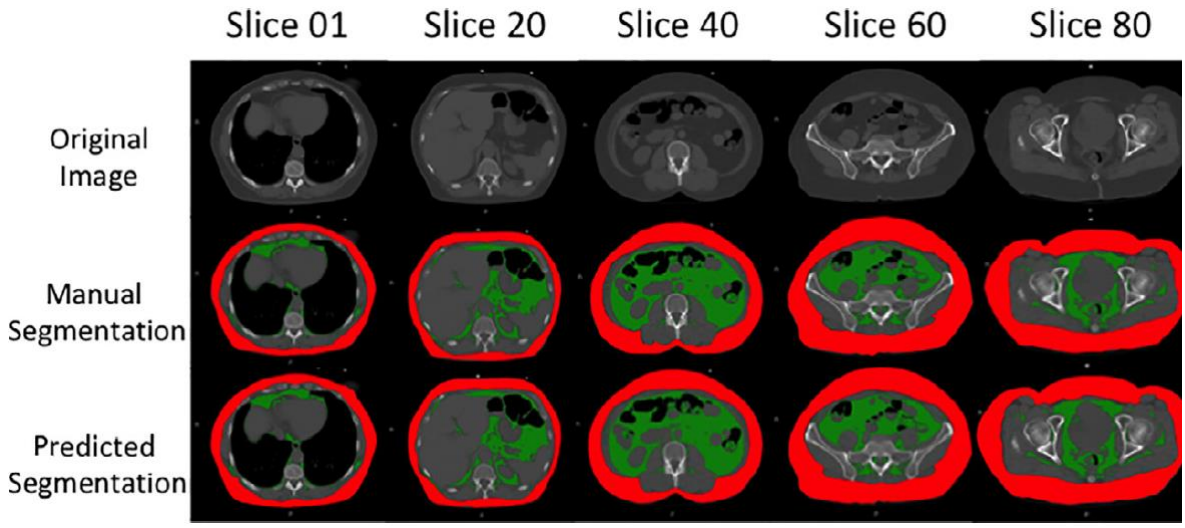

Figure 1.5. Comparison between manual and automatic segmentation (predicted by using a deep learning algorithm) of the subcutaneous adipose tissue (red area) and visceral adipose tissue (green area) from a computed tomography scan. Image adapted from [99] (figure reprinted with permission of the copyright holder, Copyright © 2020, IEEE).

AI applications have shown astonishing results in terms of accuracy and sensitivity and are a promising tool in healthcare that is becoming the key for process automatization. In surgical interventions, manual tasks such as pathology detection and quantification have always been time-consuming for medical professionals, increasing surgical planning time. Right now, many of these processes could be automated, reducing this extensive dedication. Nevertheless, more work needs to be done to provide these solutions in other clinical workflows. For this reason, we believe that AI should be introduced in additional surgical scenarios to reduce manual tasks that are time-consuming for medical professionals.

1.6. Combination of these technologies

In the previous sections, we have presented how different technologies are boosting personalized medicine in surgical treatments. However, we believe that each one has several characteristics that limit their use in other fields. This section will first show their potential when combined within the same workflow by reporting the state-of-the-art. After that, we will explore different areas in surgical treatments that could benefit from combining of these technologies.

Tracking systems provide real-time position of medical instruments in surgical navigation. Still, image-to-patient registration is sometimes difficult to perform in orthopedic oncology, increasing registration error since predefined anatomical landmarks are complicated to identify in the OR [104]. Additionally, commercial surgical navigation systems do not extend to many orthopedic surgical procedures since they lack patient and case personalization [20]. Nevertheless, 3D printing could offer a perfect combination with tracking systems to overcome these drawbacks, since additive manufacturing creates personalized tools that adapt to the specificness of the patient. For example, Schulz et al. have combined surgical navigation and 3D printing in complex bone tumors of the trunk to enhance surgical planning. They reported that the combination of 3D printing with other techniques could contribute to an improved personalized medicine [105].

On the other hand, as mentioned in previous sections, AR systems have shown great potential in surgical treatment. Nevertheless, there are some restraints if they are applied in surgical treatments in terms of portability, calibration and tracking. These disadvantages make it difficult to register the augmented data with the real-world space [106]. Up to now, patient registration has been achieved by applying manual alignment (**Figure 1.6**) [107], or with optical/electromagnetic tracking systems [108], [109]. These solutions seem to work in some specific applications, but require extra hardware, add complexity to the workflow, increase procedure time, and may not be accurate enough.

Furthermore, many navigation AR proposals are validated with methodologies that are difficult to generalize or do not follow a rigorous error analysis [110], [111]. In this context, tracking systems (such as EMTS or OTS) could be a perfect gold standard for error measurements in AR systems [112]. Additionally, 3D printing could be implemented to validate in-vitro navigation by manufacturing 3D printed phantoms based on patient data [113].

Moreover, AR and 3D printing technologies have improved orientation, guidance and spatial skills in surgical treatments when used independently. However, long 3D printing manufacturing times for large 3D models and AR depth perception are important limitations in medical applications that could be solved by combining both technologies. Wake et al. showed that the visualization of 3D models, either with AR visualization or 3D printed objects, reported an increased value in patient education [114]. On the other hand, the integration of both technologies has facilitated the explanation of medical conditions to the patient by simulating

the proposed treatments in transcanal endoscopic procedures [115] or percutaneous pulmonary interventions [116].

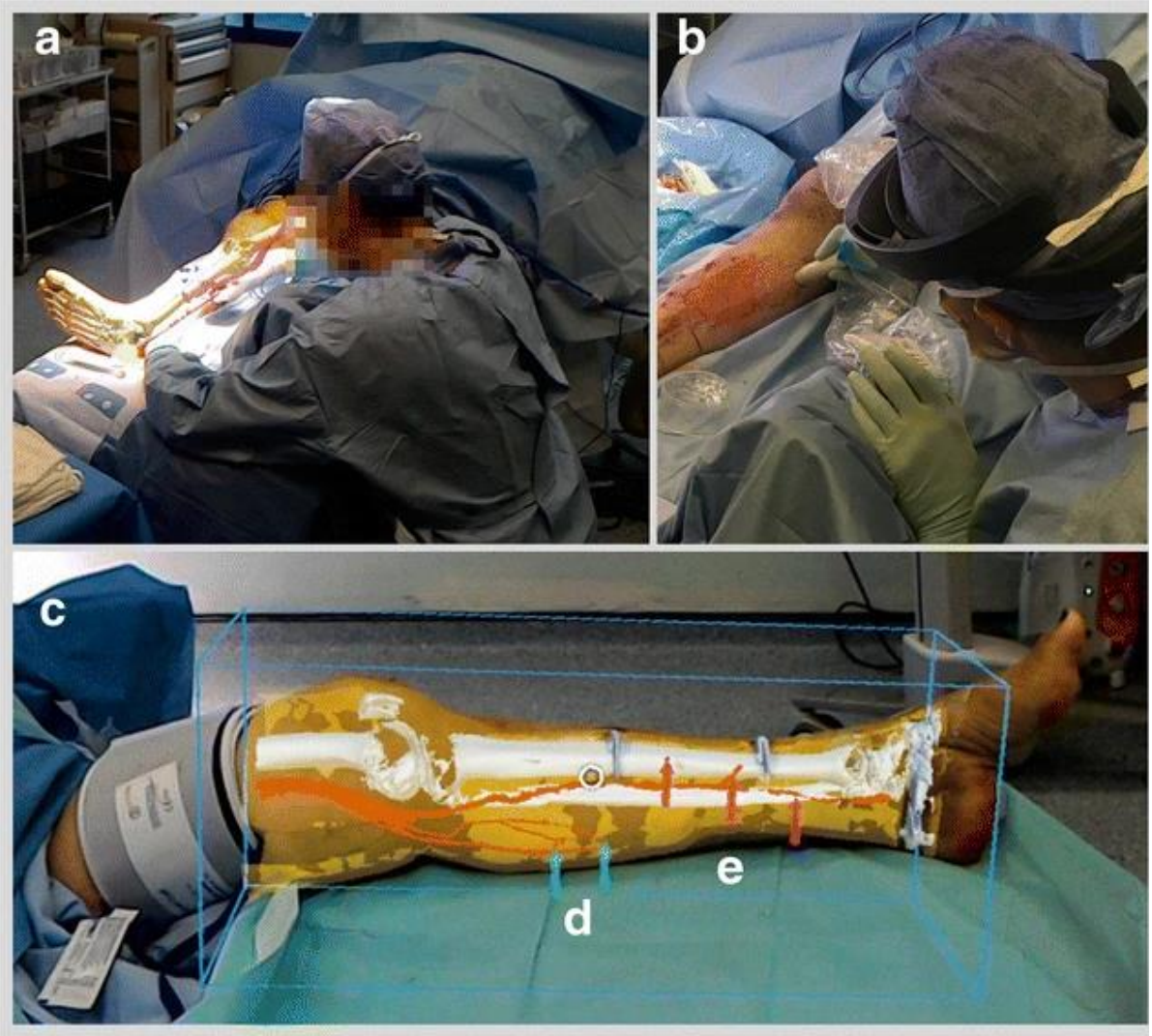

Figure 1.6. Usage of Microsoft HoloLens in the operating room to aid identification, dissection and execution of vascular pedunculated flaps during reconstructive surgery. Image adapted from [107] (figure reprinted with permission of the copyright holder, Springer Nature).

Anatomical segmentation of affected areas in surgical treatments is based on manual methodologies, which require extensive time from medical professionals during preoperative planning. ML algorithms could be an alternative to automatize these models in order to reduce processing times considerably. Izard et al. proposed using AI to automatically segment and reconstruct anatomical models that would be used in an AR and VR platform prior to surgery, reducing complexity in the surgical workflow [117].

These technologies used independently are valuable in surgical treatments. However, their combination could be crucial to improve navigation accuracy, reduce preoperative times and navigation complexity, and add surgical value. We believe that their use is still limited and that, combined, they can have an essential role in surgical guidance.

2

Motivation and Objectives

2.1. Motivation

In surgical treatments, personalization has been possible thanks to key technologies in surgical navigation that allow physicians to provide individualized treatment adapting to patients' features and anatomy. Tracking systems, augmented reality (AR), 3D printing, and artificial intelligence (AI) have been part of this process by manufacturing patient-specific tools, bringing new ways of visualizing patient information or reducing complexity and time by automatically performing cumbersome tasks [28], [46], [69], [102]. However, their independent contributions show several limitations in terms of lack of flexibility to adapt to the requirements of each case, patient-to-image registration, and large preoperative planning times.

Commercial navigation systems have already been implemented with great success in many surgical procedures, mainly where rigid structures, such as bone, are involved [28]–[30]. However, when they are designed for specific treatments, they are not promoted to other procedures due to their possible reduced market, the expenses, logistics and certification involved. Therefore, these constraints avoid their use in specific treatments regardless of the possible benefits. The combination of open-source software and tracking devices could be an alternative in cases where commercial systems are not enough [35], [36]. Nevertheless, the implementation of these systems is still reduced due to limited patient personalization tools.

Moreover, one of the main challenges when dealing with tracking systems is the patient-to-image registration. It is commonly solved by applying a fiducial-based registration with anatomical landmarks that are visible during surgery. However, these landmarks are difficult to identify in some procedures, such as orthopedic oncology [37], [38], increasing the

registration error. Furthermore, registration methodologies in AR navigation systems are still constrained by technological restrictions, such as portability, calibration and tracking. Up to now, patient registration has been achieved by applying manual alignment [107], or with optical/electromagnetic tracking systems [108], [109]. These solutions seem to work in some specific applications, but require extra hardware, add complexity to the workflow, increase procedure time, and may not be accurate enough, making their implementation impossible in many cases.

It is worth mentioning that augmented reality technology has brought tangible benefits in medical procedures by guiding surgeons during clinical interventions in many medical fields [45]–[50], but we are still far from their everyday use. The adoption by medical professionals is still restricted since they require extensive knowledge of engineering and software development, limiting their use not only in surgical treatments, but also in surgical planning and patient communication.

Additionally, anatomical segmentation of the patient's anatomy from medical imaging is essential in surgical treatments since it contributes to identifying healthy organs or pathological lesions. Nevertheless, current segmentation procedures are based on manual or semi-automatic methods, which require ample time from the medical. During the past years, artificial intelligence (AI) has overcome this issue by performing these cumbersome tasks automatically, helping to obtain relevant information from the patients' medical images almost instantaneously [83], [85], [89], [94], [100]–[103]. However, the implementation of these techniques has only been validated on local institutions, and it is not straightforward to spread their use into more clinical workflows.

These technologies used independently are very valuable in surgical treatments. However, their combination could be crucial to improve navigation accuracy, reduce preoperative times and navigation complexity, and add surgical value. We believe that their use is still limited and that, combined, they can have an essential role in surgical guidance.

2.2. Objectives

The main objective of this thesis is to increase patient personalization in surgical treatments by combining key technologies such as tracking systems, augmented reality, 3D printing and artificial intelligence. The combination of these technologies will bring surgical navigation to new complex cases, create new patient registration methods with patient-specific

tools, facilitate access to augmented reality by the medical community, and automate surgical workflows. The objectives of this thesis are the following:

(1) To develop a new surgical workflow that combines 3D printing and open-source navigation software to navigate acral tumor resection surgeries by manufacturing patient-specific 3D printed molds to ensure patient-to-image registration and proper margin removal, reducing errors and increasing surgeon's confidence.

(2) To design and evaluate an augmented reality navigation system that uses a patient-specific 3D printed surgical guide with a reference marker for patient-to-image registration in orthopedic oncology tumor resection surgery.

(3) To accelerate the adoption of AR and 3D printing technologies by medical professionals by proposing an augmented-reality smartphone application to visualize anatomical 3D models of patients using a 3D printed reference.

(4) To design and evaluate a new surgical framework that combines AR and 3D printing for their integration in orthopedic oncology surgeries by manufacturing 3D printed patient-specific models and developing an AR smartphone application to assist during preoperative planning, patient communication, and surgical intervention.

(5) To propose and evaluate two different navigation systems in an advanced surgical framework to guide electrode placement in sacral neurostimulation surgeries designed to reduce surgical time, minimize patient discomfort, and improve surgical outcomes.

The work presented in this thesis has been developed at Universidad Carlos III de Madrid in collaboration with the Department of Orthopedic Surgery and Traumatology of the Hospital General Universitario Gregorio Marañón and the Department of General Surgery of the Hospital Universitario La Paz in Madrid, Spain. Additionally, some methods are the result of a collaboration with the Applied Chest Imaging Laboratory (ACIL) research group from the Radiology Department of the Brigham and Women's Hospital and Harvard Medical School in Boston, Massachusetts, United States.

3

Surgical Navigation and 3D Printing in Acral Tumors

3.1. Introduction

Surgical navigation allows relating the pose of specific instruments to the patient's imaging studies in real-time by means of a tracking system and patient-to-image registration [118]. This technology has shown potential benefits in orthopedic oncology surgeries on pelvic, sacral, spinal, and bone tumors [119]–[122]. Nevertheless, some of these authors have not found strong evidence supporting a better surgical outcome for navigated operations compared to conventional surgery [123]. Commercial navigation systems have been designed explicitly for orthopedic procedures, such as OrthoPilot (B. Braun, Melsungen, Germany), ORTHOsoft (Zimmer Biomet, IN, USA), or NAV3i (Stryker Corporation, MI, USA). However, there are two limitations of these solutions in orthopedic tumor surgery: the lack of flexibility, necessary to adapt the system to the requirements of every case, and the high cost of these devices. Very particular procedures, such as the resection of acral tumors (those located in distal extremities such us hands or feet), have no clear benefit from navigation because it is complicated to adapt commercial systems to the necessities of those surgeries [20], [32]. Nevertheless, due to the low amount of surrounding tissue, sometimes it is hard for the surgeon to ensure enough resection margin. Surgical navigation could provide the surgeon with the tumor's location, leading to a more precise surgical margin outcome than conventional surgery. However, these locations introduce a significant challenge during surgical navigation due to their large number of joints with complex movements (e.g., hand exhibits 27 degrees of freedom). This causes

preoperative images not to correspond to the actual limb position during surgery, so the rigid transformation commonly applied for image-to-world registration will compromise navigation accuracy.

To solve these problems, we propose to adapt the image-guided surgery (IGS) workflow using two enabling technologies: open-source software and three-dimensional (3D) printing. Software solutions such as 3D Slicer [34] can be an alternative in surgical navigation, offering extra flexibility that enables the development of innovative solutions not available in commercial systems [35], [36], [124], [125]. 3D printing, also known as rapid prototyping or additive manufacturing, allows anyone to easily convert 3D models into physical objects using a layering technique. During the last decade, the applications of 3D printing have increased exponentially in the medical area [126], including preoperative planning, bioprinting, and physician training. 3D printing already has an increasing impact in surgical practice, where the ability to interact with the patient's anatomy is crucial: anatomical models, surgical instruments, and implants/prostheses are the main areas identified in the recent literature [127]–[130]. Orthopedic surgery is an area of particular interest [66] since 3D printed models facilitate the pre-contouring of plates, and cutting guides can be designed and printed adapted to each case [69], [70]. Several companies offer support for manufacturing these tools. However, there is also a trend to implement desktop 3D printing inside the hospital [79], keeping the interaction with the printing process in-house and improving the involvement of the clinical staff in the workflow.

3.2. Objective

3D printing may expand the possibilities of other techniques such as surgical navigation, where patient-specific implants have enabled IGS in complex tumor resections [131]. In this study, we suggest combining desktop 3D printing and open-source software to navigate acral tumor resection surgeries. To do so, we propose a surgical workflow that includes patient-specific 3D printed molds to ensure that the distal extremity position depicted in preoperative images resembles the one found during surgery. We also designed a specific 3D printed attachment to track a surgical tool. An open-source navigation software has been adapted for guiding the resection of these tumors. The accuracy of our solution was measured with patient-specific 3D printed phantoms and tested during two tumor removal surgeries.

3.3. Methods

3.3.1. Patient studies

We evaluated the feasibility of the suggested workflow in two patients. The first patient (case 1) presented a soft-tissue sarcoma located in the thenar eminence of the right hand (**Figure 3.1**a). The second patient (case 2) showed a soft-tissue sarcoma in the dorsal area of the right foot (**Figure 3.1**b). The study was performed in accordance with the principles of the 1975 Declaration of Helsinki as revised in 2013. The anonymized patient data and pictures included in this paper are used after written informed consent was obtained from the participant and/or their legal representative, in which they approved the use of this data for dissemination activities including scientific publications.

3.3.2. Medical image acquisition and processing

A preoperative computed tomography (CT) scan of the affected distal extremity was acquired for both cases with slice thickness of 2.00 mm and axial in-plane pixel size of 0.80 mm (case 1) and 0.95 mm (case 2). Moreover, magnetic resonance images (MRI) were also acquired for both cases to examine tumor boundaries in the soft tissue (T2 sequences for both cases with resolution of 0.20 × 0.20 × 3.85 mm for case 1 and 0.30 × 0.30 × 4.4 mm for case 2). Preoperative images were acquired 102 days before the surgical intervention for case 1 and 70 days for case 2. 3D slicer [34] version 4.8 was used for the registration of the medical images and segmentation of the anatomy of both patients. The soft-tissue tumor and surrounding anatomical region were segmented on the CT image, taking into account information from the registered MR images, using semi-automatic methods (thresholding, manual contour, and island effects). The results were exported as virtual 3D models (stereo lithography files, STL). 3D models were post-processed using smoothing (median filter with kernel size 3 × 3 × 1 pixels) and hole filling (kernel size 7 × 7 × 3) in 3D Slicer to optimize 3D printing quality and minimize manufacturing time. **Figure 3.1** shows the real picture and the virtual 3D model of the extremities and tumor (in green) for both cases.

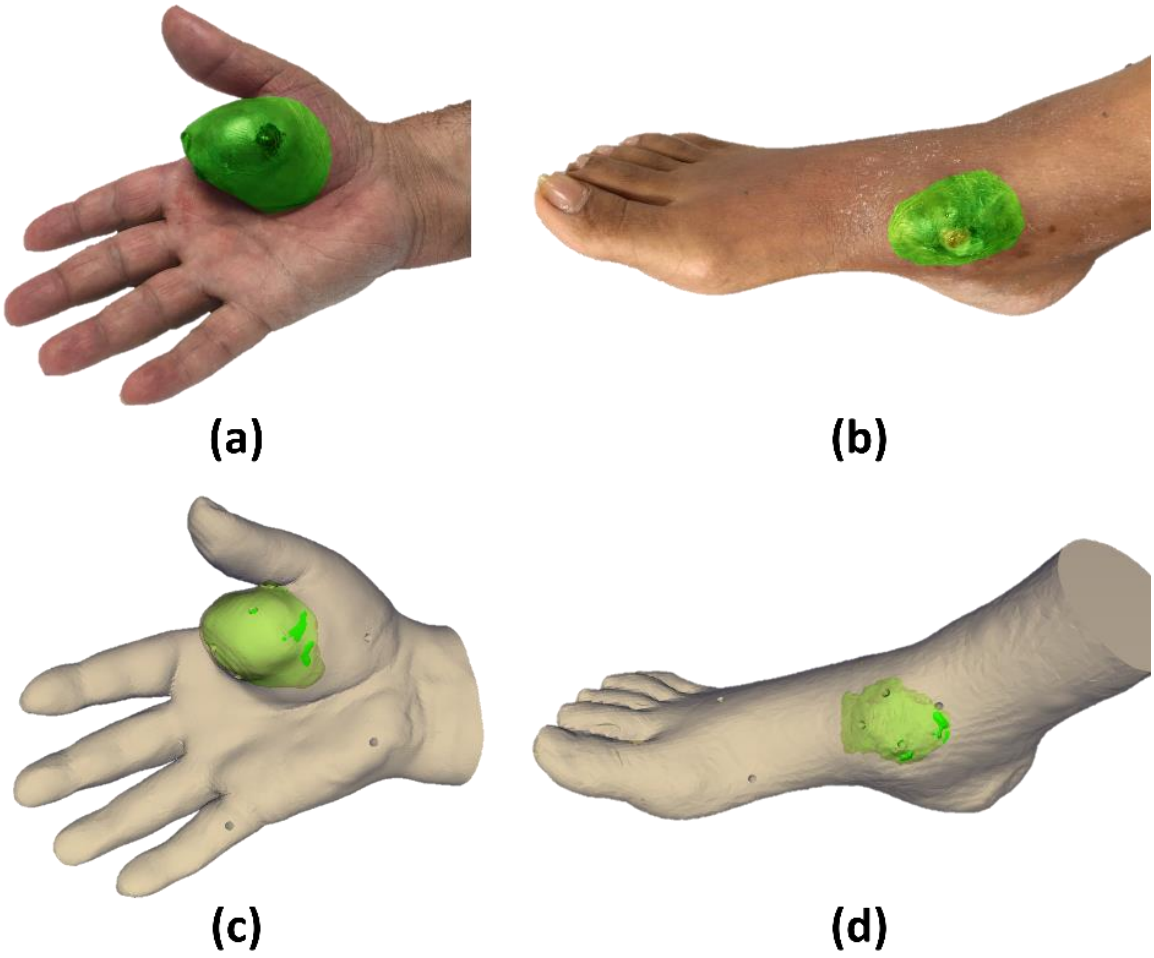

Figure 3.1. Representation of the clinical cases. Case 1: patient with a soft-tissue sarcoma (green) located on the right hand. (a) Real image and (c) virtual image. Case 2: patient with a soft-tissue sarcoma (green) in the right foot. (b) Real image and (d) virtual image.

3.3.3. Computer-aided design and manufacturing

We designed and manufactured several tools and models in this study: a mold to ensure the position of the limb for each patient, a customized cap to enable navigation of the surgical scalpel, and phantoms obtained from the limb of each patient to evaluate the navigation error in a controlled scenario. This section describes the methodology followed to create each object.

Each mold was designed in Meshmixer (Autodesk Inc., CA, USA) software by extruding the surface of the limb's 3D mesh. This holder allows the limb to be fixed during the surgical procedure in the same position as in the preoperative CT image. The design of the mold considered the surgical approach and working area, to facilitate easy management during

surgery, and presented a smooth surface on the limb side to limit any harm to the patient. It also included an attachment for retro-reflective optical markers (rigid body, RB) to enable navigation. The position of these markers was determined to avoid possible occlusions during navigation. Furthermore, we included several conical holes (Ø 4 mm × 3 mm depth) on the mold surface for point-based registration and error measurement. We also designed a customized cap with optical markers to track the electric scalpel during surgery.

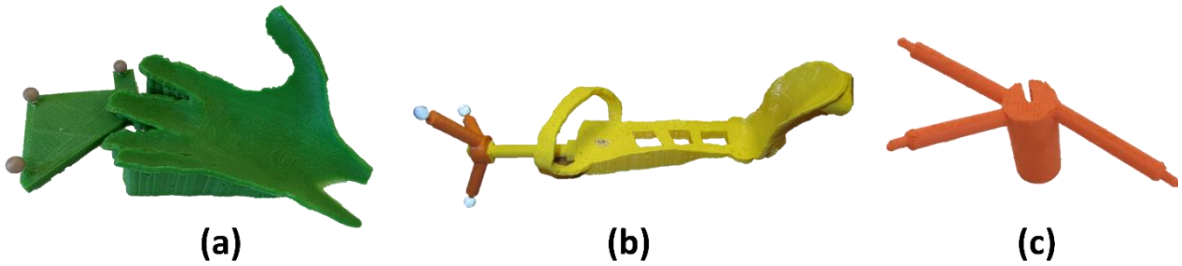

Figure 3.2. Three-dimensionally (3D) printed models with a rigid body (RB) attached to them: (a) patient-specific mold for case 1; (b) patient-specific mold for case 2; (c) electric scalpel customizable cap.

3D models (molds and the customized cap for the surgical tool) were manufactured with a desktop 3D printer (Witbox-2, BQ, Madrid, Spain) using polylactic acid (PLA) (**Figure 3.2**). The RB attachment included in the mold design of case 2 was 3D printed separately since the whole design did not fit in the printer bed (dimensions 297 × 210 mm). 3D printed tools were sterilized to maintain asepsis of the surgical field as they may be in contact with the patient. The sterilization technique was based on ethylene oxide (EtO) at 37 °C to avoid deformation (the glass transition temperature of PLA is around 55–65 °C). It involved extensive degassing to remove the residual EtO [132]. The spherical markers used for navigation were attached during surgery, since they are supplied in individual bags in sterile condition.

A patient-specific phantom was manufactured for each patient case to evaluate the performance of the IGS system before surgery (**Figure 3.3**a,d). Each phantom included a 3D printed copy of the mold made for surgery and the affected extremity limb with several conical holes (Ø 4 mm × 3 mm depth) on the model surface used to evaluate the accuracy of the navigation. Original 3D models of the mold and the limb from both cases are available in the supplementary material as **3D Model S1** (case 1 mold), **3D Model S2** (case 1 limb), **3D Model S3** (case 2 mold), and **3D Model S4** (case 2 limb).

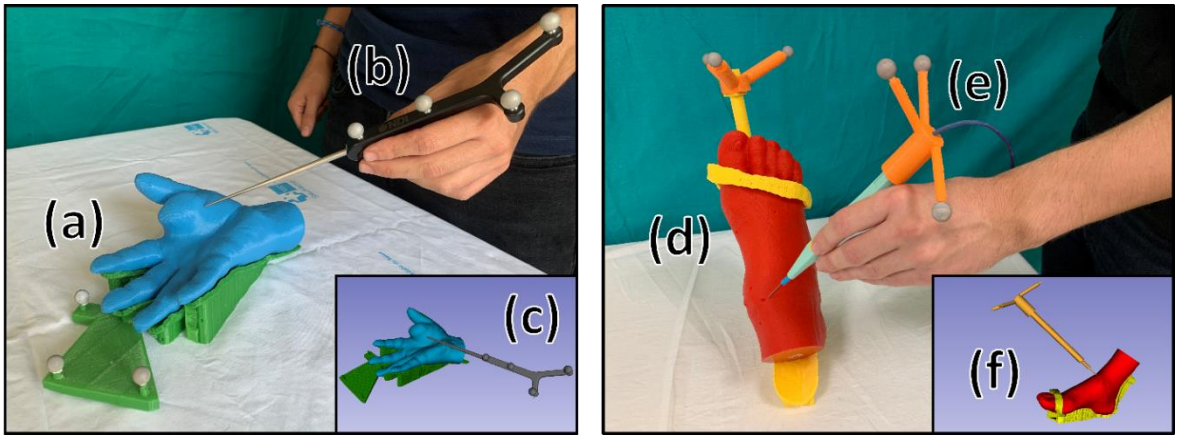

Figure 3.3. Image-guided surgery simulation on patient-specific 3D printed phantoms based on case 1 (left) and case 2 (right). The user is recording points from the conical holes made on the surface of the 3D printed phantoms (**a**,**d**) with the commercial pointer (**b**) in case 1, and with the electric scalpel (**e**) in case 2. The corresponding virtual scenes are shown in (**c**,**f**).

3.3.4. Navigation software and hardware

A specific software application named *AcralTumorNavigation* was developed as a module in the 3D Slicer platform to facilitate the surgical navigation of acral tumors [34], [133]. OptiTrack multi-camera optical tracking system (NaturalPoint Inc., OR, USA) provided real-time tool tracking during the accuracy experiments and surgery. This system is accurate and very robust for IGS navigation in large clinical scenarios, thanks to the use of multiple cameras. Even if the surgical team occludes the line-of-sight between some cameras and the tracked tools, the system will provide correct tracking data [134]. Eight near-infrared cameras (model OptiTrack Flex 13) were distributed around the operating room (OR) to cover the working area (**Figure 3.4**a). The tracking system transfers the positioning data to the *AcralTumorNavigation* module using *PLUS-toolkit* [33] and the *OpenIGTLink* communication protocol [135]. Two different tools were used as reference pointer during the surgical procedure: a passive 4-marker probe (Northern Digital Inc. [NDI], ON, Canada) (**Figure 3.3**b) and an electric scalpel with a specific optical marker configuration attached to a customized 3D printed cap (**Figure 3.3**e). A pivoting procedure [136] enabled to obtain the relationship between the RB attached to the reference pointer and its tip. Both pointer tools were sterilized before surgery (the probe and the customized cap using a protocol based on EtO at 37 °C and the scalpel in autoclave).

The limb mold ensures that the patient is in the same position as in the preoperative image, granting an automatic registration between the IGS system and the patient. This holder

included an RB that allowed the tracking device to compensate for any movement of the patient's limb during surgical navigation. For this purpose, the RB needs to be registered to the mold. We proposed two alternative approaches to solve this registration problem. First, the RB and the mold could be 3D printed together, so no external registration would be necessary as the relative position is already known from the 3D model design. Second, if the RB and mold could not be printed together or if the RB was displaced right before surgery, registration could be calculated applying a fiducial-based rigid registration algorithm [136] by recording points on the conical holes made on the surface of the mold. This method could be employed intraoperatively.

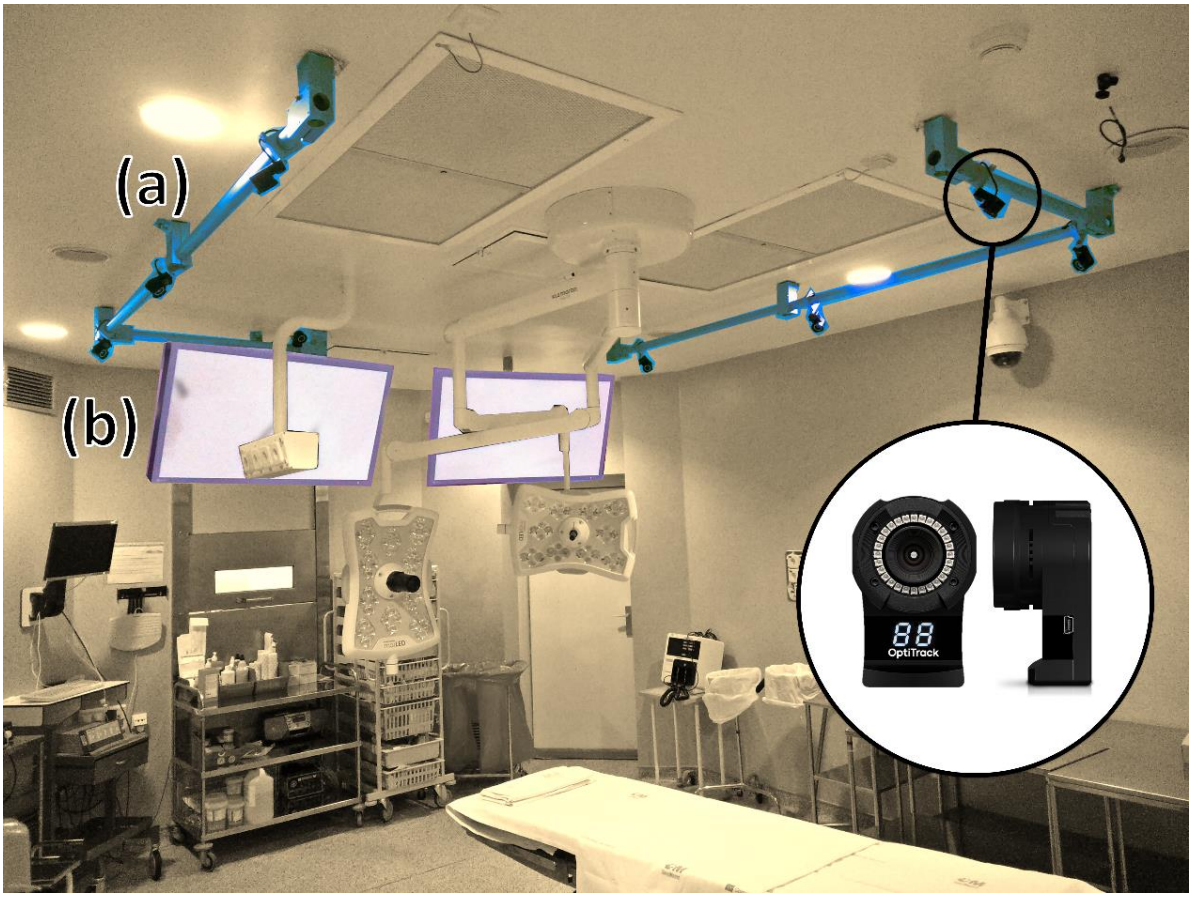

Figure 3.4. Operating room where surgeries of case 1 and 2 were performed, showing the distribution of the eight optical tracking system cameras in blue (**a**) and two surgical monitors in pink (**b**).

An external screen available in the OR (**Figure 3.4**b) displayed the *AcralTumorNavigation* software during the intraoperative navigation. First, virtual 3D models and preoperative images of the patient were loaded in the navigation software. Then, the surgeon selected the reference pointer (commercial probe or an electric scalpel) to be used

during navigation and performed pivot calibration. If any misregistration between the limb mold and its corresponding RB was detected, the application allowed the physician to calculate an intraoperative registration by recording points on the mold's conical holes using the reference pointer previously selected. Once the patient's extremity was placed on the limb holder, the program displayed the real-time position of the reference pointer with respect to the medical images and virtual 3D models of the patient. Moreover, *AcralTumorNavigation* could calculate the real-time distance of the reference pointer tip to any 3D model (e.g., tumor), giving visual feedback to the surgeon. It also enabled real-time visualization of the patient's volume-rendered image, or virtual 3D models, depending on surgeons' interest. Furthermore, the software could store point coordinates from the tip of the reference pointer, which were later used for surgical validation of the tumor resection margin.

3.3.5. Surgical workflow

Once the patient was under anesthesia, surgeons prepared the affected area for the surgical intervention by covering the patient's limb with sterile gauzes. This step protected the patient while the extremity was placed on the mold and avoided limb movement during the intervention. Then, the patient limb was fixed on the sterile mold to resemble the distal extremity position from the preoperative planning. The next step was to calibrate the reference pointer tip with respect to the RB attached to it by pivot calibration procedure. The surgeon verified that the IGS system was correctly registered to the patient by moving the reference pointer to known anatomical points on the patient and confirming that they corresponded to the correct position on the virtual models and CT image. Then, physicians proceeded with the resection of the tumor. While performing the resection task, surgeons used the navigation system several times to confirm they reached the margin area preoperatively planned. Once the tumor was removed, surgeons recorded several points around the resection area to verify the tumor resection margin. We calculated the Euclidian distance from these points to the segmented tumor after surgery. The suggested surgical framework is summarized in **Figure 3.5**.

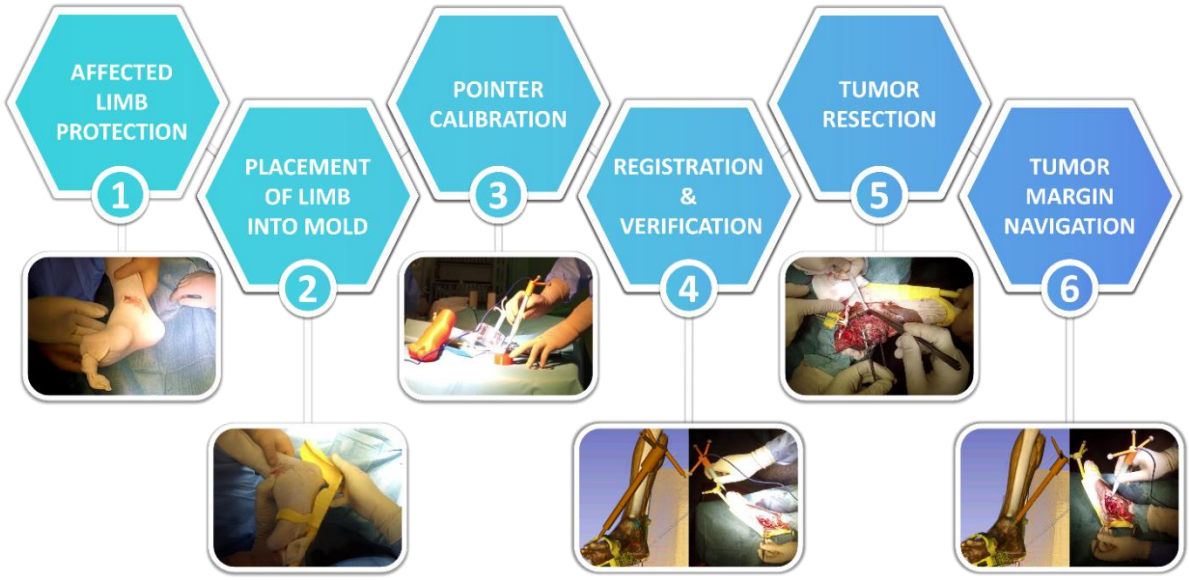

Figure 3.5. Proposed workflow for acral tumor resection surgeries.

3.3.6. Framework evaluation

We evaluated three different aspects of the proposed framework. First, the deformation of the 3D printed limb molds caused by the sterilization procedure. Second, the navigation system accuracy on patients' phantoms before surgery. Last, the feasibility of the proposed surgical navigation workflow during surgery.

Evaluation of mold deformation and sterilization

Sterilization processes might modify the shape of the mold from its original design and consequently increase navigation errors. To evaluate this error, we obtained a CT image from each 3D printed mold before and after sterilization. We measured the possible deformation by calculating the Euclidian distance between each mesh point from the model before sterilization to the closest mesh point in the sterilized model. These models were obtained from CT images after segmentation by intensity thresholding. The CT acquisition scan parameters were voltage 100 kV, exposure 400 mAs, and voxel size 0.9 × 0.9 × 0.5 mm. 3D models were initially pre-registered using the conical holes included during the design of the molds. This alignment was refined with iterative closest point registration algorithm. For case 1, the RB attachment was removed from the hand mold virtual model in order to have a fairer comparison between both cases, as the RB attachment of the case 2 mold could not be printed within the same design

Surgical simulation

Prior to surgery, the navigation procedure was simulated on the 3D printed phantoms to validate the software and to evaluate IGS system accuracy. Both reference pointers (the NDI pointer and the navigable electric scalpel) were tested during these simulations. The workflow included several steps: (1) pivot calibration of the reference pointers (only once at the beginning of the simulation); (2) fixing the limb to the mold; (3) recording the position of the conical holes (nine cones for the case 1 and 8 cones for case 2) with each reference pointer. Steps 2 and 3 were repeated four times by one user, for each phantom and each pointer, removing and placing back again the 3D printed limb on its mold. Navigation accuracy was calculated as the Target Registration Error (TRE) on the conical holes on the limb for each case. This value corresponded to the Euclidian distance between the recorded coordinates and the ones obtained from the same position in the virtual models. In case 2, it was necessary to register the RB and its mold before the simulation. **Figure 3.3** represents a user performing the simulation on the 3D printed phantoms

Evaluation during the surgical procedure

The proposed framework was tested during the tumor removal surgeries in both cases. We obtained qualitative feedback from the surgeons and a quantitative validation of the navigation system. For this purpose, we measured the distance from the surgical tumor margin, calculated from points recorded after tumor resection, to the tumor segmented on the preoperative CT image. This distance should correspond to the pre-planned resection margin.

3.4. Results

The error results obtained by comparing the 3D models from CT images before and after the sterilization processes are displayed in **Figure 3.6**. The mean error between 3D models is 0.13 ± 0.14 mm for case 1 (**Figure 3.6**a) and 0.17 ± 0.15 mm for case 2 (**Figure 3.6**b). For case 1, the surface finger area of the pinky, ring finger and middle finger and the middle surface area of the posterior part of the hand presented a higher error than the rest of the holder. The maximum error (2.30 mm) was located in some small specific points of the pinkie and ring finger. In case 2 (foot mold), some areas of the arch that tied the toes up and the surface that is in contact with the top part of the sole of the foot presented a higher error than the rest of the

mold. The maximum error (2.77 mm) was located on small parts on the arch and back of the mold. No strong deformation is detected in any of the holders.

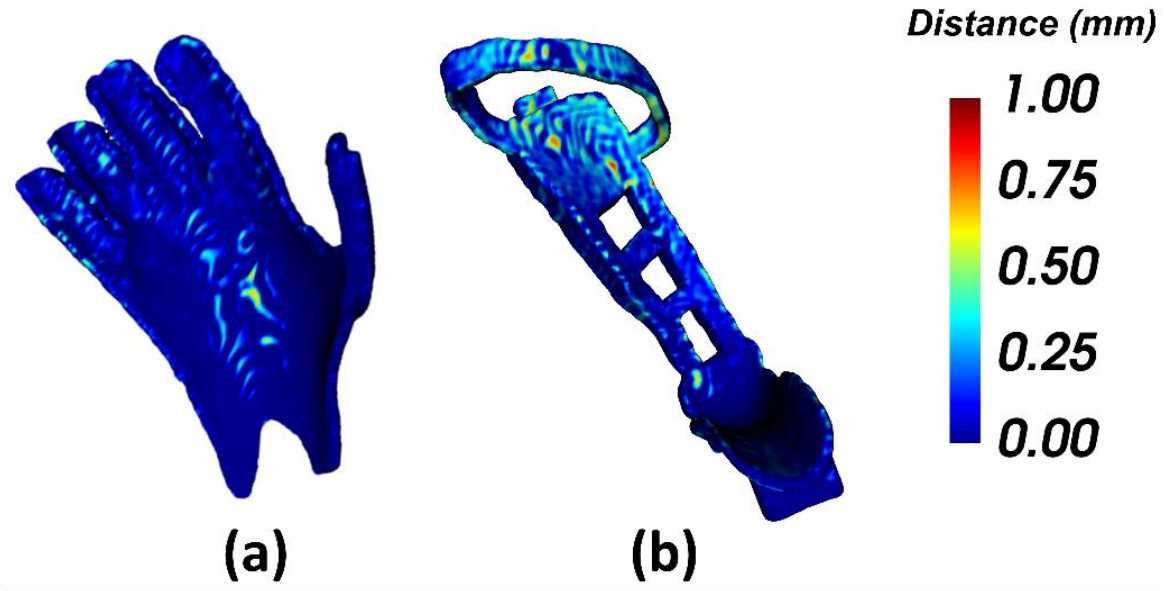

Figure 3.6. Distance comparison between the 3D models of the limb mold obtained from CT images before and after the sterilization process: (**a**) Case 1 hand mold; (**b**) case 2 foot mold.

The performance evaluation results of the IGS system on the two patient-specific 3D printed phantoms using both, the commercial pointer and the electric scalpel, are presented in **Table 3.1**. Each repetition corresponds to removing and placing back again the 3D printed limb on the mold. In case 1, the total root-mean-squared error (RMSE) across four repetitions was 1.88 ± 0.18 mm (NDI pointer) and 1.57 ± 0.11 mm (electric scalpel). In case 2, the RMSE was 2.12 ± 0.18 mm (NDI pointer) and 1.95 ± 0.43 mm (electric scalpel). In both cases, the electric scalpel obtained a lower RMSE than the commercial pointer. Sixty percent of the points taken with both tools presented an error below 1.97 mm.

The IGS workflow was feasible in both clinical cases during surgery. For case 1, the hand was fixed to the mold by using elastic bands on the fingers (**Figure 3.7**b). The position of the hand was corrected several times because it was slipping on the mold. The NDI pointer was used as the reference pointer. For case 2, the foot was put into a bandage to avoid the slipping encountered during surgery for case 1. In this surgical procedure, the electric scalpel was chosen as a reference pointer. After the patient's limb was positioned into the mold, we observed that the navigation information was not correct on the screen. We presumed that this

problem was caused by incorrect placement of the RB, so we registered the RB with the mold. Once this new position of the RB was established, the navigation continued with no further problems. Registration required less than 1 min. Video recordings of both clinical cases can be found in **Video S1** (surgery of case 1) and **Video S2** (surgery of case 2).

Table 3.1. Target Registration Error (TRE) (mm) obtained using each reference pointer (NDI pointer and scalpel) for cases 1 and 2 as well as the combined results for both cases and reference pointers. (RMSE: root-mean-squared error).

Case	TRE Metrics (mm)	NDI Pointer	Scalpel	All Reference Pointers
Case 1	**Mean**	1.80 ± 0.57	1.48 ± 0.53	1.64 ± 0.57
	RMSE	1.88 ± 0.18	1.57 ± 0.11	1.72 ± 0.22
	Min	0.87 ± 0.21	0.84 ± 0.12	0.85 ± 0.17
	Max	2.60 ± 0.37	2.42 ± 0.27	2.51 ± 0.33
Case 2	**Mean**	2.06 ± 0.54	1.84 ± 0.77	1.95 ± 0.68
	RMSE	2.12 ± 0.18	1.95 ± 0.43	2.04 ± 0.34
	Min	1.33 ± 0.23	0.70 ± 0.13	1.02 ± 0.37
	Max	2.94 ± 0.31	2.80 ± 0.41	2.87 ± 0.37
All Cases	**Mean**	1.92 ± 0.57	1.65 ± 0.68	1.78 ± 0.64
	RMSE	2.00 ± 0.22	1.76 ± 0.37	1.88 ± 0.32
	Min	1.10 ± 0.32	0.77 ± 0.15	0.94 ± 0.30
	Max	2.77 ± 0.38	2.61 ± 0.40	2.68 ± 0.40

The navigation allowed the surgeon to evaluate the current position of the reference pointer with respect to the tumor, and to check the surgical margins after tumor resection (**Figure 3.7**). Once the surgeon finished the tumor resection, he recorded points around the resection area with the reference pointer to verify the mean distance from the margin to the tumor. The distribution of the Euclidian distances from each point to the tumor is shown in **Figure 3.8**. The tumor-margin distance for case 1 was 4.54 ± 2.80 mm (average obtained from 189 recorded points), and 6.35 ± 2.17 mm from 175 recorded points for case 2. In both cases, the values obtained are above a minimum distance of 4 mm that was preoperatively planned by the surgeons. Therefore, the navigation results showed an adequate margin.

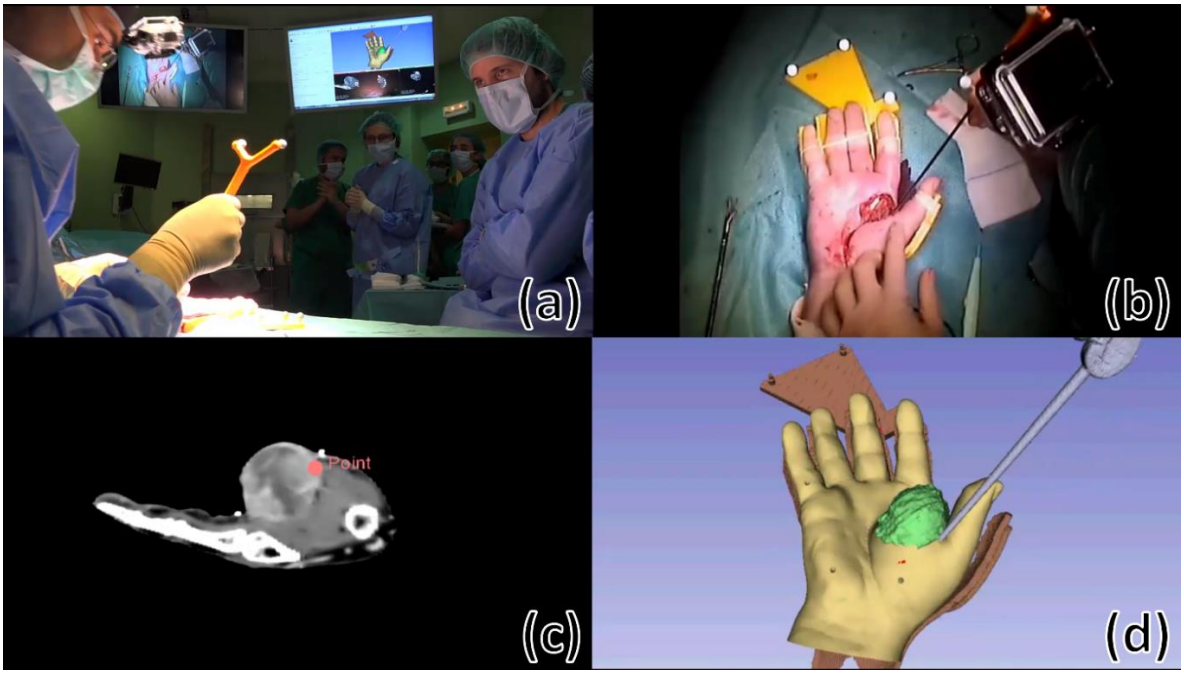

Figure 3.7. Image-guided surgery (IGS) during acral tumor resection surgery of case 1: (**a**) surgeons in the operating room (OR); (**b**) case 1 affected limb after tumor resection; (**c**) CT image; (**d**) *AcralTumorNavigation* software visualization of virtual 3D models. The red point in the CT image depicts the pointer tip. The green 3D model represents the tumor. All images are synchronized at the same moment of the surgery (**Video S1**).

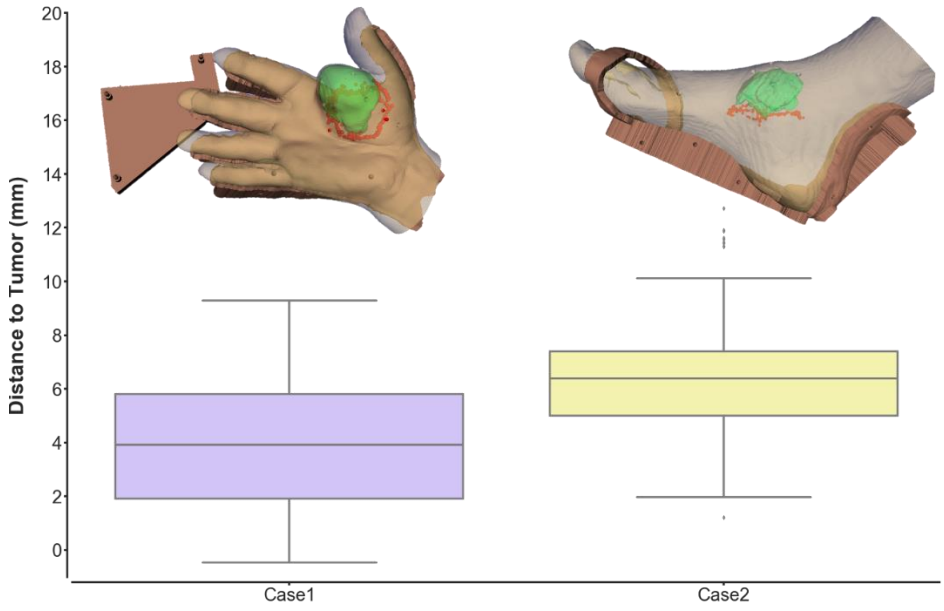

Figure 3.8. Distribution of the distances between the recorded points and the tumor for both clinical cases. Points were collected along the tumor margin during surgery. Top images represent virtual models for each case including the tumor (green) and recorded points (red).

3.5. Discussion and conclusion

Here In this study, we have presented a novel framework for acral tumor resection combining desktop 3D printing and surgical navigation. We used 3D printing technology to create a patient-specific mold that maintained the same position of the distal extremity during IGS as in the preoperative images. Furthermore, 3D printing allowed us to design a customized tracking attachment to navigate specific surgical tools. The feasibility of the suggested workflow has been evaluated on two patients with a malignant tumor in one extremity.

Patient-to-image registration is a crucial step in surgical navigation. Still, the anatomical locations of our clinical cases include a large number of joints with complex movements, hindering an accurate alignment between the patient and the images. Our research proposes a solution to this problem, but several sources of error could limit the final navigation accuracy: the 3D printed mold, the navigation system performance, and the integration of this solution in the surgical procedure.

The proposed molds are 3D printed in PLA and have to be sterilized before surgery. This process, based on EtO at 37 °C, may still deform the objects decreasing navigation accuracy. To evaluate this error, we compared the virtual 3D models obtained from CT images acquired before and after the sterilization process. The results showed that the sterilization process produced a similar error in both cases below 0.2 mm. Higher errors were found in localized points, far from the target, which will not influence the results close to the tumor during resection. We believe that these errors are caused by the limited resolution of the CT scan, which may cause small inconsistencies during the segmentation step. Nevertheless, PLA has a low glass transition temperature, limiting its use in many hospitals where low temperature sterilization is not available. For this reason, other alternative materials could be used, such as stereolithography resins. Some of these resins withstand the high temperatures from more common sterilization techniques (e.g., autoclave), and have proved lower shape deformation after sterilization [137].

Simulation of the IGS system with patient-specific 3D printed phantoms before surgery is not only valuable to facilitate preoperative planning, but it also allows the evaluation of the system accuracy before the intervention. The TRE of the whole system in these phantoms was below 1.9 mm. Our error values are higher than those reported in [131], where the authors placed an implant on a phantom using a Polaris Vicra Tracking System (Northern Digital Inc.,

ON, Canada). However, this difference is expected, since our framework includes an additional source of error arising from the positioning of the limb on the mold. Moreover, we achieved similar errors to [138], in which a multi-camera optical tracking system was also used. The errors were similar in both clinical cases, showing that the proposed methodology may be adapted to different extremity locations without altering the accuracy of the system.

Commercial IGS systems do not only lack flexibility when adapting to specific requirements of tumor surgeries, but they are also limited by the tools that can be tracked during navigation. In this study, we were able to track not only a commercial pointer but also a surgical tool (scalpel), with a lower TRE during the simulations. This might be due to differences in the tip shape and how it fits in the conical holes while performing the experiment. The scalpel has a more rounded tip that might be positioned in a more consistent way when the location of the conical holes was recorded. These results encourage us to consider creating more tracking attachments for other surgical instruments, such as different scalpel models or drills, commonly used in tumor resection surgeries.

The proposed workflow offered two different options for the image-to-patient registration during surgery. The combined design of the mold and the rigid body (RB) used for tracking allowed us to avoid the registration step in case 1. In contrast, for case 2 we had to use the conical holes to calculate the corresponding registration. This happened both during simulation and real surgery. The mold for case 2 was too large to be 3D printed in one session, so we had to separate the mold from the RB and, when both parts were combined, the result was not completely equivalent to the design. The additional time required for the registration was negligible, and our results show that errors obtained during simulation and real surgery are similar for both cases. The 3D printed mold with integrated RB allowed tracking the limb automatically, avoiding the need to repeat any registration step.

The surgical outcome was evaluated by measuring the distance from the resection margin to the pre-operative tumor. In both cases, the resulting mean distance was higher than 4 mm. This value is within the distance preoperatively planned. Additionally, the distance to the tumor feature from the navigation system gave real-time information on the position of the reference pointer tip with respect to the tumor, allowing surgeons to verify the adequate margin during the resection task.

There are several limitations in our workflow. We did not consider tissue deformation during surgery, or any change in tumor size from the acquisition of preoperative images due to

tumor reduction or inflammation. This limitation is found in any navigation system based on preoperative images. Surgeons must take into account this source of error during the procedure. Despite that, their feedback from this proposal is positive, suggesting that our solution could be beneficial in acral tumor resections, although further evaluation is needed due to our limited sample size.

In conclusion, we have shown that the combination of open-source navigation software and desktop 3D printing provides an interesting solution for surgical navigation in oncological orthopedic surgery. The simulation with 3D printed limbs and its application in two clinical cases have demonstrated the viability of the suggested framework in acral locations. This solution could be adapted to specific patients or more complex anatomical locations such as spine or pelvic girdle. In those cases, a surgical guide could be designed to fit on the patient's bone and include a tracking RB, allowing automatic registration between the surgical navigation system and the patient.

Supplementary Materials: The following are available online at https://zenodo.org/record/4313267#.X9Eq9GhKguV, **Video S1**: Surgical video recordings of the clinical case 1, **Video S2**: Surgical video recordings of the clinical case 2. **3D Model S1**: 3D model of the mold design from the clinical case 1 in STL format, **3D Model S2**: 3D model of the clinical case 1 limb in STL format, **3D Model S3**: 3D model of the mold design from the clinical case 2 in STL format, **3D Model S4**: 3D model of the clinical case 2 limb in STL format.

The content of this chapter has been published in Applied Sciences journal as part of the special issue "Computer-aided Biomedical Imaging 2020: Advances and Prospects":

R. Moreta-Martinez, J. A. Calvo-Haro, R. Pérez-Mañanes, M. García-Sevilla, L. Mediavilla-Santos, J. Pascau. "Desktop 3D Printing: Key for Surgical Navigation in Acral Tumors?". Applied Sciences, vol. 10, no. 24, p. 8984, Dec. 2020.

4

AR in Orthopedic Oncology based on a 3D Printed Reference

4.1. Introduction

Augmented Reality (AR) is a powerful tool in the medical field, where it gives the opportunity to offer more patient information to the physician by including relevant clinical data in the sight between him and the patient. This medical information can be obtained from imaging studies of the patient (e.g., computed tomography [CT], magnetic resonance [MR], positron emission tomography [PET]) that can be displayed overlaid on the physical world, enabling user interaction and manipulation. During the past two decades, AR has facilitated medical training or surgical planning and guidance. A powerful application of AR in tumor resection surgery is the visualization of a 3D model of the segmented tumor over the patient [139], providing relevant information to the surgeon about location and orientation. AR has also been evaluated in training applications [140][141], where novel physicians were able to improve their skills in terms of spatial vision and surgical ability. All these examples, while showing the possibilities of AR in different medical scenarios, have some limitations in terms of portability, calibration and tracking [142]. Recent technological developments could overcome some of these restrictions. Devices such Microsoft HoloLens, a compelling head

mounted display, or new software development kits (SDKs) such ARToolKit [143] for mobile devices, will facilitate cheaper and simpler to set-up AR systems spreading their use.

One of the main difficulties for introducing AR in surgical guidance procedures is registering augmented data to the real-world space [106]. Up to now, patient registration has been achieved with optical or electromagnetic tracking systems [109][108], applying manual alignment [107] or more advanced algorithms such as speed up robust feature (SURF) [144]. These are solutions that seem to work in some specific applications, but require extra hardware, add complexity to the workflow, increase procedure time and may not be accurate enough.

Previous research in integrating desktop 3D printing with surgical guidance could solve some of the identified limitations of AR in surgical applications. Patient specific designs, created from CT or MR studies and then 3D printed in-hospital, have already shown their advantages in orthopedic surgery in scenarios such as open-wedge high tibial osteotomy [145] or femoral varization osteotomy [146]. These guides are designed to fit precisely in a planned position on the patient. The combination of these surgical guides with a 3D printed AR tracking pattern would avoid the registration problems previously identified.

Recent studies have shown applications of this approach in maxillofacial surgery, attaching a tracking marker to a specifically designed tool that fits in the mandibula of the patient enabling AR registration [147]. Even though this technique showed good accuracy, the attachment of the tracking marker and the occlusal splint was manual, requiring a surface scan for registration, which includes a complex step in the workflow.

4.2. Objective

To overcome the previous limitations, we propose an AR approach that uses a desktop 3D printer to create patient-specific tools with a tracking marker attached, enabling automatic registration between AR and real-world spaces. This patient-specific tool fits on the patient only in the place it was designed for. The clinical data to be included in the AR scene is previously referenced to the tracking marker and can be easily visualized. This solution was developed as an AR application on Microsoft HoloLens. Accuracy and user experience were evaluated on a patient-based phantom replicating an extraosseous Ewing's sarcoma (EES) of the distal leg scheduled for tumor resection surgery. In addition, the AR approach was tested by the surgeons during the actual surgical intervention.

4.3. Materials and methods

The AR solution we present includes two main components: an AR application developed for Microsoft HoloLens and a 3D printed patient-specific tracking marker. The accuracy evaluation of the proposed system was performed on a 3D printed phantom replicating a real clinical case: a patient with an EES of the distal leg. Our institution has previous clinical experience 3D printing surgical guides to facilitate the resection of this kind of sarcomas [146]. The addition of relevant clinical data, such as the visualization of the tumor to resect, over the patient during surgery was achieved adding the tracking marker to this surgical guide.

For this specific clinical case, the 3D printed phantom included the tumor and surrounding anatomical structures (tibia and fibula). The solution for registration fits perfectly into this case; first, because the tracking marker is added to a surgical guide that was already used for this surgery; second, the modification of the guide does not interfere with the surgical working area; and last, the surgical guide is positioned on a rigid structure, the tibial bone, which means that its position could be replicated during surgery. The accuracy of this placement was also validated on the 3D printed phantom

4.3.1. AR application

The AR software application was developed on Unity version 2017.4 LTS using C#. The detection of the tracking marker was performed using Vuforia [148], a pattern recognition SDK. Vuforia includes a recognition algorithm implemented for HoloLens which provides the 3D position of a tracking marker with respect to HoloLens spatial mapping coordinate space. This algorithm enables the developed AR application to display custom 3D models with respect to the tracking marker in the HoloLens virtual environment.

The AR application (**Figure 4.1**) has the following functionalities to facilitate tumor resection surgery:

- *3D Model Visualization*: Visualization of different anatomical 3D models representing anatomy of the patient. A virtual canvas allows the user to select which models to visualize. Anatomical models used in this clinical case included skin, bone and tumor.
- *Preoperative Imaging Visualization*: A virtual canvas allows the user to select the slice and the axis (axial, sagittal or coronal) to be augmented. The images are obtained from

any 3D modality (CT in this case) and are displayed in their actual position with respect to the patient.

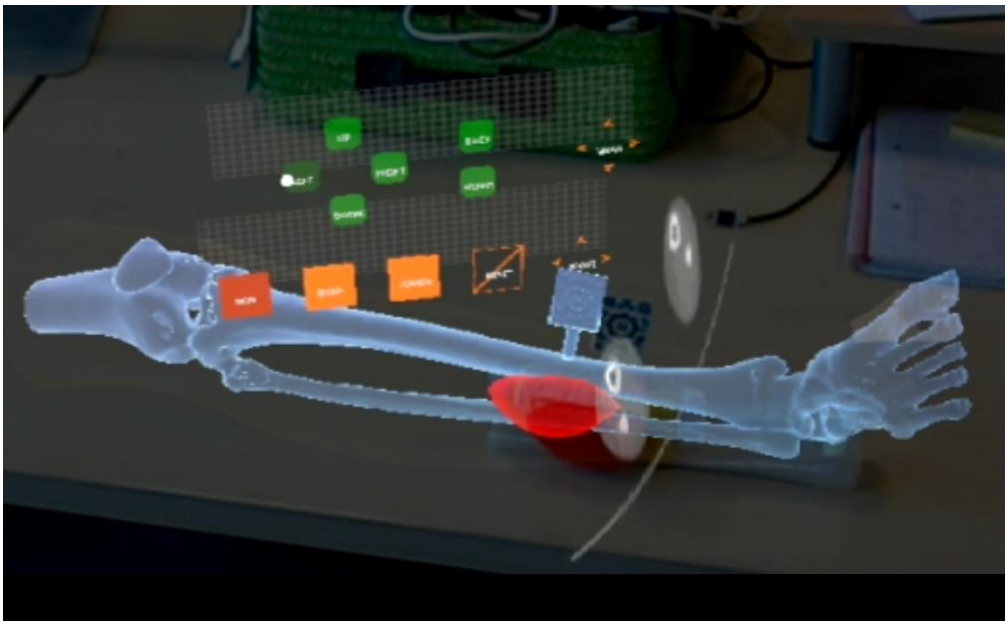

Figure 4.1. Anatomical 3D models and axial CT slice display on HoloLens application.

4.3.2. Workflow

The proposed workflow is based on the actual clinical procedure, minimizing the additional steps to limit the interference with their actual work.

Augmented reality images

The augmented reality images are based on preoperative imaging studies (CT, MR, PET) acquired from the patient. 3D Slicer platform was used to rigidly register the studies and to obtain segmentations and anatomical 3D models (polygonal meshes) from the skin, distal leg bone and sarcoma. These models were used for visualization, phantom 3D printing and to design the surgical guide.

Surgical guide design

Based on the generated 3D models of the bone tissue and tumor, a surgical guide was designed to be attached to the tibia close to the location of the sarcoma. The following aspects were considered in the design: section of the bone exposed during surgery, bone surface

features to obtain a reproducible placement and surgical working area. Meshmixer version 3.4 (Autodesk, Inc., USA) software was used for surgical guide design.

Tracking marker design

The tracking marker was designed using Autodesk Inventor 2017 (Autodesk, Inc., USA) following the instructions provided in Vuforia website [148] to obtain accurate tracking results. The marker was then virtually merged to the surgical guide using the same software.

3D printing

Models were 3D printed with polylactic acid (PLA) on a dual extrusion Ultimaker 3 Extended (Ultimaker B.V., Netherlands) desktop 3D printer. Two sets of 3D models were printed: one for validation purposes (including conical holes in the design) and other for surgical use. Each set of 3D models included a phantom (section of the tibia, section of the fibula and sarcoma) and a surgical guide containing the tracking marker (**Figure 4.2**). Furthermore, the physicians used the 3D printed phantom to inform the patient about the intervention and to assist in surgical planning by presenting the location and size of the tumor.

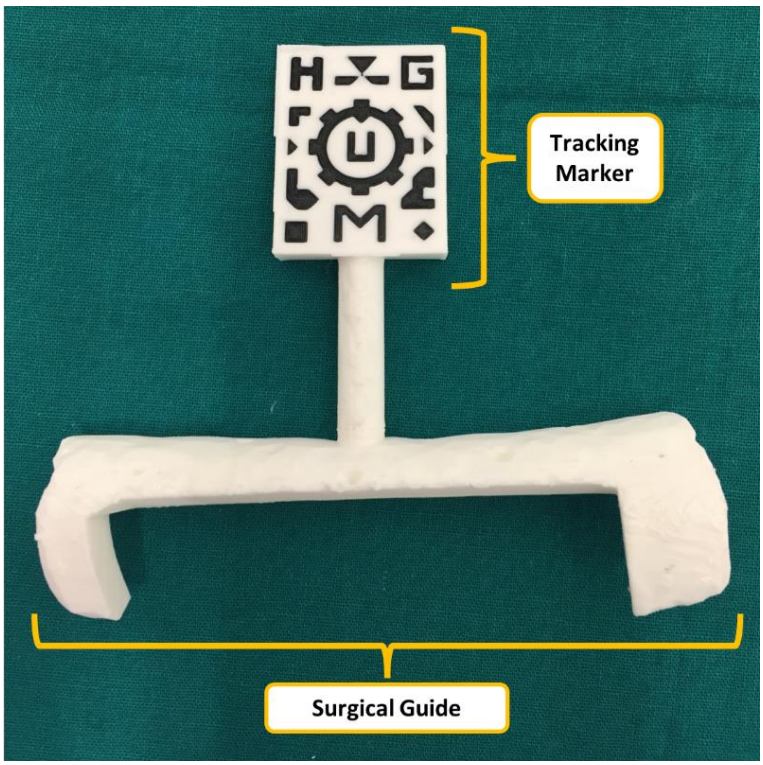

Figure 4.2. Surgical guide containing visual marker.

Prior to surgery, PLA must be sterilized to maintain asepsis of the surgical field by a sterilization technique based on ethylene oxide (EtO) at 37º to avoid deformation (the glass transition temperature of PLA is around 55 - 65 °C) and extensive degassing to remove residual EtO [149].

4.3.3. Validation

The surgical guide placement error and the AR point localization error were evaluated. A set of phantom and surgical guide 3D printed models was used. These models contain 20 and 6 conical holes, respectively. Conical holes were used as reference points for registration and error measurement. An optical tracking system [Polaris, (Northern Digital, Inc., Canada)] was used as a gold-standard for the positioning measurements. A reference pointer with optical markers was used for point recording.

In addition, a qualitative assessment of the workflow and the functionality were performed during the use of the AR application in surgery by expert clinicians.

Surgical guide placement error

The assessment of the surgical guide placement accuracy was performed by attaching the surgical guide to the phantom and recording the position of the 6 conical holes with the optical tracking system. This process was repeated three times by removing and placing back again the guide on the phantom. The required point-based registration was computed using the conical holes included in the validation phantom.

AR point localization error

To validate the AR visualization, a simulation of the surgery was performed using the HoloLens application. First, the surgical guide was positioned on the phantom and the tracking pattern was used to register the AR scene. Afterwards, 15 randomly distributed spherical models (3 mm diameter) were augmented on the surface of 3D phantom model. The tip of the reference pointer was positioned on every projected spherical model, using just the augmented data as reference, and the position of the tip (provided by the optical tracking system) was recorded (**Figure 4.3**). The Euclidian distance between this recorded position and actual location was measured to quantify the AR tracking error. This experiment was performed by three different users and each user repeated the steps three times.

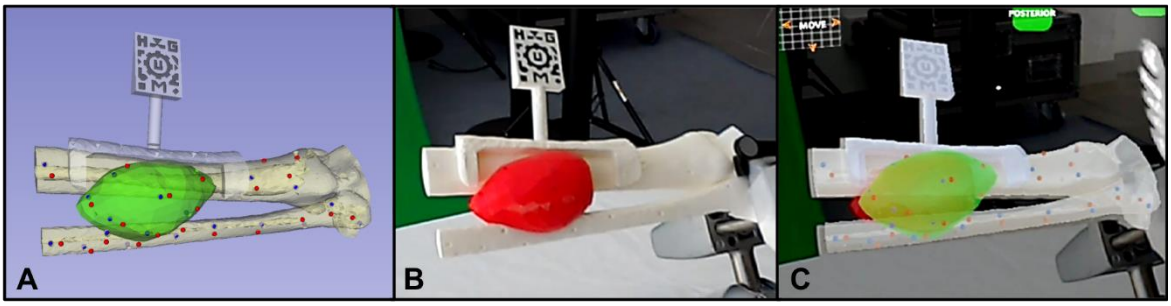

Figure 4.3. Point recording on phantom. (**A**) Virtual view, (**B**) real view and (**C**) AR view.

AR at the operating room

Once the AR application was tested and validated on the 3D printed phantom, the workflow was evaluated in the surgical intervention of the patient. Surgeons used HoloLens device and a sterilized patient-specific surgical guide (**Figure 4.2**) in the operating room. The developed AR application projected the preoperative images and 3D models of the tumor and bone on the patient for surgical guidance.

4.4. Results and discussion

The detection of the tracking marker (dual-color 3D printed pattern on the surgical guide) by Vuforia SDK was feasible and almost immediate. One of the limitations for the pattern detection was the required proximity, around 20 cm, to be correctly identified. Nevertheless, once the marker is detected an optimal visualization is achieved at longer distances, since the marker detection is required only once at the beginning of the navigation process. The dependence of this process with light conditions was not evaluated. However, the OR scenario presented very intense and focused light sources that did not hinder this step of the workflow.

The accuracy results for the repeated placement of the surgical guide on the 3D printed phantom are displayed on **Figure 4.4**: the average placement root-mean squared error (RMSE) across all three repetitions was 1.87 mm. Several factors other than the surgical guide placement contribute to this error: 3D printing accuracy of the models (phantom and surgical guide), conical holes localization error using the tracked tool and intrinsic error from the optical tracker.

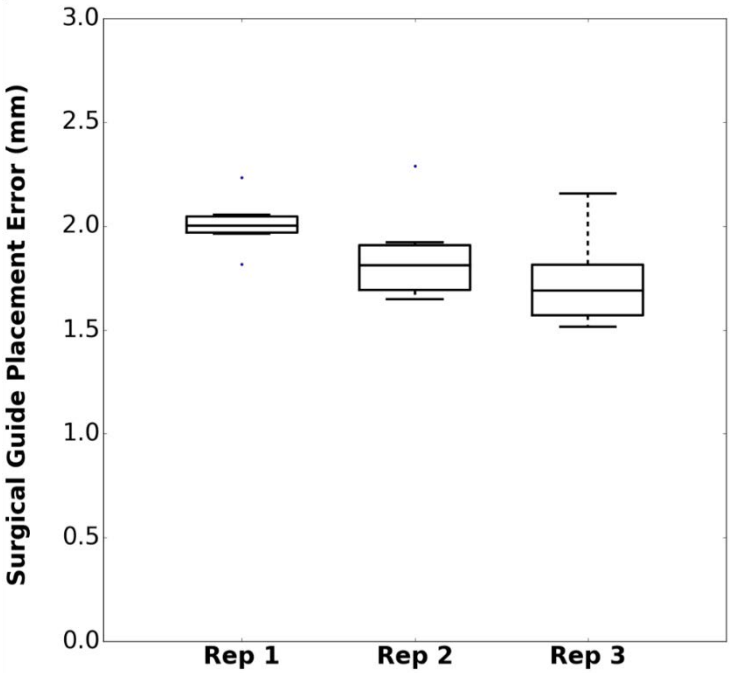

Figure 4.4. Surgical guide placement error for three repetitions.

Regarding the AR visualization error with HoloLens, the average RMSE for all users and repetitions on the 15 points distributed along the surface of the phantom was 2.90 mm (**Figure 4.5**). This result is mainly influenced by the pointer tip positioning with respect to the holograms due to the depth perception, the size of the projected spheres in the AR environment and the positioning of the surgical guide. All error sources described for the surgical guide placement evaluation have also influence in this value. Nevertheless, the system is considered sufficiently accurate for many AR applications in the OR.

Once the feasibility and accuracy of the proposed workflow were demonstrated, the developed software application was tested by several physicians with extensive experience in surgical navigation and AR on the phantom, receiving positive feedback. The registration methods based on the positioning of the surgical guide presented an optimal accuracy and did not interfere with the usual surgical workflow. The limitation regarding the required proximity for marker detection could be overcome, so physicians believed that the application was ready to be used in a real clinical case.

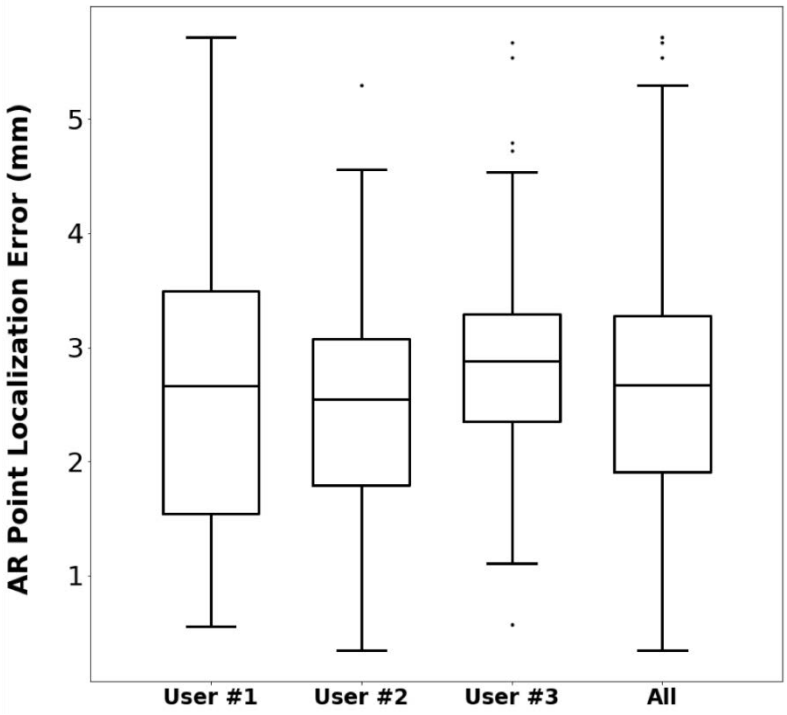

Figure 4.5. AR point localization error for three users.

Finally, an expert surgeon evaluated the complete workflow during surgery. HoloLens device was attached and fixed prior to the sterilization procedure. Once the area was cleared and the tumor was visible, the surgeon placed the guide on the bone (**Figure 4.6**). The surgical guide was easily placed and fitted as planned in the desired area. A second surgeon manually held the guide until it was detected by the HoloLens application, and then it was removed from the scene since it was not necessary during the navigation step. No quantitative error measurements were obtained during surgery, although according to the surgeons experience the alignment between the augmented data and the actual anatomy was accurate.

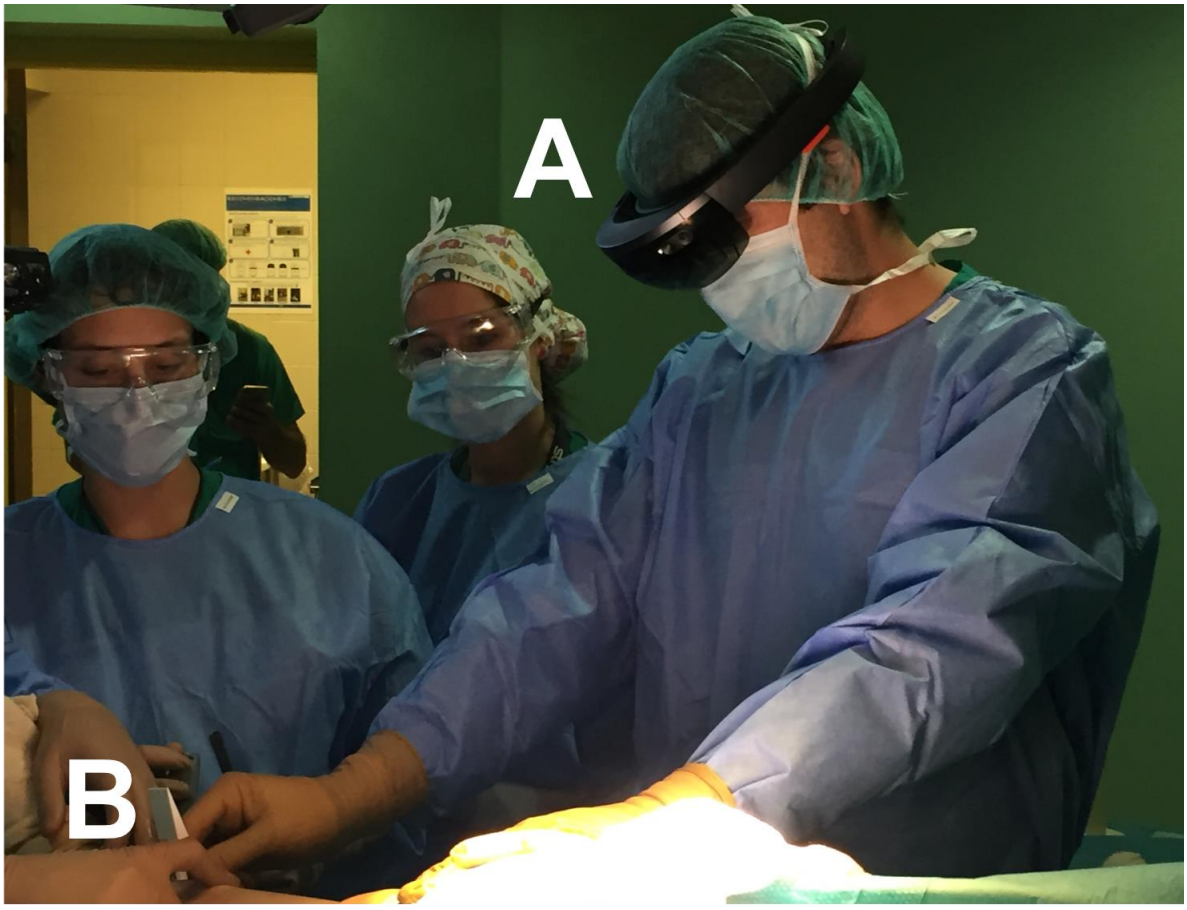

Figure 4.6. Surgeon placing surgical guide in patient's tibia. (**A**) HoloLens and (**B**) surgical guide.

4.5. Conclusion and future work

AR can be an interesting technology for clinical scenarios as an alternative to surgical navigation. However, the registration between augmented data and real-world spaces is a limiting factor. In this work, we propose a method based on desktop 3D printing to create patient specific tools containing a visual pattern that enables automatic registration. This custom guide fits in a unique region in the bone surface, avoiding placement errors. This solution has been developed in a software application running on Microsoft HoloLens. The workflow was first validated on a 3D printed phantom replicating the anatomy of an Ewing's sarcoma patient, and then on the actual surgery of this clinical case. The application allowed physicians to visualize skin, bone and tumor location overlaid on the phantom. This workflow can be applied in cases where hard body structures such as bones are involved, so it could be extended to many clinical applications in the surgical field and also for training and simulation.

Although we have tested our workflow on wearable AR devices, we believe that a similar approach can be applied to other devices such as tablets or smartphones.

The evaluation results show that the surgical guide that includes the tracking pattern can be placed precisely onto the reference bone anatomy, with accuracy of approximately 2 mm. The addition of the AR component results in an overall localization error of around 3 mm, which can be considered accurate considering that tracking information is obtained from the HoloLens RGB camera. Moreover, the clinical experience during surgery demonstrated the feasibility of the proposed workflow for AR guidance during surgical interventions.

The main advantages of our proposal are the simplicity, the easy interaction with the AR environment and the accurate registration using patient-specific 3D printed tools. No objective evaluation was performed regarding the added value provided by the AR guidance on the surgical scenario. However, we think that the results from this work will encourage the development of simple and efficient AR systems for educational, simulation and guidance purposes on the medical field.

The content of this chapter was presented at the 21st International Conference on Medical Image Computing & Computer Assisted Intervention (MICCAI) 2018, and published in the journal Healthcare Technology Letters:

R. Moreta-Martinez, D. García-Mato, M. García-Sevilla, R. Pérez-Mañanes, J. A. Calvo-Haro, J. Pascau. "Augmented reality in computer-assisted interventions based on patient-specific 3D printed reference". Healthc. Technol. Lett., vol. 5, no. 5, pp. 162–166, 2018.

5

Protocol to Combine AR and 3D Printing for Medical Applications

5.1. Introduction

Augmented reality (AR) and three-dimensional (3D) printing are technologies that provide increasing numbers of applications in the medical field. In the case of AR, the interaction with virtual 3D models and the real environment benefits physicians in education and training [41], [140], [141], multidisciplinary communication [150], and guidance during clinical interventions [45], [46], [48], [107], [151], [152]. Likewise, 3D printing has become a powerful solution for developing patient-specific customizable tools [145], [146], [153] or 3D anatomical models, which can improve preoperative planning and clinical interventions [154], [155].

Both AR and 3D printing improve orientation, guidance, and spatial skills in medical procedures; thus, their combination is the next logical step. Previous work has shown that their joint use can increase value in patient education [114], facilitating explanations of medical conditions and proposed treatment, optimizing surgical workflow [115], [116], and improving patient-to-model registration [156]. Although these technologies have grown exponentially in recent years, their adoption by physicians is still limited since they require extensive engineering knowledge and software development.

Furthermore, in previous works, AR patient-to-image registration has been calculated manually [107], with surface recognition algorithms [152] or has been unavailable [41]. These methods have been considered somewhat limited when an accurate registration is required [156]. We propose more accurate and straightforward patient-to-image registration methods by combining AR technology and 3D printing to overcome these limitations.

5.2. Objective

The purpose of this work is to describe a step-by-step methodology that enables the use of AR and 3D printing by inexperienced users without broad technical knowledge. The proposed protocol describes how to develop an AR smartphone app that allows superimposing any patient-based 3D model onto a real-world environment using a 3D printed marker tracked by the smartphone camera. In addition, we describe an alternative approach for automatic registration between a 3D printed biomodel (i.e., a 3D model created from a patient's anatomy) and the projected holograms. The described protocol is entirely based on free and multi-platform software. Moreover, the solution is generic and can be applied to any medical imaging modality or patient. To illustrate the methodology, we present a real clinical case of a patient suffering from distal leg sarcoma.

5.3. Protocol

This section briefly explains each step of the protocol, the material provided and some visual examples of the results. The complete step-by-step methodology is available in video and written format at the Journal Of Visualized Experiments website [157].

This study was performed in accordance with the principles of the 1964 Declaration of Helsinki as revised in 2013. The anonymized patient data and pictures included in this paper are used after written informed consent was obtained from the participant and/or their legal representative, in which he/she approved the use of this data for dissemination activities including scientific publications.

5.3.1. Materials

A computer with Microsoft Windows 10 or Mac OS as operating system is needed to complete the protocol with the following software installed: 3D Slicer (v 4.10.2), Meshmixer

(v3.5), Unity (v. 2019) and Xcode (last version) for iOS deployment. All software tools necessary for completing the protocol can be freely downloaded for personal purposes.

Our institution has uploaded a freely available repository in GitHub platform (GitHub Inc., San Francisco, CA, USA), found at https://github.com/BIIG-UC3M/OpenARHealth, containing the following material needed to complete the protocol, including a clinical case of a patient suffering from distal leg sarcoma that is used as an example to illustrate the methodology:

- A CT scan of a patient suffering from distal leg sarcoma.
- 3D biomodels of the patient (bone and tumor).
- 3D Slicer module *ARHealth: Model Position* for positioning 3D models with respect to the 3D printed marker.
- Markers that can be 3D printed, which will be detected by the AR application to position the virtual 3D models. There are two markers available.

Moreover, the user needs a 3D printer (with a single or dual extruder), 3D printing material (Polylactic acid, PLA; acrylonitrile butadiene styrene, ABS) and a smartphone (either Android or iOS devices) to complete the augmented reality application guide.

5.3.2. Protocol description

The protocol consists of a total of six sections, which are represented in **Figure 5.1**. The diagram shows the results at each step using the clinical case as reference example.

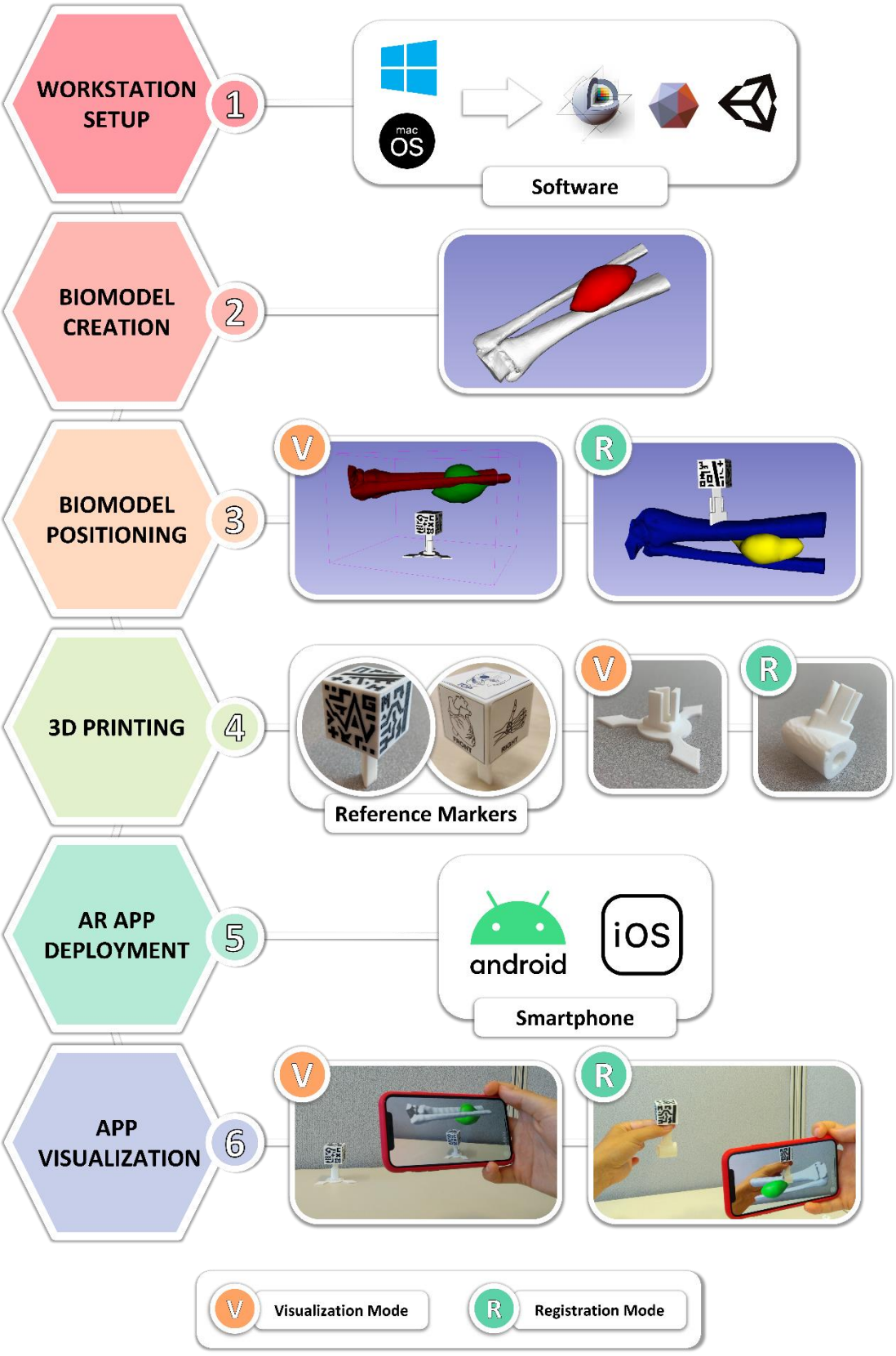

Figure 5.1. Proposed step-by-step protocol to develop a medical augmented reality smartphone application with the assistance of 3D printing technology.

The protocol starts with section 1, describing the workstation set-up and necessary software tools. Section 2 describes how to use 3D Slicer software to easily segment target anatomies of the patient from any medical imaging modality, obtaining the 3D models. This step is crucial, as those are the virtual 3D models displayed in the final AR application.

In section 3, 3D Slicer is used to register the 3D models created in the previous section with an AR marker. During this registration procedure, patient 3D models are efficiently and simply positioned with respect to the AR marker. The position defined in this section will determine the hologram relative position in the final app. This solution reduces complexity and multiplies the possible applications. Section 3 describes two options for defining the spatial relationships between the models and AR markers: *Visualization* and *Registration* mode. The first option, *Visualization* mode, allows the 3D models to be positioned anywhere with respect to the marker and displayed as the whole biomodel. This mode provides a realistic, 3D perspective of the patient's anatomy and allows moving and rotating of the biomodels by moving the tracked AR marker. The second option, *Registration* mode, allows attachting a marker adaptor on any part of the biomodel, offering an automatic registration procedure. With this option, a small section of the 3D model, including the marker adaptor, can be 3D printed, and the app can display the rest of the model as a hologram.

Section 4 provides guidelines for the 3D printing process. First, the user can choose between two different markers: the "dual color marker" and "sticker marker". The whole "dual color marker" can be 3D printed but requires a dual extruder 3D printer. In case this printer is not available, the "sticker marker" is proposed. This is a simpler marker that can be obtained by 3D-printing the cubic structure, then pasting the images of the cube with sticker paper or sticker glue. Furthermore, both markers were designed with extensible sections to perfectly fit in a specific adaptor. Thus, the marker can be reused in several cases.

Section 5 describes the process to create a Unity project for AR using the Vuforia software development kit. This step may be the most challenging portion for users with no programming experience. Still, with these guidelines, it should be easy to obtain the final application that is presented in section 6. The app displays the patient's virtual models over the smartphone screen when the camera recognizes the 3D printed marker. In order for the app to detect the 3D marker, a minimum distance of approximately 40 cm or less from the phone to marker, as well as good lighting conditions, are required.

5.4. Application examples

The proposed protocol has been designed to apply AR and 3D printing technology in any clinical scenario. In this section, we want to show what anyone can achieve following the guide by giving multiple application examples in different medical procedures. Four different cases are presented in **Figure 5.2**, showing screenshots of the final AR application.

In the first case, we have developed a smartphone application for a neurological surgery demonstration. The AR application shows on the display virtual models of the skull (white), brain (light orange) and tumor (red) on top of a commercial skull phantom (**Figure 5.2**A). To register the virtual models with the phantom, the cubic marker was positioned on a 3D printed guide that was designed to fit on a unique position on top of the nasal bone. The goal of this AR app is to practice the correct surgical approach.

The following example was implemented in the same clinical case provided in the protocol. This time, the patient's phantom was 3D printed in two colors, representing the tibia and fibula bones in white and the tumor after radiation therapy in red. The main objective of the designed application was to compare the reduction of the tumor before (blue virtual model with some transparency) and after radiotherapy (3D printed in red) (**Figure 5.2**B). The marker was registered with the phantom using a surgical guide that was explicitly designed for the intervention of the same clinical case.

Maxillofacial surgery is another discipline where AR and 3D printing can provide great value. **Figure 5.2**C represents the visualization of the AR application by superimposing the preoperative planning virtually, in this case the tumor and its safety margin in blue, on top of a phantom based on data from a patient suffering from a carcinoma on the palate. AR offers an enriched perspective of the location of the tumor before surgery.

In the last case, we designed an app for orthopedic surgery to visualize pre-defined osteotomy planes and the remaining affected area in a patient suffering from a pelvis sarcoma. The cutting planes are represented in orange, green and blue virtual models, and the remaining pelvis is visualized in white (**Figure 5.2**D). It is worth mentioning that combining both technologies, AR and 3D printing, in this case, we have reduced material waste and 3D printing time by representing the whole affected area overlaid on a small 3D printed section of the pelvis.

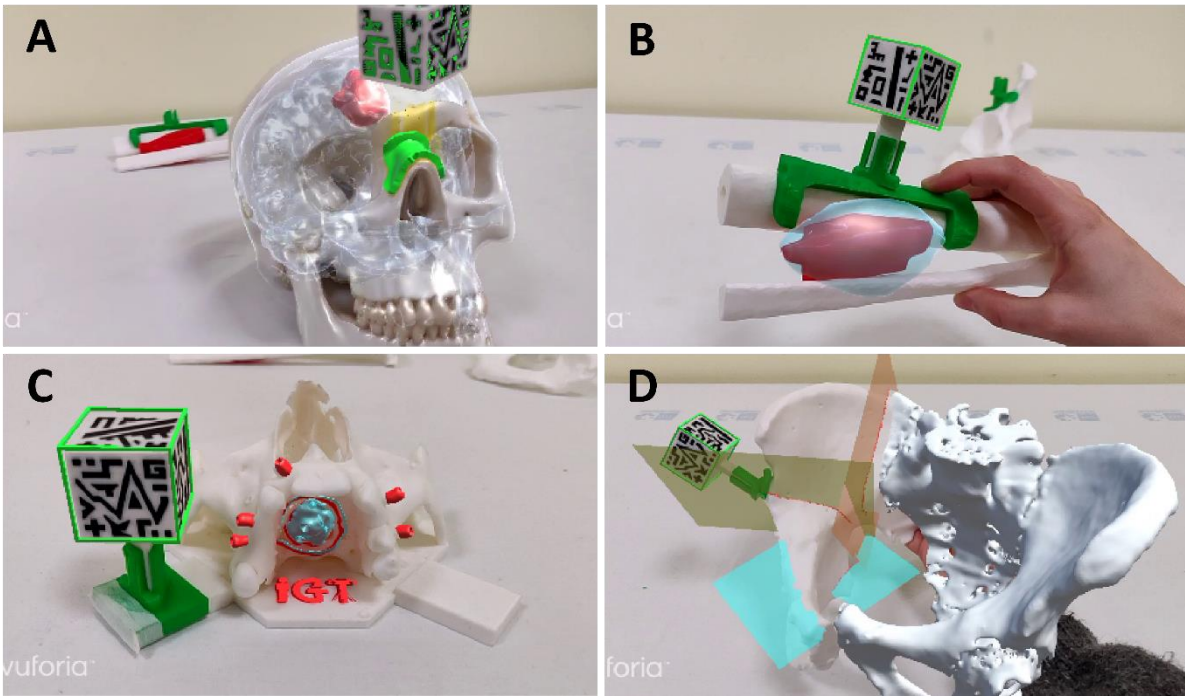

Figure 5.2. AR visualization from a smartphone application applied to four different clinical cases. (**A**) Tumor visualization on a skull phantom. (**B**) Virtual tumor visualization (blue) on top of the 3D printed phantom (bone in white, reduced tumor in red) to compare how the tumor was reduced after radiation therapy. (**C**) Virtual visualization of the tumor (blue) and pre-defined tumor margin (blue) on top of a phantom based on a patient suffering from a palate carcinoma. (**D**) Augmented reality visualization of the whole pelvis (white virtual model) and pre-defined cutting planes (blue, green and orange) on top of a small portion of a 3D printed pelvis.

5.5. Results and discussion

The final visualization of the holograms was clear and realistic, maintained the real sizes of the biomodels, and positioned them accurately. When using the smartphone application, the AR marker needs to be visible by the camera for the app to correctly display the holograms. In addition, good and constant scene illumination is required for proper marker detection. Bad light conditions or reflections on the marker surface hinder the tracking of the AR marker and cause malfunctioning of the app.

The time required to create the app depends on several factors. The duration of section 1 is limited by the download speed. Regarding anatomy segmentation (section 2), factors affecting segmentation time include complexity of the region and medical imaging modality (i.e., CT is easily segmented, while MRI is more difficult). For the representative example of the tibia, approximately 10 min were required to generate both 3D models from the CT scan.

Biomodel positioning (section 3) is simple and straightforward. Here, it took approximately 5 min to define the biomodel position with respect to the AR marker. For the 3D printing step, the duration is highly dependent on the selected mode. The "dual color marker" was manufactured at high quality in 5 h and 20 min. The "sticker marker" was manufactured in 1 h and 30 min, plus the time required to paste the stickers. The final section for app development can be time-consuming for those with no previous experience in Unity, but it can be easily completed following the protocol steps. Once the AR markers have been 3D printed, the development of an entirely new AR app can be performed in less than 1 h. This duration can be further reduced with additional experience.

AR holds great potential in education, training, and surgical guidance in the medical field, and its combination with 3D printing opens new possibilities. This protocol describes a detailed methodology that enables inexperienced users to create a smartphone app combining AR and 3D printing for the visualization of anatomical 3D models, created from medical images of any patient, with 3D printed reference markers.

One of the most interesting clinical applications of AR and 3D printing is to improve patient-to-physician communication by giving the patient a different perspective of the case, improving explanations of specific medical conditions or treatments. Another possible application includes surgical guidance for target localization, in which 3D printed patient-specific tools (with a reference AR marker attached) can be placed on rigid structures (i.e., bone) and used as a reference for navigation. This application is especially useful for orthopedic and maxillofacial surgical procedures, in which bone tissue surface is easily accessed during surgery.

One of the main expectations when designing this protocol was that this method might accelerate the adoption of AR by medical professionals, since it does not require broad knowledge of medical imaging or software development, does not depend on complex hardware and expensive software, and can be implemented on a short time. On the journal website (**Figure 5.3**), we can see that the video has reached more than 10.000 views between January 2nd of 2020 and October 6th of 2021 (in less than two years). Moreover, up to the day this thesis was submitted, several journal articles have presented solutions combining AR and 3D printing in several disciplines citing our work. This shows a genuine readers' interest on these technologies in the biomedical field.

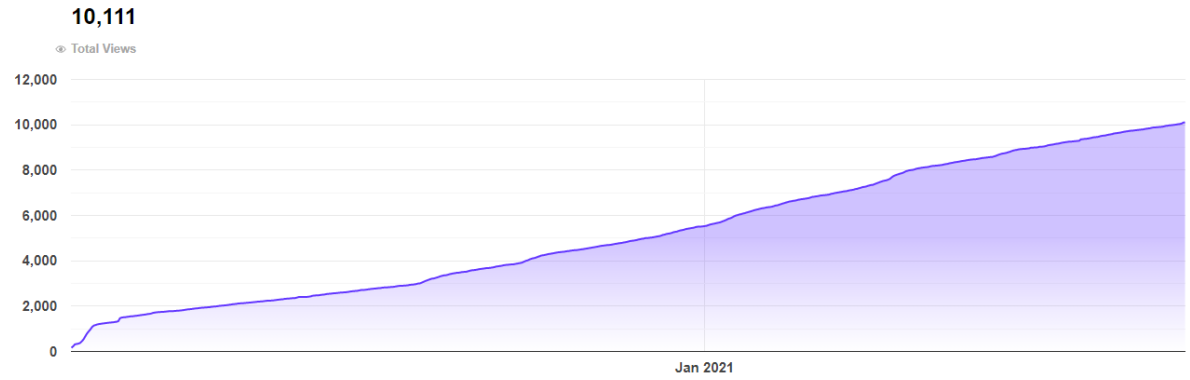

Figure 5.3. Cumulative page views of the submitted paper on the Journal of Visualized Experiments in video and written format [157].

To conclude, we believe that medical AR applications will keep growing thanks to new technological advances, as the one proposed in this work. Our solution brings AR solutions closer to the final clinical user, combining free and open-source software with an open access protocol. This way we expect to contribute to the paradigm shift that AR and 3D printing represent for the medical community.

The content of this chapter has been published in the Journal of Visualized Experiments (JoVE):

R. Moreta-Martinez, D. García-Mato, M. García-Sevilla, R. Pérez-Mañanes, J. A. Calvo-Haro, J. Pascau. "Combining Augmented Reality and 3D Printing to Display Patient Models on a Smartphone". J. Vis. Exp (155), e60618 (2020).

6

Improving Surgical Workflows with AR

6.1. Introduction

Orthopedic oncology involves the treatment of patients diagnosed with tumors in bone and soft tissues, including bone metastases, sarcomas, benign and cancerous tumors [158]. Even though these tumor types are uncommon and represent less than 1% of all new cancer diagnoses [159], they are considered a real challenge to clinicians as five-year survival rate is 50% [160].

The standard treatment of these tumors includes their complete surgical resection, ensuring a safety margin of healthy tissue, usually followed by external radiation therapy [161], [162]. However, the local recurrence rate is up to 27% after a marginal resection [163]. For this reason, it is essential to efficiently plan the surgical approach preoperatively to improve surgical outcome, leave enough surgical margin, and reduce the risk of local recurrence or metastasis [164]–[166]. Preoperative imaging techniques, such as computed tomography (CT) or magnetic resonance imaging, allow estimating the size and location of the tumor and other surrounding anatomical structures [167], [168]. However, this information is not always available during the intervention to better identify healthy and tumorous tissue differences. This means that the surgical procedure still depends on previous experience and subjective judgment of the surgeon to achieve complete tumor removal [169].

During the last decade, surgical navigation techniques have improved tumor resection accuracy, decreasing local occurrence, and improving surgical outcomes [38], [170]. However, navigation systems present several limitations. They require point-based patient-to-image registration with anatomical landmarks that are difficult to identify during surgery. Besides, real-time navigation information is displayed on external screens, requiring the surgeon to move his attention away from the patient.

Recent technologies, such as three-dimensional (3D) printing and augmented reality (AR), have increased their adoption in many medical areas with exciting benefits. 3D printing allows the rapid manufacturing of 3D solid objects from a digital file [171]. In the medical field, this includes patient-specific anatomical 3D biomodels useful for surgical planning and patient communication [54], [58], [115]. On the other hand, AR superimposes 3D virtual models onto physical objects in the real space, enabling the simultaneous interaction with both of them [172]. Physicians have found significant advantages when AR is applied to medical training [173], surgical navigation [112], [139], or needle insertion [151]. These two technologies could overcome the limitations identified for surgical navigation by improving surgeon's spatial perception of the anatomy and displaying relevant patient information on-site during surgical procedures.

Despite the number of medical specialties in which 3D printing and AR have been applied, there are not many publications reporting the use of these technologies in orthopedic oncology. Some studies have presented patient-specific 3D printed models of the affected bone and tumor for preoperative planning, reporting improved surgical outcomes in blood loss, operative time, and surgical incision [174], [175]. Others propose an "in-house" workflow with desktop 3D printers designing patient-specific surgical guides to delimit the tumor or the osteotomy cutting plane during the surgical intervention [176], [177]. Regardless of the clear benefit of these technologies, the 3D printing time and material required for large anatomical models limit their application [174]. On the other hand, AR-based navigation systems have been beneficial for improving the tumor's location before and during surgery, since it can be overlaid on top of the patient's anatomy when the target is difficult to identify [111], [178]. However, one limitation of AR for surgical guidance is the registration of virtual and real data. Manual alignment [107] or electromagnetic tracking systems [108] have been tested to overcome this problem, although they provide limited accuracy and may involve extra instrumentation or time [179].

The combination of 3D printing and AR could overcome these limitations and improve surgical outcomes. Previous studies have shown some initial results of this approach: Witowski et al. designed a workflow that reduced anesthetic time, morbidity and postoperative complications [116]; our group implemented an AR system that enabled automatic registration with a 3D printed patient-specific surgical guide [156]. The integration of 3D printing and AR could be useful not only during the surgical intervention, but also in all surgical workflow stages [157].

6.2. Objective

In this study, we propose a new surgical framework including both technologies through the treatment process in orthopedics oncology. First, to support surgical planning, displaying the anatomical structures in three dimensions and real size. Then, assisting during patient communication to explain the pathology and treatment approach. Finally, providing surgical guidance by projecting the tumor and other structures over the patient's anatomy. This solution has been developed as an AR-based smartphone application. It displays the patient's anatomy and the tumor's location using a 3D printed reference marker designed to fit in a unique position of the affected bone tissue, thus enabling automatic registration. To evaluate the contribution of both technologies, we tested the proposed system on six 3D printed patient-specific phantoms obtained from orthopedics tumors in a variety of anatomical locations. The solution was clinically evaluated during the whole surgical workflow in two patients, reporting physicians' and patients' perspectives using surveys.

6.3. Materials and methods

We describe the proposed orthopedics oncology surgical workflow in the following subsections. First, we present the patients involved in this study (**Section 6.3.1**). Then, **Section 6.3.2** describes the preoperative image acquisition protocol and the design and manufacturing of the different tools. Next, we explain the proposed augmented reality system (**Section 6.3.3**) and the evaluation of its performance on patient-specific 3D printed phantoms (**Section 6.3.4**). The last section shows the deployment of this technology at each stage of the surgical workflow (**Section 6.3.5**). A summary of the proposed surgical framework is presented in **Figure 6.1** in comparison with the traditional one.

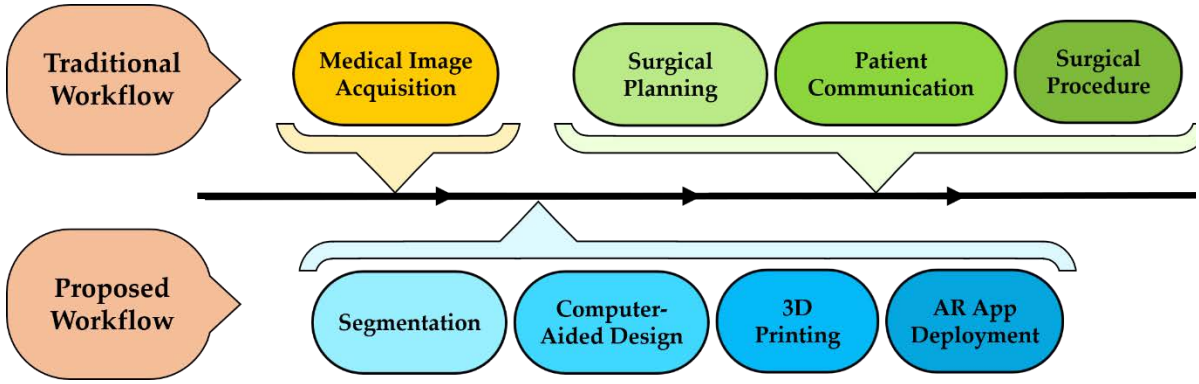

Figure 6.1. Proposed step by step orthopedics oncology medical workflow.

6.3.1. Patient selection

We evaluated our proposal on data from six patients with tumors in bone or soft tissue treated by the Department of Orthopedic Surgery and Traumatology at Hospital General Universitario Gregorio Marañón. In order to maintain the anonymity of the patients, an alphanumeric code was assigned to each of them. The selected cases included tumors on different bones and anatomical regions (thorax, femur, hip and tibia) to ensure the added value of our workflow in a wide range of orthopedic oncology procedures. **Table 6.1** summarizes the diagnosis, tumor size, and location for each patient. The study was performed in accordance with the principles of the 1975 Declaration of Helsinki as revised in 2013 and was approved by the Research Ethics Committee at Hospital General Universitario Gregorio Marañón. The anonymized patient data and pictures included in this paper are used after written informed consent was obtained from the participant and/or their legal representative, in which they approved the use of this data for dissemination activities, including scientific publications.

Table 6.1. Patient demographics involved in this study.

Case ID	Gender/Age	Diagnosis	Tumor Location	Tumor Size [cm]
AR3DP0002	M / 62	Myxofibrosarcoma	Right buttock	18 × 19 × 17
AR3DP0003	F / 71	Liposarcoma	Right periscapular region	3 × 3 × 6
AR3DP0004	M / 19	Ewing Sarcoma	Left iliac crest	13 × 19 × 16
AR3DP0005	F / 66	Fibrous dysplasia	Left femur	4 × 2 × 8
AR3DP0006	M / 79	Myxofibrosarcoma	Left thigh	10 × 15 × 12
AR3DP0007	F / 84	Undifferentiated pleomorphic sarcoma	Right calf	10 × 8 × 14

6.3.2. Image processing and model manufacturing

The proposed workflow includes steps such as medical image segmentation, computer-aided design, and 3D printing. From our experience, for each new patient, these three steps can be completed in less than 24 hours.

Medical image acquisition and segmentation

A CT scan was acquired for each patient and used as reference image for segmentation. CT pixel size and time span between image acquisition and surgery are displayed in **Table 6.2**. We segmented the tumor and the surrounding bone tissue on 3D Slicer version 4.10 [34]. An initial bone mask was obtained with intensity thresholding and further refined with the islands tool, removing components such as the clinical bed. The tumor volume mask was extracted with manual painting and erasing tools. Finally, the segmentation masks were post-processed with hole filling (kernel size 7 × 7 × 3) to optimize 3D printing quality and minimize manufacturing time.

Table 6.2. Resolution of the CT scan acquired for each patient and time span between image acquisition and surgery.

Case ID	CT Resolution [mm]	CT – Surgery Time Span [Days]
AR3DP0002	0.93 × 0.93 × 1.00	13
AR3DP0003	1.31 × 1.31 × 3.00	101
AR3DP0004	0.98 × 0.98 × 2.50	137
AR3DP0005	0.78 × 0.78 × 0.80	92
AR3DP0006	1.10 × 1.10 × 5.00	94
AR3DP0007	1.13 × 1.13 × 3.00	83

Computer-aided design

The segmentation results were exported from 3D Slicer as virtual 3D models (stereo lithography files, STL) to be processed on Meshmixer software (Autodesk Inc., San Rafael, CA, USA). We used this program to design and extract several models for each patient: surgical guides for automatic registration, small bone fragments for surgical planning, and virtual models to display on the AR system.

Surgical guides are patient-specific tools designed to fit only in one specific location of the anatomy, usually bone tissue, during surgery. They can serve as physical models that mark the tumor limits during the surgery, or as cutting guides to resect the bone following the planes

decided during surgical planning [69], [176]. To design a surgical guide, the bone area on which it was intended to fit was selected, extracted, and extruded to create the surgical guide surface as a negative of the bone surface. In such a way, it had the specific curvature of the bone, perfectly fitting in that region and ensuring its unique positioning. The surgeons considered several parameters of the intervention to define the location of the surgical guide: the expected position and orientation of the patient, the line of sight of the physicians (that has to be preserved), and the surrounding tissue. Each guide included holes (Ø 5 mm) to attach it to the bone using screws, and a holder for the AR tracking marker that will allow automatic patient-to-image registration. The registration transformation was obtained with a previously developed 3D Slicer module [157].

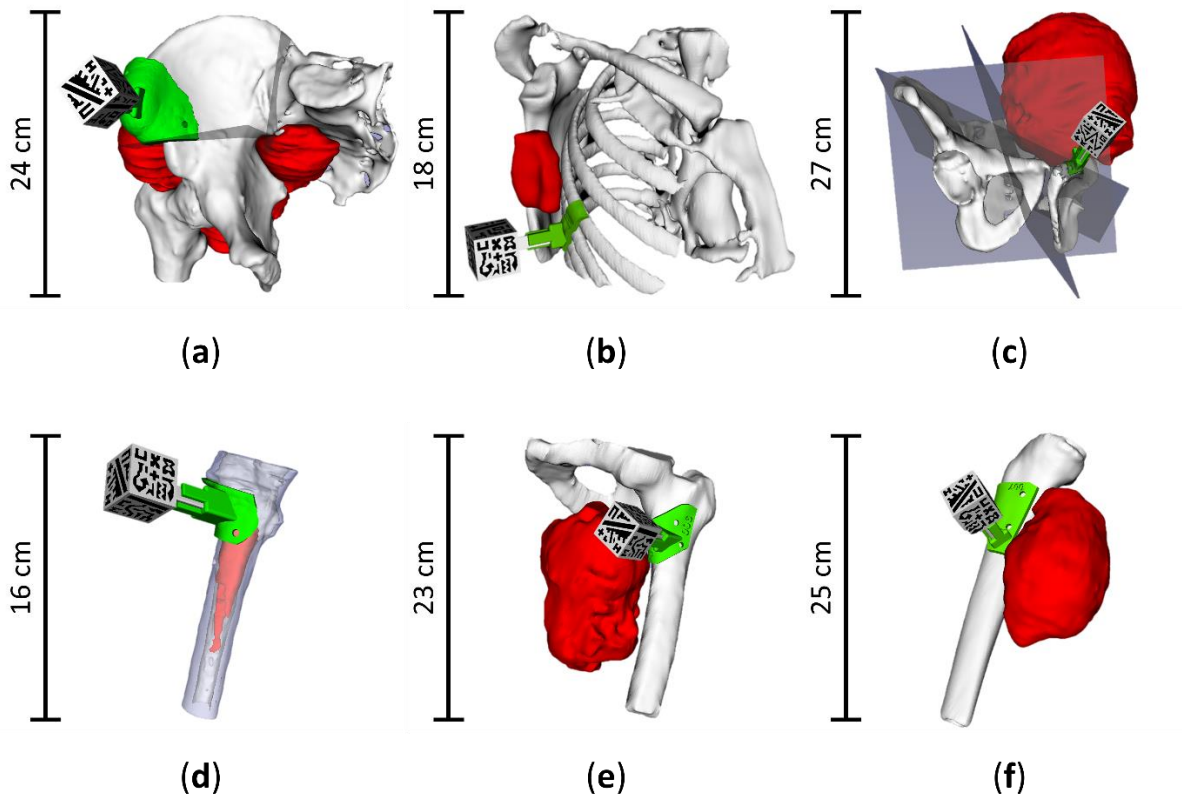

Figure 6.2. Virtual 3D models from patients: (**a**) AR3DP0002; (**b**) AR3DP0003; (**c**) AR3DP0004; (**d**) AR3DP0005, with some transparency in the bone to display the inner tumor; (**e**) AR3DP0006; (**f**) AR3DP0007. Tumors are represented in red, bones in white and surgical guides in green. Surgical cutting planes are illustrated in semi-transparent gray in the cases that required them: (**a**) and (**c**). The 3D printed marker reference is positioned in the surgical guide.

For each case, we also extracted several bone fragments, smaller than the segmented bone structure, corresponding to the area of the bone in which the surgical guide was intended to fit. They were used to practice with the positioning of the surgical guide before and during

the intervention. Finally, other models, such as cutting planes, were designed when required by the surgeons. **Figure 6.2** shows the complete 3D models of the six patients included in this study with bone (white), tumor (red) and the surgical guide (green) in its corresponding position. When cutting planes were defined during surgical planning, they are displayed (semi-transparent gray).

3D printing

Once the 3D models had been defined, surgical guides and bone fragments were manufactured with desktop 3D printers. These tools were printed using a different technique depending on the expected use of the models.

Surgical guides were fabricated using the stereolithography 3D printer Form 2 (Formlabs Inc., Somerville, MA, USA) with BioMed Clear V1 resin material (Formlabs Inc.). This resin is a USP class IV certified material, allowing contact inside the patient for long periods of time (more than a week) [180]. The 3D printed surgical guides were sterilized before surgery with ethylene oxide (EtO) at 55° C [132]. The pieces will not deform under these sterilization conditions, since this material withstands high temperatures without distortion [137].

Fused deposition modeling (FDM) desktop 3D printers Ultimaker 3 Extended and Ultimaker S5 (Ultimaker B.V., Utrecht, The Netherlands) were used to manufacture all the other tools in polylactic acid (PLA). Bone fragments and a copy of the surgical guide were 3D printed using different color materials. A copy of each bone fragment was sterilized using EtO at low temperature (37° C) (this sterilization has shown to avoid low deformation in PLA [181]) to be used as guidance during the surgical intervention. These tools will not be in contact with the patient.

6.3.3. Augmented reality system

The smartphone application, *ARHealth*, was developed in Unity (version 2019.3), using C# programming language, and is compatible with Android and iOS devices. The app uses Vuforia SDK (Parametric Technology Corporation Inc., Boston, MA, USA) to identify the patterns of a cubic reference marker [157] in the smartphone camera field of view (FOV) and project the virtual models overlaid onto the real-world image. These models will be correctly registered with the patient since their relative coordinates are computed and stored using a

previously developed 3D Slicer module [157], and then recovered by *ARHealth*. We designed the cubic marker ($30 \times 30 \times 30$ mm^3) to contain unique patterns in black and white on each face (**Figure 6.3**). It also included an adaptor on one face to attach it to the corresponding holder in the surgical guide. This cubic reference was 3D printed in PLA using the dual extruder 3D Printer Ultimaker 3 Extended (Ultimaker B.V.) in white and black color materials, and it was sterilized with EtO at low temperature (37° C) [181] before surgery.

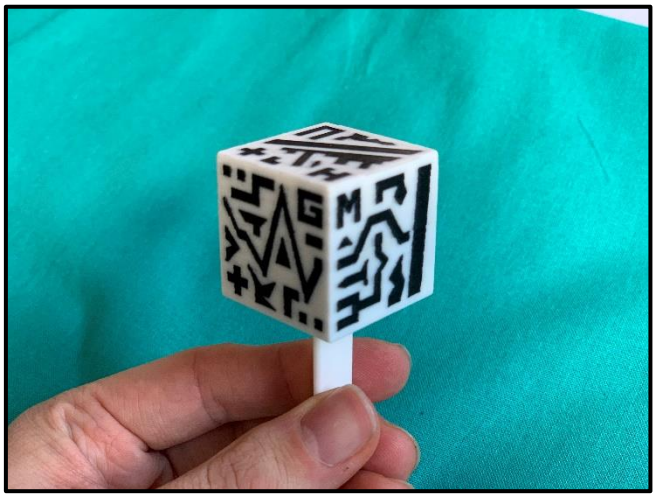

Figure 6.3. 3D printed augmented reality cubic marker used in the augmented reality system.

The smartphone application presents a main menu where the patient of interest is selected. Once chosen, it displays a second menu that offers three visualization modes: Demo, Clinic and Surgery.

- In the *Demo* mode, all the virtual 3D models are displayed around the AR marker, without any patient registration (**Figure 6.4**a). The AR marker can be rotated to show the virtual models from any point of view.
- *Clinic* mode displays the virtual 3D models in their corresponding position with respect to the surgical guide, which is registered to the cubic marker (**Figure 6.4**b). This mode is designed to be used with the surgical guide fixed on a 3D printed bone (or fragment), allowing for surgical planning and training.
- *Surgery* mode will be used during the actual surgical intervention. The surgical guide will be attached to the patient's bone, solving the registration between the patient and the AR system. The main difference with *Clinic* mode is that those models that will be essential to the surgeon, such as tumor or cutting planes, are augmented on top of the patient to guide the operation in real-time. Besides, an occlusion texture could be

assigned to the bone model within the app, covering the models behind it, providing the same visualization as if the actual bone was occluding these elements (**Figure 6.4**c).

(**a**) (**b**) (**c**)

Figure 6.4. ARHealth smartphone application. (**a**) Demo mode using patient AR3DP0005 3D models, tumor is represented in red inside the bone, which is displayed in white with transparency texture; (**b**) Virtual visualization (tumor in red, bone in white with transparency texture) overlaid on top of the 3D printed bone fragment (solid white) of patient AR3DP0007 using Clinic mode; (**c**) Surgical mode visualization of patient AR3DP0004 (tumor is represented in blue and cutting planes in semi-transparent green). A green frame surrounding the AR marker indicates that the reference is being tracked by the system.

The incorporation of a new case to the app is a simple process: once the necessary biomodels have been created, they are uploaded to the Unity project. The user interface and biomodel visualization parameters are then automatically updated. The smartphone app is then compiled and copied to our institutional smartphone. This procedure preserves data security since all patient related information is compiled in the app and cannot be exported or accessed. Besides, the app currently runs on our local smartphone devices.

6.3.4. Augmented reality system performance

The performance of the proposed augmented reality system was evaluated on six 3D printed patient-specific phantoms, corresponding to each of the patients participating in the study. They were designed by selecting a representative region of the patient's anatomy (including part of the bone and the tumor) and attaching to them some supports and bases. The supports joined parts that were not connected in the original anatomy in order to obtain a rigid phantom. The resulting models could stand over their base to maintain stability during the validation process. Eight small conical holes (Ø 4 mm × 3 mm depth) were added to the model surface for point-based registration and error measurement. Additionally, the surgical guides (that included the support for the AR marker) were also modified, adding three to five conical holes (Ø 4 mm × 3 mm depth), depending on the guide size. Those holes were used for error measurement. The phantoms dimensions are summarized in **Table 6.3**. These phantoms were 3D printed in PLA with the dual extruder FDM 3D printers in two different colors. The surgical guide specifically designed for validation was 3D printed in resin material to simulate the surgical intervention. **Figure 6.5** displays the six resulting phantoms.

Table 6.3. Size dimensions of the manufactured patient-specific 3D printed phantoms.

Case ID	Phantom Dimension [cm]
AR3DP0002	17 × 15 × 13
AR3DP0003	12 × 11 × 9
AR3DP0004	22 × 22 × 19
AR3DP0005	16 × 10 × 5
AR3DP0006	17 × 15 × 10
AR3DP0007	22 × 12 × 11

Surgical Guide Placement Error and the Augmented Reality Tracking Error were evaluated to assess the precision and accuracy of the AR system. A Polaris Spectra (Northern Digital Inc., Waterloo, ON, Canada) optical tracking system (OTS) managed by 3D Slicer was implemented as a gold-standard for the performance evaluation, following the methodology from a previous study [156]. Additionally, the distance range for marker detection of the system was also studied.

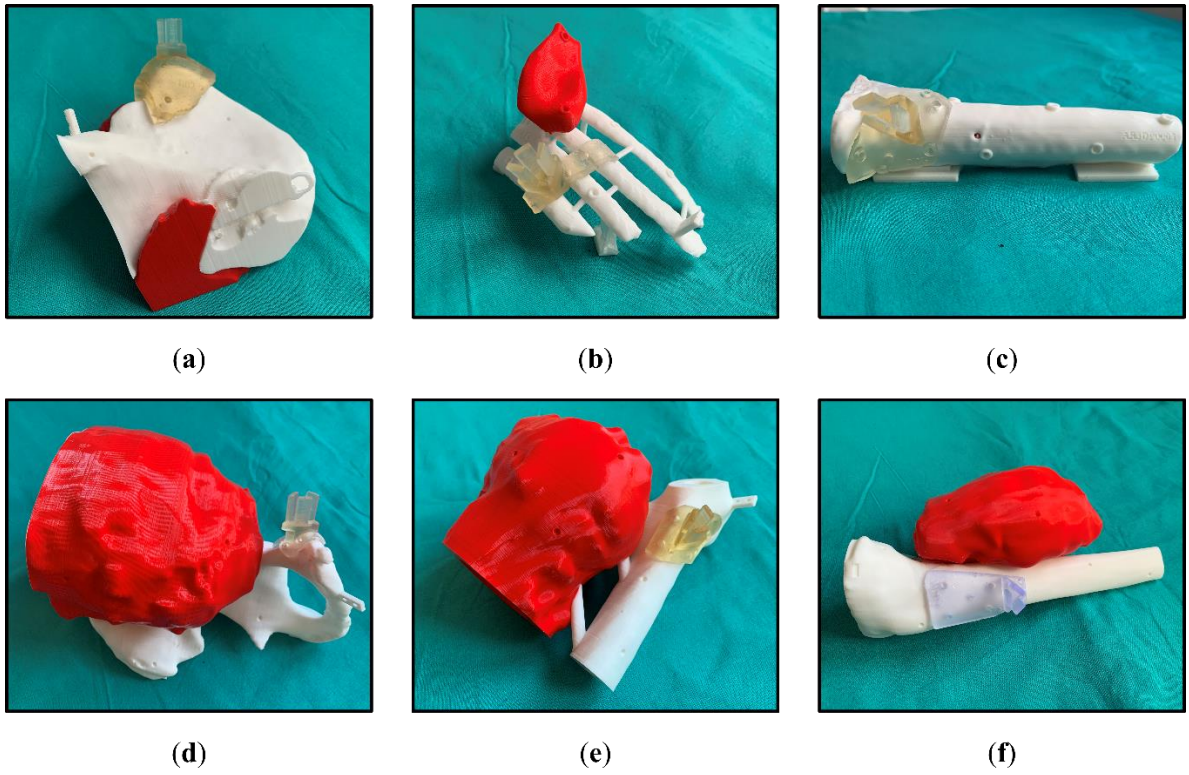

Figure 6.5. 3D printed patient-specific phantoms from patient: (**a**) AR3DP0002; (**b**) AR3DP0003; (**c**) AR3DP0004; (**d**) AR3DP0005; (**e**) AR3DP0006; (**f**) AR3DP0007. Bones are in white, the tumors are in red, and the resin surgical guides are fitted on their corresponding position.

Surgical guide positioning error

This error was analyzed to assess the uniqueness of the surgical guide positioning on the bone. We attached the surgical guide to each phantom and recorded the position of the conical holes (from 3 to 5, depending on the guide) with a pointer tracked by the OTS. The Euclidean distance between the recorded coordinates and those obtained from the virtual models allowed us to determine the Surgical Guide Placement Error. This process was repeated five times by two users, removing and placing back again the guide on each phantom. We calculated the required point-based registration [136] between the 3D printed phantom and its virtual model using conical holes included in the validation phantom.

Augmented realty tracking error

The overall AR system performance was determined using a modified version of the *ARHealth* app on a Google Pixel 4 XL smartphone (Alphabet Inc., Mountain View, CA, USA). First, the surgical guide was positioned and fixed on the phantom. Then, the AR reference

marker was placed on the surgical guide enabling automatic registration between the AR system and the phantom. Once the AR system tracked the marker, 14 virtual spheres (Ø 3 mm) were randomly augmented on the surface of the 3D printed phantom. Each user positioned the tip of a tracked pointer on the virtual spheres by looking at the smartphone screen, and that location was recorded with the OTS. The Euclidean distance between the recorded positions and true positions of the spheres was calculated to evaluate the Augmented Reality Tracking Error. Each experiment was repeated five times by two different users, removing and placing back the surgical guide. **Figure 6.6** shows the phantom of the Patient AR3DP0002 (buttock tumor) and the smartphone with the modified version of *ARHealth* displaying the augmented spheres in deep blue.

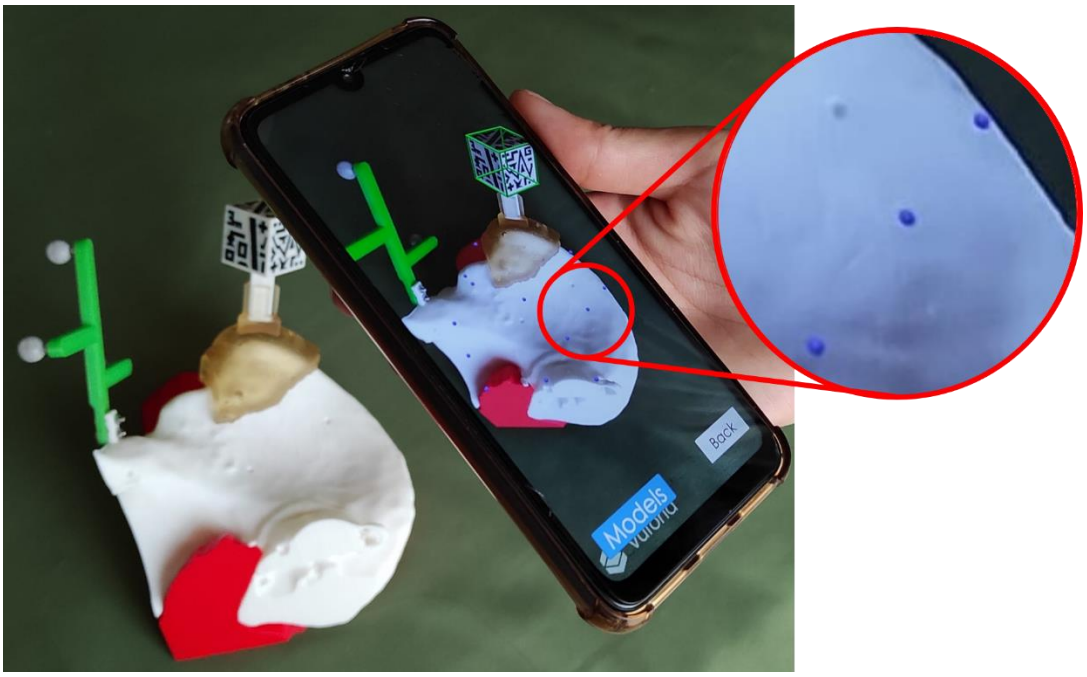

Figure 6.6. Phantom of patient AR3DP0002 (buttock tumor) and smartphone with the ARHealth validation app. The Augmented Reality Tracking Error validation spheres are augmented on the phantom surface in deep blue.

6.3.5. Integration of the augmented reality System in the Surgical Workflow

The proposed AR System was implemented during the whole surgical workflow of patients AR3DP0006 and AR3DP0007. *ARHealth* was used at the three steps of the workflow: by the surgeons during surgical planning, to show the virtual anatomical models to the patients before surgery, and during the surgical intervention to display the tumor margins. Finally, a

survey was designed to qualitatively record the opinion of the surgeons and the patients about the proposed AR-based system.

During surgical planning, surgeons used *Demo* and *Clinic* modes from the *ARHealth* app installed in a Google Pixel 4 XL smartphone. First, the user selected *Demo* mode from the main menu, and holding the phone with one hand, he pointed with the camera to the AR marker to detect it. The virtual models, such as bone and tumor, were projected on the smartphone display. The AR app would track the cubic reference movements, and the virtual models moved according to the face detected. *Demo* mode was used to take a first glimpse of the case without needing any 3D printed biomodel. Then, *Clinic* mode was selected from the main menu of the app. This time, the surgeon took the 3D printed surgical guide of the corresponding patient and fixed it into the PLA bone fragment. Then, the cubic marker was placed on the surgical guide, and with the smartphone camera pointing at it, the system displayed all the models with respect to the bone fragment. This mode was used to practice with the visualization before the surgery and with the surgical guide placement. The *Clinic* mode could also help analyze and discuss alternative strategies for the surgical procedures, compare possible approaches or instruct inexperienced surgeons.

During the last medical appointment with the patient prior to the surgery, physicians used *ARHealth* as a reinforcement to explain the tumor location and the treatment they were going to receive. With the *Clinic* mode selected on the smartphone, patients pointed with the camera to the cubic marker, which was already attached to the surgical guide and the bone fragment. They were able to rotate the marker and tailor the transparency of the models to comprehend the details of their condition more easily.

Our proposed technology was also evaluated as guidance for tumor resection. The system provided the tumor's location thanks to the automatic registration between the reference marker and the surgical guide. An iPhone 6 (Apple Inc., Cupertino, CA, USA) was used as the AR-device during the procedure. The surgical intervention was developed without modifications until the tumor was completely removed, leaving the bone tissue exposed. After that, the smartphone was introduced in a sterilized case (CleanCase, Steridev Inc., Lansing, MI, USA) held by one surgeon. One of the surgeons opened the *ARHealth* app on the smartphone and selected the *Clinic* mode. The physician placed the surgical guide with the cubic marker attached on the sterile bone fragment and verified its position, ensuring that the app was working as expected. The next step was to place the surgical guide on the patient's

bone target area. Surgeons used the *Surgery* mode to visualize the bone and ensure the correct placement of the guide, validating the automatic registration. Then they fixed it in the bone with medical screws. One of the surgeons selected the occlusion bone mode and used the smartphone to project the tumor on the patient in real-time through the AR display. They could rotate the smartphone at any orientation to better evaluate the resection margin. Finally, they removed the surgical guide and continued with the procedure.

We designed two different questionnaire surveys, one for the patients and the other for the surgeons, to qualitatively assess the impact of the proposed workflow from their point of view and identify possible aspects that could be improved. Ten surgeons from the Department of Orthopedic Surgery and Traumatology filled the 16 questions from the surgeon's questionnaire (**Document S1**). Survey's questions were scored on a 5-point Likert scale. All participating surgeons were familiar with the AR system. The survey presented to the patients consisted of 6 questions (**Document S2**) and was completed by the two patients involved in the clinical validation.

6.4. Results

The detection of the AR cubic marker by the smartphone application was feasible and practically immediate if they were at an appropriate distance. We zoomed in and out the Google Pixel 4 XL and iPhone 6 smartphones, both under optimal and dim light conditions, to determine the distance at which the marker was detected (zoom in) and lost (zoom out). In all the cases, the AR marker was detected at 30 cm. Once the pattern was identified, it was possible to move the phone further away from the marker up to 50 cm and maintain the visualization (provided that the AR cube was always on the camera's FOV).

6.4.1. Augmented reality performance

Figure 6.7 displays the results obtained during the validation of the Surgical Guide Placement Error for each phantom by two users and five repetitions each. The last column includes the measures on all phantoms. The error obtained for Patient AR3DP0005 could not be analyzed due to technical errors during the corresponding evaluation experiment. The overall Surgical Guide Placement Error was 1.75 ± 0.61 mm.

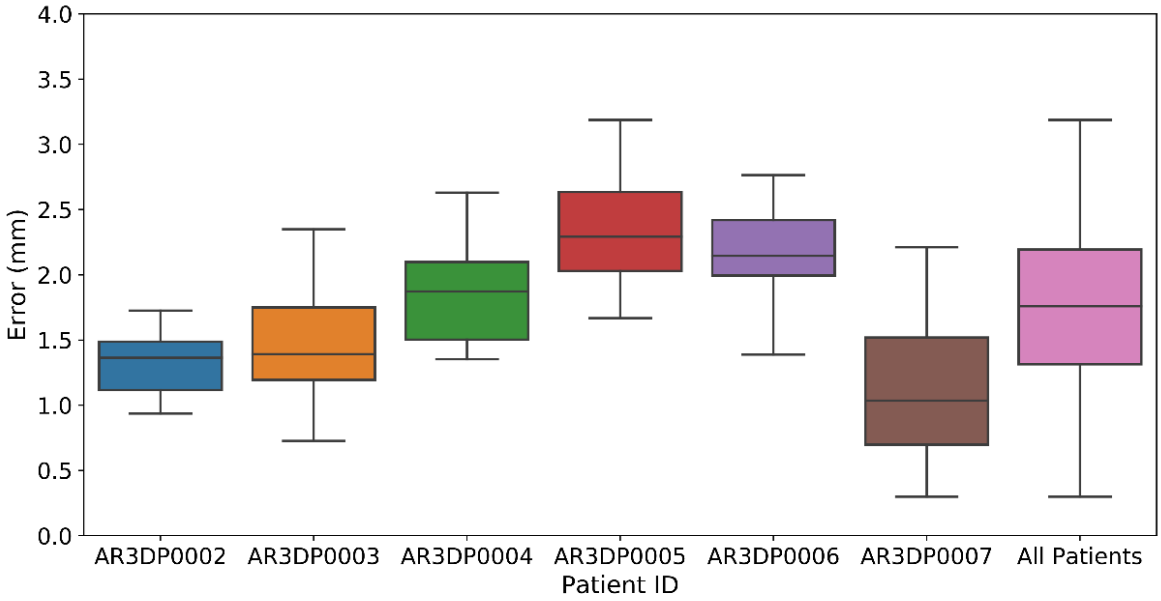

Figure 6.7. Surgical Guide Placement Error obtained for each patient phantom. The upper and lower limits for each box represent the first and third quartile of the dataset, and the middle line indicates the median. The whiskers stand for the highest and lowest values (±1.5 times the standard deviation).

The Augmented Reality Tracking Error validation experiments were designed to demonstrate the system's accuracy and independence from the user. **Figure 6.8** represents the error values for five repetitions on each phantom. The minimum mean error is obtained for case AR3DP0007 (2.1 ± 0.9 mm) and the maximum for AR3DP0004 (4.2 ± 1.5 mm). To determine the user-dependency of the error values, we performed a paired t-test comparing the data obtained by both users in each phantom under the null hypothesis that there is not a significant difference between their results, obtaining a p-value > 0.05 in all cases. Overall, the mean error of the system was 2.80 ± 0.98 mm.

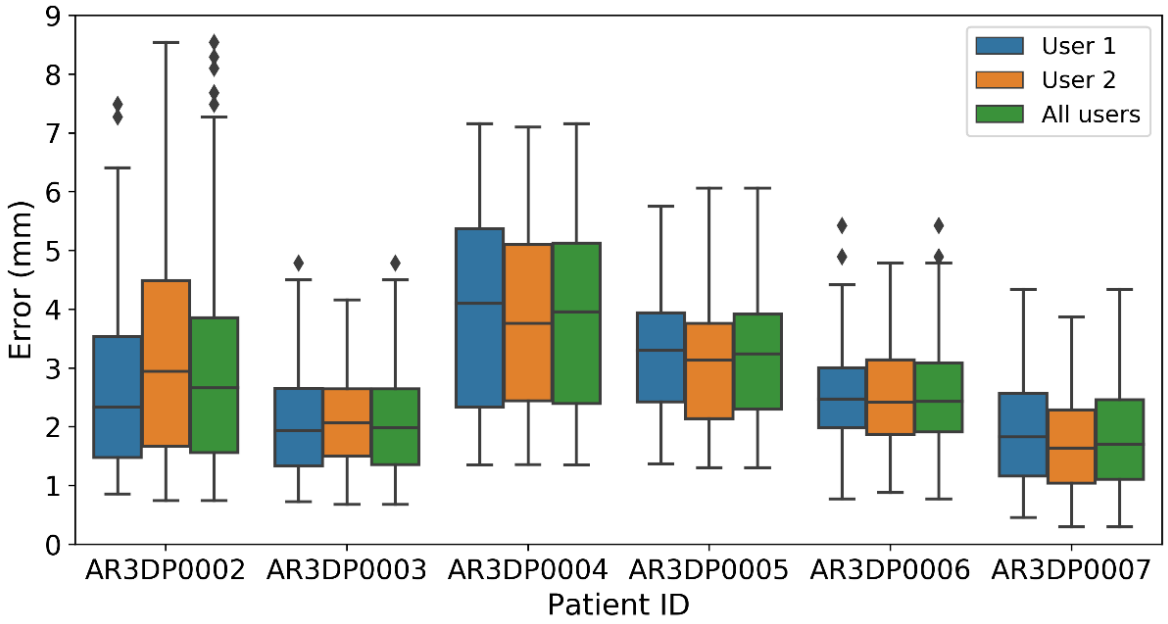

Figure 6.8. Augmented Reality Tracking Error for all the patients separated by user. The upper and lower limits for each box represent the first and third quartile of the dataset, the middle line indicates the median. The whiskers stand for the highest and lowest values (±1.5 times the standard deviation).

6.4.2. Integration of the Augmented Reality System in the Surgical Workflow

The integration of *ARHealth* was feasible on all the surgical workflow steps for patients AR3DP0006 and AR3DP007. During the preoperative planning, surgeons used *Demo* and *Clinic* mode from the *ARHealth* app to reinforce their knowledge about each patient case. It allowed physicians to discuss the surgical approach anywhere in the hospital, thanks to the portability of the system (**Figure 6.9**a,b). During the last clinical appointment, both patients held the smartphone and tracked the AR marker easily. Patients understood how this technology worked with just one explanation from the physician, and both used the system for approximately 5 minutes. **Figure 6.9**c,d shows one of the patients using the AR system during the clinical appointment. Detection of the cubic marker was fast, and no problems were encountered during these two steps of the medical workflow.

During the surgical intervention, the smartphone was placed on the sterile case without complications. The 3D printed bone fragment was useful in both cases to verify the position of the surgical guide before placing it on the real bone. Moreover, surgical guides fitted as planned in the target area of the patient's bone, allowing a successful registration between the AR system and the patient's anatomy. The virtual models were projected on the patients in their

expected location. Neither blood nor different light conditions interfered with the detection of the cubic marker, and *ARHealth* could display the tumor to better evaluate the surgical margins. Additionally, the 3D printed reference stayed fixed on the surgical guide adaptor and was easily removed when it was no longer needed. The picture of **Figure 6.9**e,f was acquired during the surgical intervention of Patient AR3DP0007. One surgeon is holding the smartphone in the sterile case projecting the tumor virtual model on top of the patient after tumor resection to delimit tumor margin.

During AR3DP0006 surgical intervention, some main arteries interfered with the cubic marker detection after placing it into the surgical guide. However, thanks to the cubic shape of the tracking reference, the AR system detected other uncovered faces of the cubic marker, projecting the anatomical virtual models in the right position on the patient.

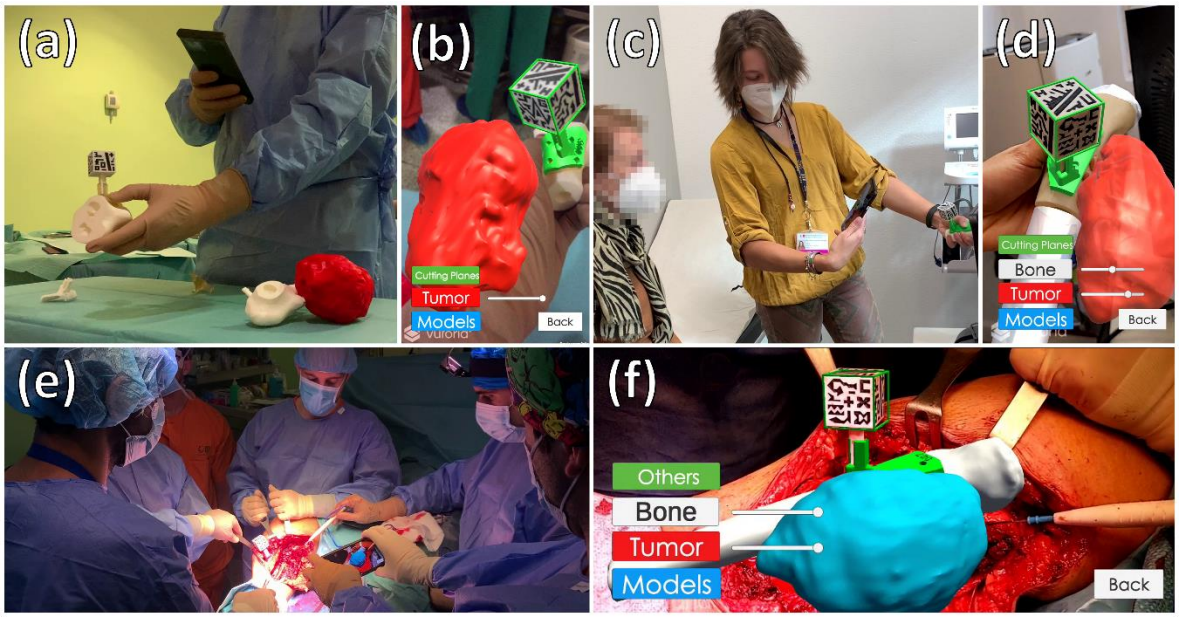

Figure 6.9. Integration of the augmented reality system at each step of the medical workflow. (**a**,**b**) Physician using ARHealth during surgical planning of patient AR3DP0006; (**c**,**d**) Medical staff explaining patient AR3DP0007 her condition using ARHealth; (**e**,**f**) One physicians using ARHealth during surgical intervention of patient AR3DP0007 after the surgical guide was placed on the patient, and other surgeon delimiting surgical margin while looking at the AR-display. (**b,d,f**) Smartphone visualization at the same moment of (**a,c,e**), respectively.

Nine orthopedic surgeons answered the proposed survey. Five of them had prior experience with AR. **Table 6.4** reveals the individual scores obtained from each user. The last row and column represent the average scores per question and surgeon, and the left-most column is a condensed form of the questions asked. The total average score obtained in the

survey, considering the questions related to the smartphone application and the usability of the proposed workflow, was 4.5 out of 5. Regarding the medical fields that they considered could benefit the most from this technology as it is right now, they all selected oncologic surgery. 78% of them additionally answered orthopedic surgery and 67% chose neurosurgery, plastic surgery or minimally invasive surgery. The 44% of the physicians also picked cardiac surgery.

Patient's survey was answered by the two patients for whom the whole medical workflow was deployed (**Table 6.5**). None of them had prior experience with AR or had even seen a 3D model of their body before. Both patients gave the maximum score to the *ARHealth* system and preferred AR in the explanation of their pathology rather than a 2D image or the standard surgeon's description.

Table 6.4. Surgeons' survey scores.

Questions	Individual Scores (per surgeon)						Avg. Score
	1	**2**	**3**	**4**	**5**	**6**	
1. AR in surgeries (general)	5	4	5	5	3	5	4.5
2. AR in surgeon's operations (general)	5	4	3	3	4	5	4.0
3. DEMO: surgeon understanding	5	4	5	5	4	5	4.7
4. DEMO: surgical planning	5	4	5	5	5	5	4.8
5. DEMO: patient communication	5	5	5	5	5	5	5.0
6. CLINIC: PLA bone fragment	5	4	4	5	4	5	4.5
7. CLINIC: practice with AR	5	3	4	5	5	5	4.5
8. CLINIC: patient communication	5	3	5	5	3	5	4.3
9. SURGERY: tumor location	5	5	4	5	4	5	4.7
10. SURGERY: increase of accuracy	5	4	4	5	5	5	4.7
11. SURGERY: phone case	5	4	5	5	5	5	4.8
12. GENERIC: easiness of interpretation	5	5	4	5	4	5	4.7
13. GENERIC: patient communication	5	5	5	5	5	5	5.0
14. GENERIC: surgeon's confidently	4	4	5	5	4	5	4.5
15. GENERIC: use this workflow	5	4	4	5	4	5	4.5
Avg. Score	4.9	4.1	4.5	4.9	4.3	5	4.5

Table 6.5. Patients' survey scores.

Questions	Individual Scores (per patient)		Avg. Score
	1	**2**	
1. Pathology understanding before *ARHealth*	2	4	3
2. Pathology understanding after *ARHealth*	5	5	5
3. General opinion about AR	5	5	5

6.5. Discussion and conclusion

In this study, we present and evaluate a novel framework deployed in orthopedic oncology combining AR and 3D printing technologies to assist surgeons during different stages of the surgical workflow. Our system supports surgical planning, enhances patient communication, and provides guidance during surgical interventions. A smartphone-based AR application has been developed to visualize the patient's anatomy and the tumor locations using a 3D printed reference marker. Automatic registration between virtual and real world is achieved by patient-specific surgical guides (with a support for the reference marker) that fit in a unique region of the affected bone tissue. The precision of the system has been analyzed using the clinical data from six patients, and the feasibility has been evaluated during the whole surgical workflow on two of them.

3D printing still has significant limitations, such as long 3D printing time of large pieces and a lot of material waste in orthopedic oncology [174]. In this study, these problems have been tackled by 3D printing just small models, such as delimit fragments of the affected areas, and displaying the complete biomodels with AR. This method could be an alternative to reduce material cost and 3D printing time.

The main limitation of AR in the medical field is the required image registration between real and virtual data [182]. Some studies try to solve this issue with a manual registration [107], which might not be the best option in many cases. We adapted the automatic registration technique presented in [156], proposing a more general approach. The 3D printed surgical guide has now a marker holder attached to it. This allows the attachment of an AR marker when the surgical guide is fixed on the patient without removing the whole surgical guide. Additionally, we have demonstrated that this guide is placed in the target position with a mean error below 1.80 mm in six patient-specific phantoms of different bone types and areas. These results are comparable with those reported in [156]. The low error indicated that this registration method could be reliable for AR systems applied to orthopedic oncology.

When evaluating the Augmented Reality Tracking Error on six patient-specific phantoms the overall error was 2.80 mm. These results are similar to those reported in [156], using Microsoft HoloLens, and in [183], using a tablet-based system. However, a relevant fact is that in [156] the AR marker was two-dimensional, limiting the mobility of the AR device. Our study obtains similar tracking error results, but with a 3D printed cubic marker that can be

tracked from different points of view, providing freedom of movement, a crucial aspect specially in the OR.

The AR performance achieved comes from an accumulation of different error sources, such as the accuracy of the 3D printers, the localization of the control points, the intrinsic error of the OTS and the registration error. However, the low error obtained in our system encourages us to believe that virtual models can be displayed with enough accuracy on top of the patient to improve different steps of the surgical workflow.

The Augmented Reality Tracking Error results reveal increased variability for the biggest phantoms, suggesting an increasing error at larger distances. Nonetheless, this is common to all navigation systems [184]. Phantom AR3DP0002 and Phantom AR3DP0004 were the largest in our experiments and, therefore, had more error evaluation positions further away from the origin (the AR marker). Consequently, the error results for those phantoms are higher both in average and standard deviation. Although existing, this correlation will not affect during this type of surgeries, on which the working volumes are limited around the surgical guide. Anyway, this factor must be considered in each case.

The proposed AR system was favorably tested during the complete medical workflow of two patients. The visualization of virtual 3D models of the patients was feasible using the smartphone and the tracking marker during surgical planning, patient communication and surgical intervention. The general opinion of the surgeons is that the system would be very useful to establish a preoperative plan more confidently (by examining the case in three dimensions before surgery). The solution is portable, not requiring a personal computer. The importance of patient communication in surgical interventions was already highlighted in [185]. In our case, both patients welcomed this technology to understand their situation better, and surgeons found it very useful to accompany their explanations of the pathology and surgical approach.

Additionally, the proposed methodology was easily integrated during the two clinical interventions. The system displayed the corresponding tumor position on top of the patient with virtual anatomical elements, boosting surgeons' confidence to verify that the tumor has been adequately resected. The physicians believed this visualization could be beneficial in tumor resection surgeries. Moreover, they suggested that this technology could also be advantageous to guide osteotomy cutting planes. AR visualization offers advantages compared to image guided information shown in standard displays, since the actual anatomy captured by the

camera is combined with digital models in a natural way for the user. Our experience is still limited, so further evaluation is required in a larger sample. The system accuracy is good but may not be enough to replace surgical navigation techniques.

Finally, the survey's results revealed an overall great acceptance of this system in the hospital and endorse the applicability of our proposal from the clinical perspective, promoting further research on this area. The questions related to the medical fields that could potentially benefit from this system open the future applications spectrum of this technology.

One of our system's limitations is that we created the 3D virtual biomodels based on an CT acquired several weeks before the surgery, and the tumors may have grown, reduced or moved in that time lapse [186]. Nevertheless, this is a limitation for any navigation system based on preoperative images. Another limitation is that, to use the *ARHealth* app, one hand must continuously hold the smartphone. A mechanical arm, holding the smartphone, could be incorporated into the OR to address this issue. Even the system could be running on a head-mounted display, such as Microsoft Hololens 2, to free the surgeon's hands in the procedures and give him/her more maneuverability during surgical intervention.

With regard to the expansion of our system to other hospitals, some extra security protocols should be applied to the smartphone application in order to preserve patients' privacy. This could be implemented with OAuth 2.0 protocol [187] as an authorization framework to limit the access to the app to only qualified personnel.

In conclusion, we have shown the benefits that the combination of AR and 3D printing can bring to orthopedic oncology surgery by evaluating the proposed AR system in patient-specific 3D printed phantoms and at each stage of the surgical workflow. We believe that this work serves as a baseline for developing more AR and 3D printing systems for surgical guidance, training, and patient communication.

Supplementary Materials: The following are available online at https://www.mdpi.com/1424-8220/21/4/1370/s1, **Document S1**: Questionnaire given to surgeons to validate the AR system, **Document S2**: Questionnaire given to patients involved in this study to validate the AR system.

The content of this chapter has been published in Sensors journal as part of the special issue "Computer Vision for 3D Perception and Applications":

R. Moreta-Martinez, A. Pose-Díez-de-la-Lastra, J. A. Calvo-Haro, L. Mediavilla-Santos, R. Pérez-Mañanes, J. Pascau. "Combining Augmented Reality and 3D Printing to Improve Surgical Workflows in Orthopedic Oncology: Smartphone Application and Clinical Evaluation". Sensors, vol. 21, no. 4, p. 1370, Feb. 2021.

7

Needle Navigation in Sacral Neurostimulation

7.1. Introduction

Nonobstructive chronic urinary retention, urgency urinary incontinence, fecal incontinence, and other bowel dysfunctions are pathologies that affect millions of people globally [188]. It is estimated that 17.4% of women and 15.6% of men aged > 40 years in Europe suffer from at least one of these conditions [189]. Although conservative treatments, such as behavioral modification and drug therapy, are indicated as first-line alternatives, their effect is usually limited by patient obedience, adverse medication events, or unsatisfactory efficacy [190].

During the past two decades, sacral neuromodulation or sacral nerve stimulation (SNS) has been considered a valid alternative when conventional treatments have failed. SNS is a minimally invasive procedure where an electrode lead is implanted through the sacral foramina to stimulate the nerve modulating colonic and urinary functions [191]. This practice has shown to efficiently treat fecal incontinence [192], refractory overactive bladder [193], urinary retention [194], or constipation [195].

One of the most crucial steps in SNS procedures is the placement of the tined lead close to the sacral nerve, as the final position of the electrode will determine the efficacy of the treatment. In order to reach the sacral nerve, a needle must be inserted through the posterior sacral foramina S3 or S4, that are usually smaller than 12x8 mm [196]. Currently, surgeons

perform a combination of visual inspection to localize bony landmarks [197], [198] and conventional x-ray fluoroscopy (anterior and lateral projections) to estimate the location of the target sacral foramen, decide the initial insertion trajectory, and verify the needle's location with respect to the sacrum while positioning the lead in place [199]. However, needle insertion is very challenging for surgeons. Several x-ray projections are required to interpret the needle's position correctly. In many cases, multiple punctures are needed, causing an increase in surgical time and patients' discomfort and pain. Not to mention that the lack of general reference points in patients with anatomical sacral abnormalities may increase surgical difficulties.

Intraoperative computed tomography (CT) imaging has previously been proposed to estimate the final position of the needle in patients with abnormal sacrum where fluoroscopy has failed [200], [201]. Others have combined CT scans inside the operating room with navigation systems to track the position of the needle in real-time, guiding electrode placement, reducing procedural time, and improving surgical outcomes [202], [203]. Nonetheless, these techniques have been used in just a few cases, only when required to perform a complex surgical procedure correctly. Additionally, these systems involved an intraoperative CT, which implies additional radiation exposure to both patients and medical professionals during the intervention, restricting their integration in the clinical practice [204].

As an alternative, patient-specific 3D printed navigation templates have been proposed for accurate electrode lead placement, using a preoperative CT scan to define needle trajectory and perform patient registration [205]. Zhang et al. have shown that this technique could imply lower intraoperative radiation exposure and higher efficacy of the procedure than the traditional approach. However, the application of this proposal is limited by the long manufacturing time of the template. Also, the patient needs to have registration markers stuck on the affected surface for days, leading to discomfort and possible landmark displacements, resulting in a low registration accuracy during the procedure. Moreover, removing the template once the needle is inserted could modify the final position of the electrode lead [206]. Finally, Rubio-Perez et al. have presented an alternative application of 3D printing for fabricating patient-specific sacrum biomodels to understand possible anomalies of patients' anatomy before surgery [60].

Needle insertion guidance with tracking systems has previously been proposed in surgical procedures such as radiofrequency ablation [207], [208] or spine surgery [209]. All these navigation systems provided successful needle guidance. Nevertheless, the navigation

information is displayed on external screens, requiring the surgeon to divert his attention from the patient. In this context, augmented reality (AR) technology could overcome these limitations, providing the surgeon with real-time navigation information directly overlaid in the surgical field. AR for needle guidance has become a feasible alternative in recent years [210], [211]. Hecht et al. proposed a smartphone-based AR navigation system to display the needle trajectory in the target area for ablation and biopsy procedures, demonstrating a superior needle insertion accuracy compared to CT-guided freehand methods [110]. Besides, Kuzhagaliyev et al. presented the combination of an AR head-mounted display with an optical tracking system to guide the needle ablation during irreversible electroporation in the pancreas [212]. Although these AR navigation techniques provided needle guidance solutions for surgical treatments, they do not propose feasible patient registration methods that could be translated to real clinical scenarios.

The described works have shown how navigation systems can improve needle guidance using tracking devices or AR technology. However, these solutions have not been implemented in SNS procedures yet. In the past, our group developed an open-source navigation software to track the needle's position with respect to the patient in real-time using an electromagnetic tracking system (EMTS) [213]. The proposed solution did not require an intraoperative CT for registration, providing accurate needle guidance for SNS. Nonetheless, the proposal showed several limitations: navigation software did not indicate the target depth, preoperative CT images had to be segmented just before surgery in a very narrow time window, and the EMTS components required asepsis and were affected by metal distortions from other surgical tools.

This work will solve the restrictions mentioned above, proposing solutions that could be translated to clinical practice, based on the following hypothesis:

- Optical tracking systems would be more convenient than EMTS for SNS procedures, facilitating the asepsis and improving needle guidance.
- Augmented reality would improve the interaction of the user with the navigation information.
- Algorithms based on artificial intelligence (AI) could perform bone segmentation in the sacrum almost instantaneously [214], [215], solving one of the restrictions found during image-guided navigation [117].

7.2. Objective

In this work, we propose and evaluate two different navigation systems to guide electrode placement in SNS surgeries designed to reduce surgical time, minimize patient discomfort and improve surgical outcomes. For the first alternative, we developed an open-source navigation software to guide electrode placement by real-time needle tracking with an optical tracking system (OTS). In the second method, we introduce a smartphone-based AR application that displays virtual guidance elements directly on the affected area, using a 3D printed reference marker placed on the patient, facilitating needle insertion with a predefined trajectory. We also developed and tested an automatic sacrum segmentation method based on Artificial Intelligence to speed up the extraction of virtual models from the CT study of the patient. Both techniques were evaluated to determine which one obtained better results than the current surgical procedure in terms of the number of insertions, accuracy, procedure duration, and radiation exposure. To compare the proposals with the clinical method, we developed an x-ray software tool that calculates direct reconstruction radiograph (DRR), simulating the fluoroscopy acquisitions during the procedure. All methods were evaluated by twelve physicians (inexperienced and experienced users) on a realistic anthropomorphic phantom based on a patient that underwent an SNS procedure. Finally, we propose a feasible surgical workflow designed for clinical use to be performed during the surgical intervention, including preoperative CT imaging, automatic virtual model creation, patient-to-image registration, and surgical navigation based on each proposed method.

7.3. Previous work

7.3.1. Surgical navigation for SNS needle guidance using an EMTS

Previously, our research group proposed a surgical navigation system oriented to clinical use to improve electrode placement accuracy in SNS surgical procedures. This solution was based on an EMTS to track both the needle and the patient during the intervention. The tracking device was connected via OpenIGTlink communication protocol to an open-source navigation software (**Figure 3.1**) developed in 3D Slicer platform [34]. The proposed methodology used a CT scan of the patient as a surgical reference during needle trajectory planning.

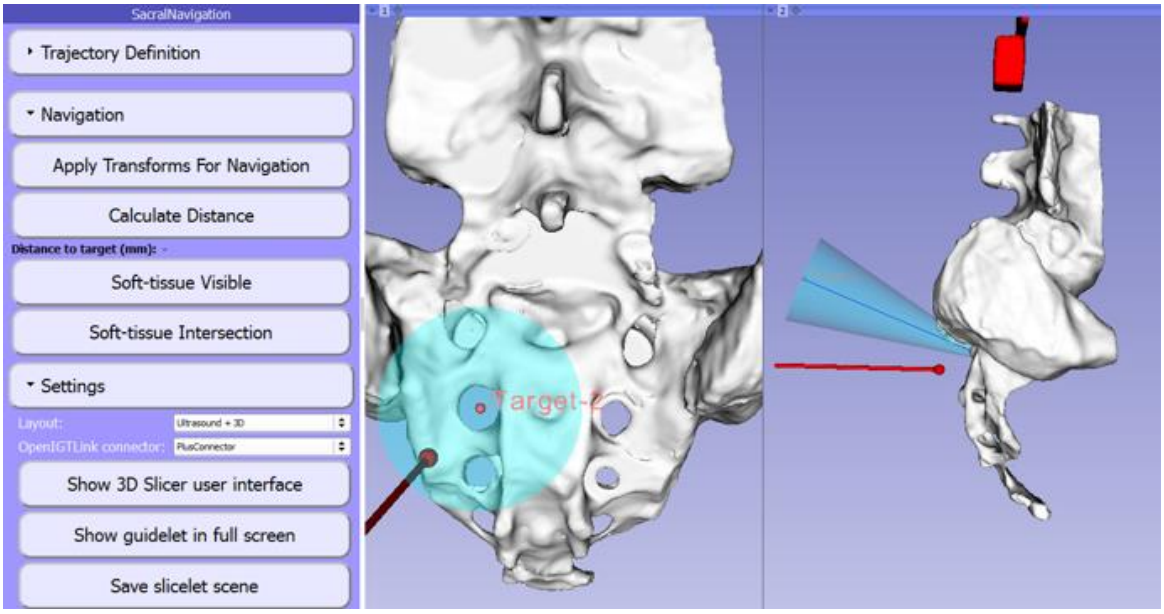

Figure 7.1. Navigation software proposal for needle guidance in sacral neuromodulation procedures. Image adapted from [213] (figure reprinted with permission of the copyright holder, Springer Nature).

The proposed workflow was defined as follows:

- 2-3 hours before surgery:
    1. Skin fiducials placement on the patient around the visible insertion area for image-to-patient registration.
    2. CT scan acquisition and manual image segmentation to obtain a virtual 3D model of the sacral anatomy.
- During surgery:
    3. Needle and pointer calibration to obtain the position of the tool's tip with respect to the tracking sensor.
    4. Image-to-patient registration, recording the location of skin fiducials with a tracked pointer.
    5. Target and optimal trajectory definition on the navigation software.
    6. Needle navigation.

An anthropomorphic phantom of the SNS affected area was manufactured to evaluate the system. This phantom included the sacrum bone, 3D printed in polylactic acid (PLA) and covered with silicone (Dragon Skin 20 Slow) to mimic the patient's soft tissue. One experienced surgeon qualitatively evaluated the complete workflow giving positive feedback in terms of navigation experience. Additionally, two SNS unexperienced users performed a

total of six needle insertions in the phantom assisted with the proposed navigation system to evaluate the procedure quantitatively. The actual needle tip position was obtained from a CT scan acquired after each needle insertion. The error with respect to the target trajectory and the time to perform the task were measured.

The results showed a final root-mean-squared error of 1.93 mm and a total procedure time of 130 ± 100 s, demonstrating that this navigation system facilitated needle insertion in SNS procedures, reducing the time needed to perform the task and achieving high accuracy. However, to finally bring the method to clinical use, some drawbacks should be solved:

- The validation metrics were not sufficient to conclude that the proposed methodology could replace the current clinical procedure, as the comparison was not based on previous literature.
- Although the phantom had a realistic appearance, the soft tissue part was made of hard silicone. Needle insertion in this material required high pressure to reach the sacral foramina compared to clinical patients. Therefore, the needle tended to bend, and the insertion experience was not accurate compared to actual clinical procedures. Furthermore, the phantom S3 and S4 foramina sizes were larger than the average [196], so inserting the needle inside the target foramen without colliding with the bone was more straightforward than with an actual patient.
- The navigation software was useful and intuitive, but it lacked depth navigation feedback.
- The use of an EMTS was not convenient in these surgical interventions due to three main limitations. First, the need to insert each EMTS sensor in a sterilized plastic bag, which implied material waste and long preparation times. Second, sensor cables interfered with the surgical field. And third, devices such as the C-Arm, surgical bed, and stimulator, interfered with the electromagnetic field produced by the EMTS. This hindered the definition of a clear volume without ferromagnetic distortion, which could affect EMTS tracking accuracy.
- The proposed workflow included the acquisition of a CT scan right before the surgery to avoid misplacements of the skin markers. This step implied that the segmentation of the preoperative images had to be performed in a very short time window. Virtual model creation could take long segmentation times, leading to delays in the surgical intervention and unnecessary pressure and stress to the staff involved in the procedure.

All these limitations led to the search for new solutions: the design of a new experiment that included evaluation metrics more comparable with the current procedure; 3D manufacturing of a more realistic phantom; developing new features in the navigation software; finding technological navigation alternatives; and developing a more automatic surgical workflow. All these proposals will be presented in this chapter.

7.3.2. Automatic segmentation

Anatomical segmentation of medical images has always been essential for pathology location and quantification in surgical treatments. However, current segmentation methodologies are mainly based on manual or semi-automatic approaches, which require extensive dedication from medical professionals. In recent years, these cumbersome tasks are being automated thanks to the new advances in machine learning (ML), a subfield of AI, algorithms which are showing great potential in disease diagnosis and prediction.

In SNS cases where a preoperative CT scan is acquired, the segmentation of the sacrum would be necessary to create a virtual 3D model and use it to define the trajectory for the needle insertion. However, in most cases the sacrum is manually segmented, leading to a long processing time. Therefore, developing tools to automatically segment these anatomical parts would benefit SNS procedures by reducing processing time and complexity.

Our research institution, in collaboration with the Applied Chest Imaging Laboratory (ACIL) research group at Brigham and Women's Hospital (Boston, MA, USA) and Harvard Medical School (Boston, MA, USA), implemented several deep learning algorithms for automatic segmentation, facilitating fast patient screening from medical images by predicting clinical outcomes. More specifically, we have contributed to two areas: development of a complete automated segmentation workflow to predict body composition measurements from thoracic CT scans (Supplementary Material, **Section 10.1**); automatic segmentation of all heart cavity chambers from non-contrast non-ECG gated CT scans (Supplementary Materials, **Section 10.2**). This experience has allowed the implementation of a workflow to segment sacral bone tissue from CT scans automatically in SNS procedures, presented in **Section 7.4.1**.

7.4. Materials and methods

In this section, we first describe the segmentation algorithm developed to automatically obtain the virtual model of the sacral bone from a CT scan (**Section 7.4.1**). Then, we present

the anthropomorphic phantom (**Section 7.4.2**) and the experimental set-up (**Section 7.4.3**) defined for evaluating all the navigation methodologies. Next, we explain in detail the proposed simulation system for SNS procedures (**Section 7.4.4**), the navigation system based on OTS (**Section 7.4.5**), and the AR system proposal for needle guidance (**Section 7.4.6**). After that, we describe how the experimental study was evaluated (**Section 7.4.7**).

7.4.1. Automatic segmentation of the sacral bone

For this study, we used a database composed of 89 cases with manually segmented abdominal bone structures, including right femur, left femur, right hip, left hip and sacrum [216]. The image dimensions are 512 × 512 × (500 ~ 700). As the sacrum delineation considered the sacral foramina as bone (we can observe on **Figure 7.2** that foramina are not visible), we applied a semi-automatic process to remove the segmented areas of the foramina prior to the training phase. This step is crucial for SNS since the location and size of the foramen will determine the needle's trajectory. 3D Slicer [34] software was used to process the data following several steps:

1. Obtain the sacrum mask from the subject.
2. Segment non-bone tissue from the CT image. For each case, we applied three thresholding operations: from -1200 to 50, 100 and 150 HU. The best one is selected in step 6.
3. Subtract the result from step 2 from the original sacrum to extract the sacral foramina.
4. Perform hole filling using a closing operator (ball structural element of size 1 × 2 × 2) for each sacrum.
5. Apply wrap solidify technique [217] on 3D Slicer. This method combines shrink wrapping, projection, and solidification algorithms to create a solid segment. (Region: Outer surface, Carve Holes values: 3, 4, 5. Best value selected in step 6)
6. For each clinical case, the best configuration (thresholding and wrap) was carefully selected by manually evaluating each segmentation according to sacrum shape and foramina sizes.

The best segmentation was adopted as the new ground truth label for the sacrum.

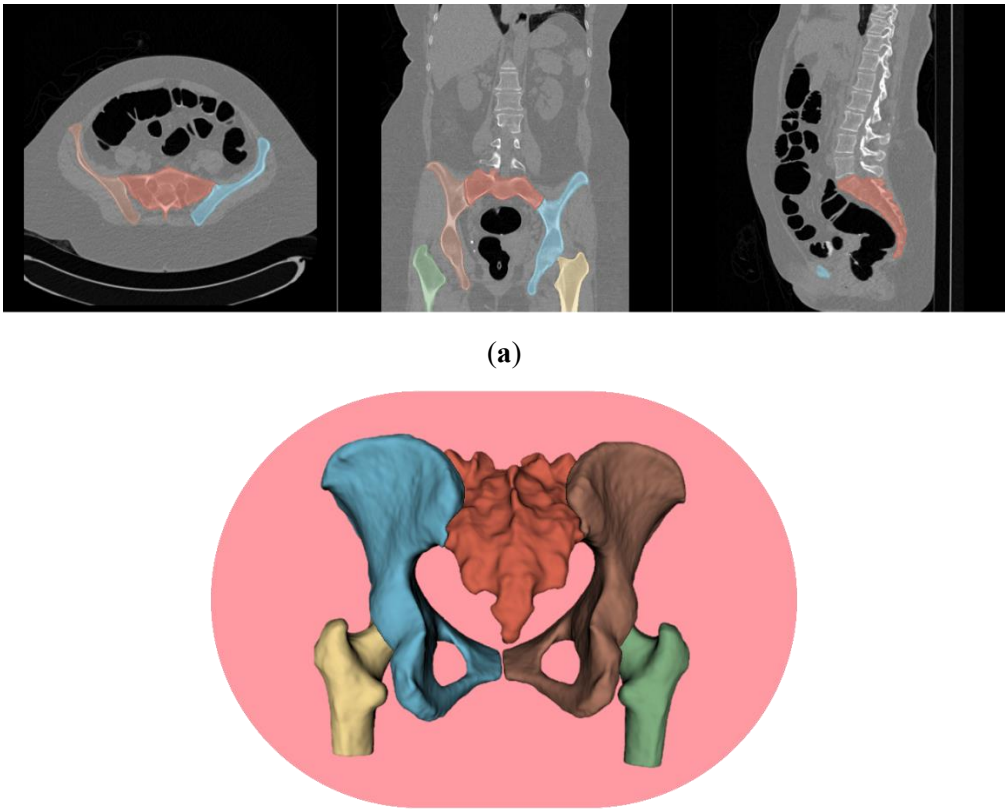

(**a**)

(**b**)

Figure 7.2. Example case from the training database [216]. (**a**) CT images, from left to right: axial, coronal and sagittal slices. (**b**) Virtual 3D models of each mask (5 in total).

After the sacral foramina were removed from the original mask, each image was classified into six classes obtained from the manual segmentation: original right femur, original left femur, original right hip, original left hip, modified sacrum, and background. The dataset was randomly divided into training (67 scans), validation (5 scans), and testing sets (17 scans). To reduce the computational burden, we resampled all the images to a pixel size of 1.20 × 1.20 × 1.43 and considered a volume of interest (VOI) of dimensions 128 × 128 × 128 centered in the sacrum. The input data always included the whole sacrum and was normalized by the mean and standard deviation of the training data. Additionally, data augmentation was performed by randomly shifting pixels (-20, 20) in all directions and randomly rotating images between -10º and 10º angles, obtaining a total of 402 images for training.

The neural network implemented in this study was based on a U-Net 3D architecture [218], represented in **Figure 7.3**. The proposed neural network consists of two different paths: a contracting path (encoder) and an expanding path (decoder). The encoder uses several blocks that include convolutional, batch normalization and max polling layers to capture the context of the image by expanding the future maps and reducing the dimension of the original data

within each block. Then, the decoder follows a symmetric expanding path which concatenates the corresponding information from the contacting path to enable precise output in the sense of both global and local features. Contrary to the contracting path, the decoder contracts the features maps and expands the dimension of the image at each block using convolutions and up-sampling steps. The end of the network reaches the original input size image with the corresponding depth map and the segmented classes. More in detail, we employed a modified version of the U-Net 3D [219] that uses strided convolutions instead of max pooling, and Leaky rectified liner unit (Leaky ReLU) as the main activation function.

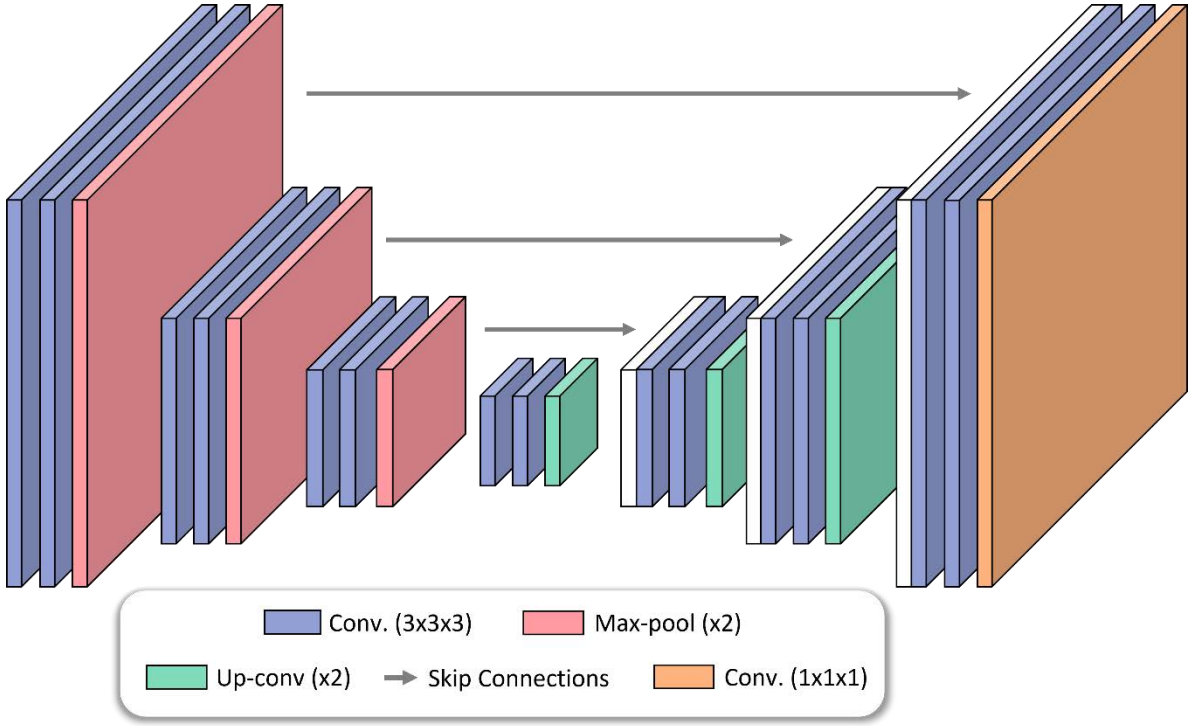

Figure 7.3. Schematic U-Net 3D architecture based on [218].

The parameters of the network were trained with dice coefficient as loss function weighting classes according to class prevalence. A batch size of 2 images and Adam optimizer [220] were used with an initial learning rate of 0.0001. This learning rate was reduced by a factor of 10 whenever the loss did not change significantly after four epochs. Initial weights and biases were selected with a He normal initializer [221]. Training was early stopped when the loss was stabilized after twenty consecutive epochs, resulting in a total of 500 epochs to converge. The network was implemented on Keras 2.1.6 framework with TensorFlow 2.4 backend and Python 3.6.8 as main programming language. The training was run in an Intel i7 workstation with 32GB RAM and GPU NVIDIA Titan X 12GB RAM.

The performance of the segmentation network in 17 subjects from the test set was studied by comparing both the ground truth and the automated segmentation method. These images were not used for tuning the parameters of the neural network model. Dice Similarity Coefficient (DSC) score, Average Surface Distance (ASD), Harsdorf Distance (HD), precision, and recall were calculated to analyze the segmentation performance. Furthermore, we visually examined the segmentation results of both the lowest and highest average DSC of the test set.

7.4.2. Sacral phantom

We evaluated the proposed surgical navigation systems on a phantom based on a patient suffering from a bowel dysfunction that underwent an SNS procedure. The patient had a standard sacrum shape, with average sacral foramina sizes. This study was performed in accordance with the principles of the 1964 Declaration of Helsinki as revised in 2013. The anonymized patient data and pictures included in this paper are used after written informed consent was obtained from the participant and/or their legal representative, in which he/she approved the use of this data for dissemination activities, including scientific publications.

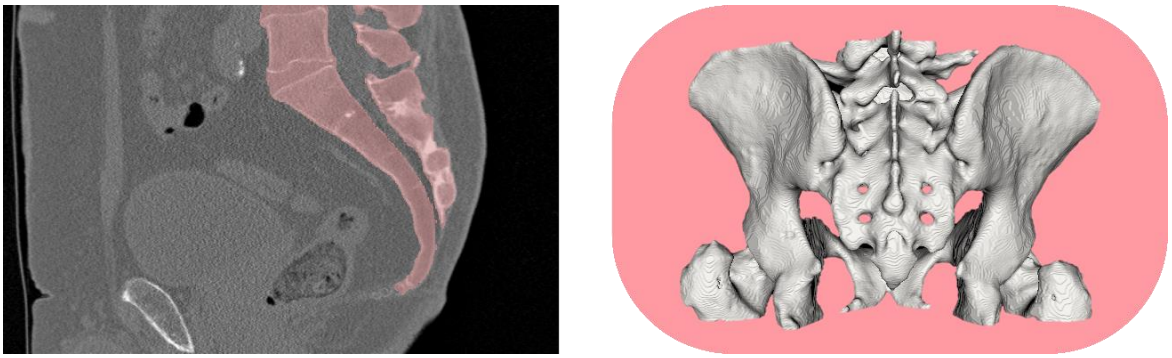

(**a**) (**b**)

Figure 7.4. Images of the patient's anatomy used in this study. (**a**) CT coronal slice image, with segmented bone in red. (**b**) Virtual 3D model of the pelvic bone structures.

A preoperative sacral CT scan (**Figure 7.4**a), obtained with the patient in prone position, was used as a template to manufacture an anthropomorphic phantom. The bone tissue, including pelvis, sacrum, vertebras and skin, were segmented from the CT image (pixel resolution of 0.625 × 0.625 × 0.330 mm) in 3D Slicer version 4.10.2 [34] applying semiautomatic methods (thresholding, manual contour and island effects). The results were exported as virtual 3D models (stereolithography files, STL) (**Figure 7.4**b) and post-processed

using smoothing (median filter with kernel size 5 × 5 × 9 pixels) and hole filling (kernel size 7 × 7 × 3) in 3D Slicer to optimize 3D printing quality.

The fabricated phantom was composed of two parts: bone and soft tissue. For the bone rigid structure, the virtual 3D model of the bone was processed using Meshmixer software (Autodesk Inc., San Rafael, CA, USA) to reduce the size by cutting the model where just the whole sacrum, a section of the iliac crest and the first vertebra were visible. Then, we included six conical holes (Ø 4 mm x 3 mm depth) on the bone model's surface to perform a point-based registration and added some features to fix the optical markers. The final design was 3D printed in polylactic acid (PLA) (**Figure 7.5**a) using a Raise 3D Pro 2 (Raise3D Inc., Irvine, CA, USA) desktop 3D printer.

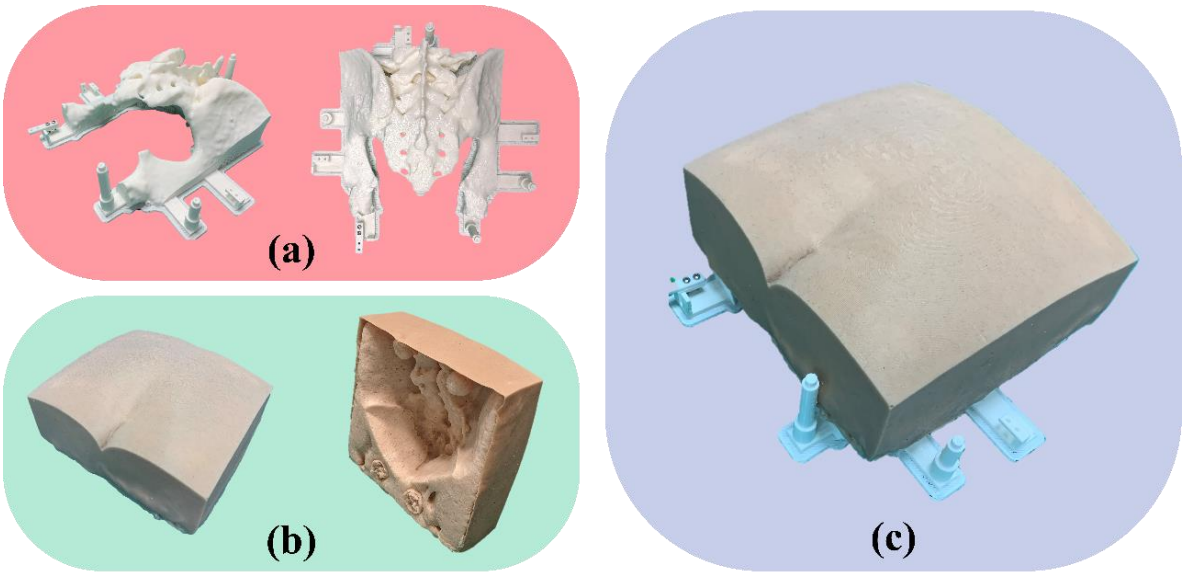

Figure 7.5. Manufactured phantom. (**a**) 3D printed bone in PLA. (**b**) Soft tissue. (**c**) Phantom assembled.

The part that mimics the soft tissue was designed to have two layers. First, an outer layer of low viscosity silicone Ecoflex 00-20 (Smooth-On, Inc., Macungie, PA, USA) 3 mm thick on the exterior of the phantom's upper side. Then, a second layer made of flexible silicone castable foam Soma Foama 15 (Smootth-On, Inx.) on the interior of the phantom (**Figure 7.5**b). A cast was designed and 3D printed to mold the silicones with the patient's shape, including the negative surface of the bone model. The first layer presents an initial resistance similar to the skin when the needle is inserted, while the second layer allows realistic feedback during needle insertion. The final phantom size was 20 × 19 cm of soft tissue and 24 × 24 cm of bone (**Figure 7.5**c). **Table 7.1** shows S3 and S4 foramina sizes (left and right).

Table 7.1. Phantom's sacrum foramina sizes.

Foramen	Axial Size [mm]	Longitudinal Size [mm]
S3 Left	7	5
S3 Right	7	7
S4 Left	9	6
S4 Right	9	7

7.4.3. Experimental set-up

For the three proposed methodologies, a common scenario was set up to perform the validation experiment. A Polaris Spectra (Northern Digital Inc. [NDI], Waterloo, ON, Canada) optical tracking system (**Figure 7.6**a) provided real-time tool tracking during the experiment. The tracking device transferred the positioning data to the navigation software using PLUS-Toolkit [33] and OpenIGTLink communication protocol [135]. The two infrared cameras of the optical tracker enabled the tracking of tools that included a configuration of three or more retro-reflective optical markers (rigid body, RB). The navigation software was displayed on an external screen when required by the navigation experiment (**Figure 7.6**b).

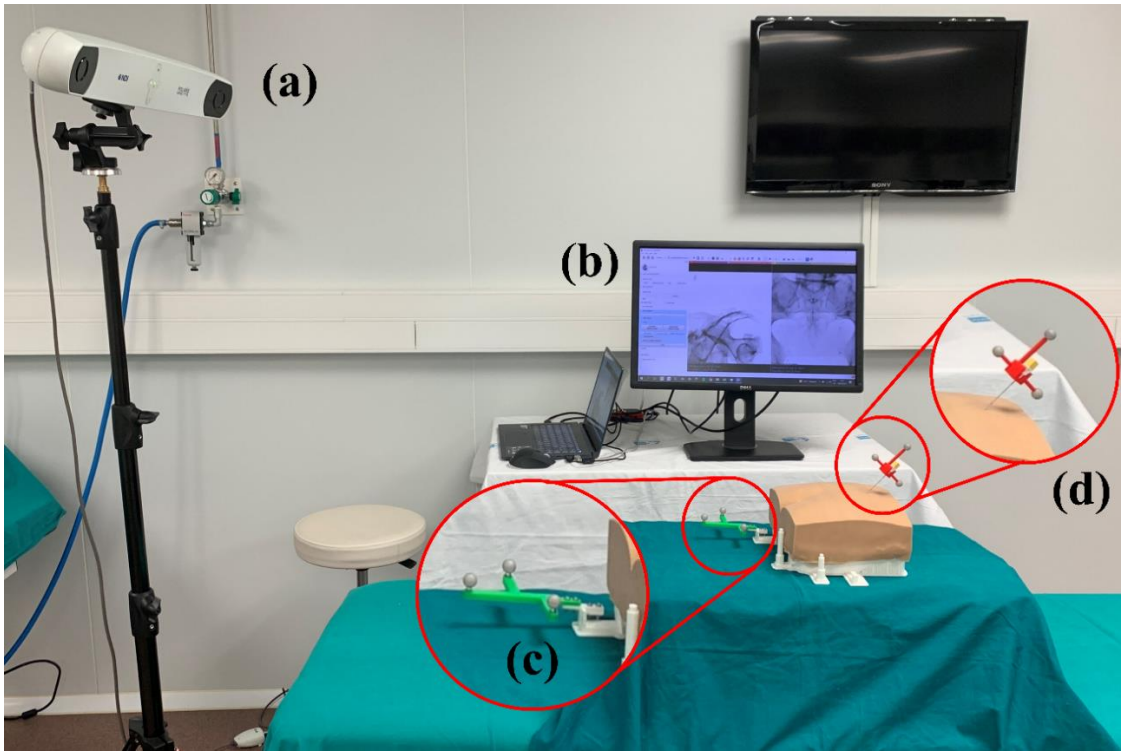

Figure 7.6. Experiment setup. (**a**) Optical tracking device. (**b**) External display. (**c**) Rigid body (RB) with spherical markers attached to the phantom. (**d**) Needle with RB attached.

A specific optical marker configuration was attached to the phantom (**Figure 7.6**c) to compensate for any possible movement during the experiment. We calculated the registration of the phantom with the navigation system by recording points on the conical holes made on the surface of the bone using a passive 4-marker probe (NDI Inc.), applying then fiducial-based rigid registration algorithm. The needle used during the experiment comes from a demonstration surgical kit from Medtronic (Model 3550-18/042294 Lead Introducer Kit, Medtronic PLC, Fridley, Minnesota, USA). We developed and a customized 3D printed cap holder with a specific optical marker configuration for the needle (**Figure 7.6**d). Pivot calibration [136] procedure was performed to calculate the relationship between the RB attached to the needle and its tip. Before each experiment, a registration of the phantom and the needle was performed. During the experiment, the needle and the phantom were always tracked, and the position given by the tracking system was used as a gold standard to compare with each navigation method

7.4.4. Simulation of the clinical method

A specific software application was developed as a module in 3D Slicer to simulate current SNS surgical procedures on the manufactured phantom. In this simulation, the user first performs a physical examination on the phantom to identify the position and orientation of the sacral bone. Then, the objective would be to reach the target foramen by inserting the needle using simulated x-ray projections for guidance. The software provides as many simulated projections as needed and gives feedback if the needle is in the selected target position when requested.

The NDI tracker provides real-time needle position with respect to the phantom. The software allows reproducing realistic anterior and lateral x-ray projections from anatomical structures of the phantom. In order to create the x-ray projection, a direct reconstruction radiograph (DRR) algorithm is applied on the CT of the patient from which the phantom was developed. The DRR program receives the CT image and the desired position for the x-ray tube focal point, calculating a projection by a bilinear interpolation [222]. To display the needle in the projection, we designed a virtual 3D needle model that is converted to a mask on the CT image coordinate system in its actual position, modifying the corresponding Hounsfield units (HU) units to metallic material (1500 HU). The software steps are summarized as follows:

1. Pivot calibration of the needle for virtual model registration.

2. Projection orientation selection.
3. Recording of needle's position with respect to the phantom.
4. Needle's virtual 3D model mask creation in phantom's CT image coordinate system, modifying the corresponding pixel values to 1500 HU.
5. DRR algorithm execution and projection simulation.
6. Simulated x-ray projection visualization on the user interface.

Figure 7.7a shows the software user interface, the phantom with the needle inserted in a target position, and the simulated lateral (left) and anterior (right) projections. Each projection is calculated almost instantaneously.

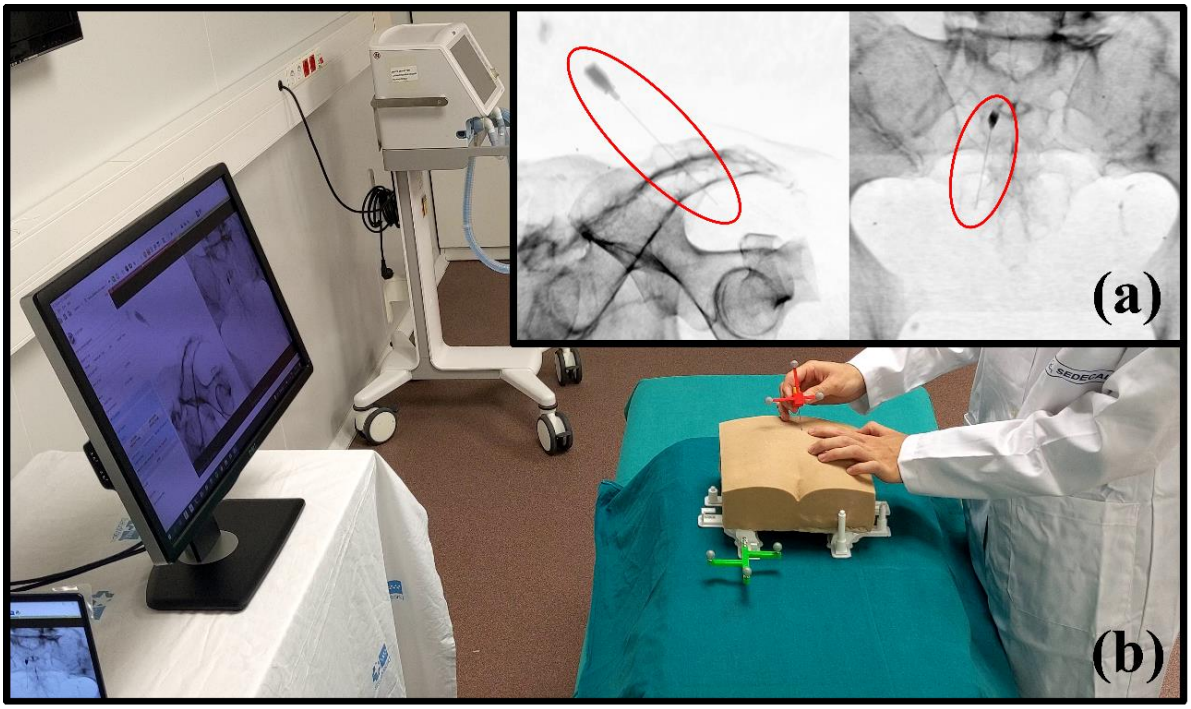

Figure 7.7. User performing the clinical method simulation. (**a**) Lateral (left) and anterior (right) projections with the needle circled in red. (**b**) User inserting the needle on the phantom.

7.4.5. Surgical navigation with optical tracking system

A software application named *SNSNavigation* was developed as a module in 3D Slicer to facilitate needle insertion in SNS procedures. This software has been adapted from López-Velázquez et. al [213]. NDI tracker transfers the position of the needle and the patient to the software in real-time. The RB attached to the phantom compensates for any movement during the experiment. *SNSNavigation* software displays information on an external screen. First, the

virtual 3D models of the patient are loaded on the navigation software in the correct orientation automatically. Then, once the target is selected, virtual models are displayed to visualize the trajectory of the needle and the target area. The software divides the screen into two sections to facilitate the guidance process, showing on the left a lateral view and an anterior view of the virtual 3D models on the right. The needle is represented as a cylinder of Ø 1.5 mm, with a sphere of Ø 2 mm on the tip. The trajectory of the needle is displayed as a red line with a sphere of Ø 2 mm representing the target point in the foramen. The anterior view plane is oriented perpendicularly to the trajectory line. A transparent green virtual model representing the target volume is displayed to indicate the expected final position. This model corresponds to the shape of the foramen hole, similar to a cylinder of diameter of the foramen size and between 1 and 2 cm of length (depending on the foramen size). If the needle's tip touches this target volume, the model will turn red, indicating that the needle has reached the target position. Additionally, the *SNSNavigation* software can calculate the real-time distance from the needle's tip to the target point.

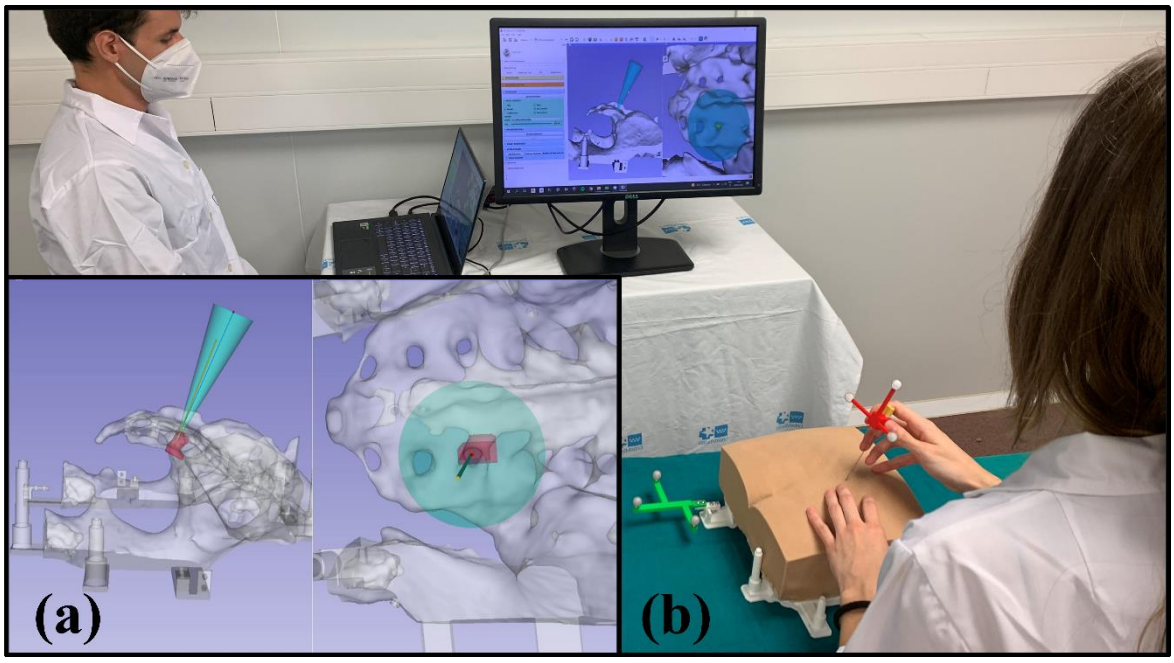

Figure 7.8. User performing needle insertion using the OTS navigation system as guidance. (**a**) Lateral view (left) and anterior view (right) of the navigation software. Green model represents the trajectory area, red model indicates that the tip of the needle is in the target position. The needle is represented with an orange virtual model. (**b**) User inserting the needle on the phantom.

To reach the target, first, the user looks at both lateral and anterior views on the navigation software (**Figure 7.8**a) while moving the needle until the tip of its virtual model coincides with the target point in the navigation software. After that, the orientation of the

needle should be corrected until it reaches the desired trajectory (given by the cone and the red trajectory line) without moving the needle's tip. Once the needle's virtual model is aligned with the position provided by the software, the user inserts the needle following that trajectory until the target volume changes from green to red in the user interface. A controller operates the navigation software while the user is performing the task, modifying the software options according to the users' needs.

7.4.6. Surgical navigation with augmented reality

We developed a smartphone AR application named *SacralNSAR* on Unity platform (version 2019.3) compatible with Android and iOS devices. This application uses Vuforia software development kit (SDK) (Parametric Technology Corporation Inc., Boston, MA, USA) to detect and track the position of a 3D printed cubic reference marker (30 × 30 × 30 mm) with unique black-and-white patterns on each face (**Figure 7.9**c) [157]. Once the marker is detected on the smartphone camera field of view, the virtual models are displayed overlaid on the real-world image in real-time.

Before navigation, the app presents a menu to select the predefined target and trajectory. Once chosen, virtual 3D models are displayed on the AR screen: the sacral bone, the optimal trajectory to reach the selected sacral foramen, the insertion point on the surface of the phantom, and the target needle insertion depth (**Figure 7.9**a).

The AR reference cube phantom (**Figure 7.9**c) was fixed to a 3D printed adaptor on top of the phantom (**Figure 7.9**b), in the superior area of the gluteus. To know the position of this marker with respect to the phantom, we performed a point-based registration obtaining the position of the conical holes designed on the marker adaptor's surface with the optical tracking system. Then, this registration transformation was transferred and updated on the smartphone (Google Pixel 4 XL, Alphabet Inc., USA). Additionally, a 3D Slicer module was developed to track the position of the needle in real-time and use it as a verification tool to know if the needle was in the correct target during the experiment.

In order to reach the target foramen while using this navigation system, the user selects the desired target from the smartphone app. Then, holding the smartphone with one hand and the needle with the other, the user points at the 3D printed marker with the camera until the app tracks it. Once the virtual models appear on the AR display, the needle's tip should be positioned on the insertion point. The orientation is corrected using the trajectory red line model

as a reference. Then, the user inserts the needle until the holding part reaches the orange insertion depth virtual model. The 3D Slicer module will verify the final position of the needle.

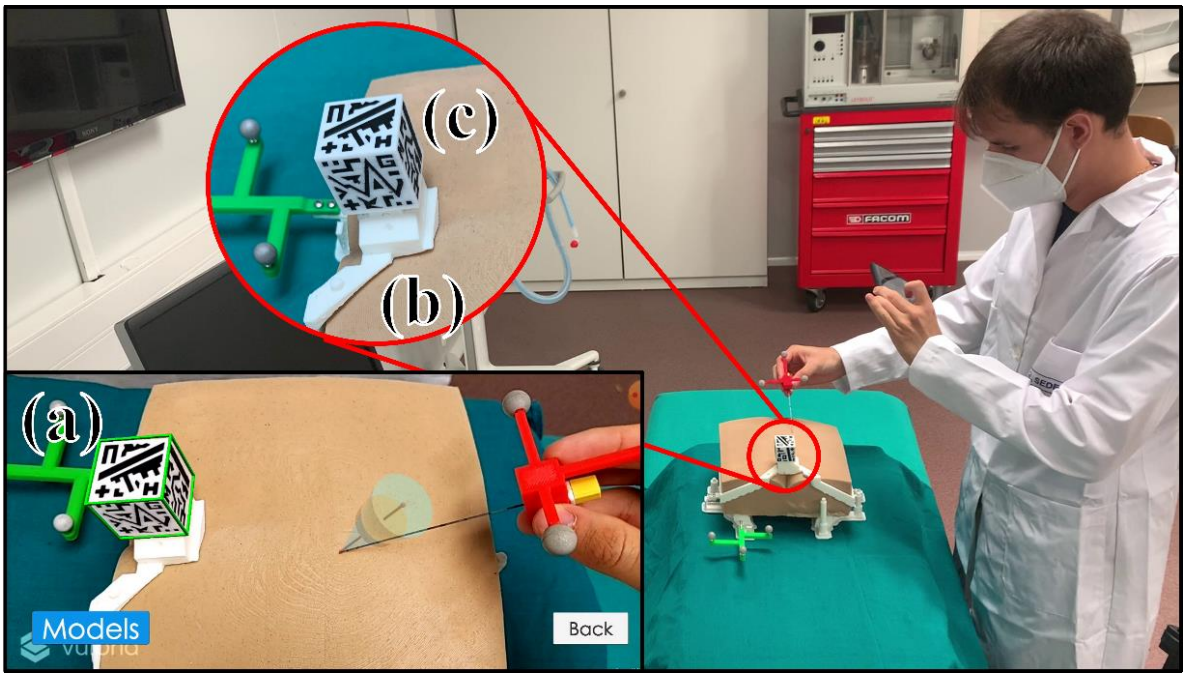

Figure 7.9. User performing needle insertion using the AR navigation system. (**a**) AR visualization on the smartphone during guidance. (**b**) 3D printed marker adaptor. (**c**) 3D printed cubic reference marker.

7.4.7. Evaluation of the navigation alternatives

Needle insertion performance was evaluated using the proposed phantom to compare the current SNS procedure with the two proposed navigation methods: optical tracking system and AR technology.

Twelve volunteers, physicians from the general surgery department at the Hospital Universitario la Paz (Madrid, Spain), participated in the experiment. Five of them were attending physicians, and seven medical residents. From the whole group, seven had prior experience in SNS procedures (experienced users), while the rest just knew about the technique (unexperienced users). None of them had previously performed the procedure as primary surgeons, and they did not have prior experience with navigation systems, neither have used them in the past nor daily.

Each volunteer followed the three navigation methods in random order. For each method, we defined the same four targets (S3 Left, S3 Right, S4 Left, and S4 Right) to be found

by each participant inserting the needle with a predefined angle and direction. For each method and user, the target order was decided randomly to control possible sequence effects. Prior to the experiment, an instructor explained each method and gave time to the participants to familiarize with the system before performing the pre-defined insertions (< 15 min). The trajectories used for training were not the same as the ones used for the examination. All the operators started with the needle in the same position on the experiment table. The insertion finishes once the needle reaches the target volume. Each time the user thought that the needle was in the target position, the actual location was obtained from the optical tracking system to check if it was correct. For the clinical method, no trajectory was predefined as physicians performed the procedure following the standard surgical practice. A total of twelve needle placements were performed by each participant, which resulted in a total of 144 needle insertions for the whole experiment.

Several metrics were recorded during each intervention:

- *Repetition total time*: the time needed to insert the needle to the target foramen.
- *Number of punctures*: the number of insertions the operator needed to reach the target. A new insertion was considered if the needle was extracted from the phantom soft tissue and inserted again.
- *Time per puncture*: time spent between each puncture: Repetition total time / Number of punctures.
- *Number of stimulations*: the number of times the user asked the instructor if the needle was in the right place.
- *Number of projections*: the number of x-ray projections taken during each repetition. This measure was only recorded during the clinical method.

After finishing the experiment, each user was asked to complete a questionnaire survey that included 31 questions to rate their experience with each technique in terms of usability, precision, and difficulty in a 5-point Likert scale.

Statistical analysis

Statistical analysis was conducted using Python 3.7 and SciPy python libraries [223]. Mann Whitney U test was used when two groups were compared. Kruskal-Wallis test was applied when comparing more than two variables, with Conover-Iman test as post hoc analysis between groups. Differences were considered to be statistically significant for p-values <0.05.

Results of the Mann Whitney U and Kruskal-Wallis tests are reported as medians, interquartile ranges (IQR) and the associated p-values, otherwise as means and standard deviations

7.5. Results

7.5.1. Sacrum segmentation performance

The segmented sacrum from the database used in this experiment had the foramina closed, which is not valid in SNS procedures as they are crucial for defining needle trajectory. We solved this limitation by removing the unwanted segmented areas with a semiautomatic method described in **Section 7.4.1**. When reviewing the segmentation masks, we detected that some areas inside the sacrum were not classified correctly, limiting the performance of the automatic segmentation algorithms. However, the shapes of the foramina were accurately segmented.

Table 7.2 shows the performance results of the network on the sacrum label for the training, validation, and testing cases. The DSC obtained on the automatically segmented sacrum is 90.35 ± 2.49. **Figure 7.10** shows the final virtual 3D model of the highest (a) and lowest (b) DSC score from the test data set. We can observe that the foramina are easily differentiated with a similar sacrum shape as the ground truth, obtaining a correct foramen size in S3 and S4 locations. However, in the worst case, it seems that the smallest foramen is almost closed in the predicted model.

Table 7.2. Sacrum performance results of the automatically segmented cases for each set (mean ± standard deviation). (DSC: Dice Score Coefficient; ASD: Average Surface Distance; HD: Harsdorf Distance)

Sacrum Performance	DSC	ASD (mm)	HD (mm)	Precision (%)	Recall (%)
Train (85%, 67)	0.971 ± 0.006	0.22 ± 0.02	7.18 ± 10.83	96.81 ± 0.71	97.47 ± 0.60
Validation (5%, 5)	0.901 ± 0.035	0.95 ± 0.33	19.05 ± 14.27	93.75 ± 3.99	88.72 ± 6.89
Test (20%, 17)	0.906 ± 0.025	0.83 ± 0.33	16.56 ± 12.12	89.11 ± 4.96	92.00 ± 4.28

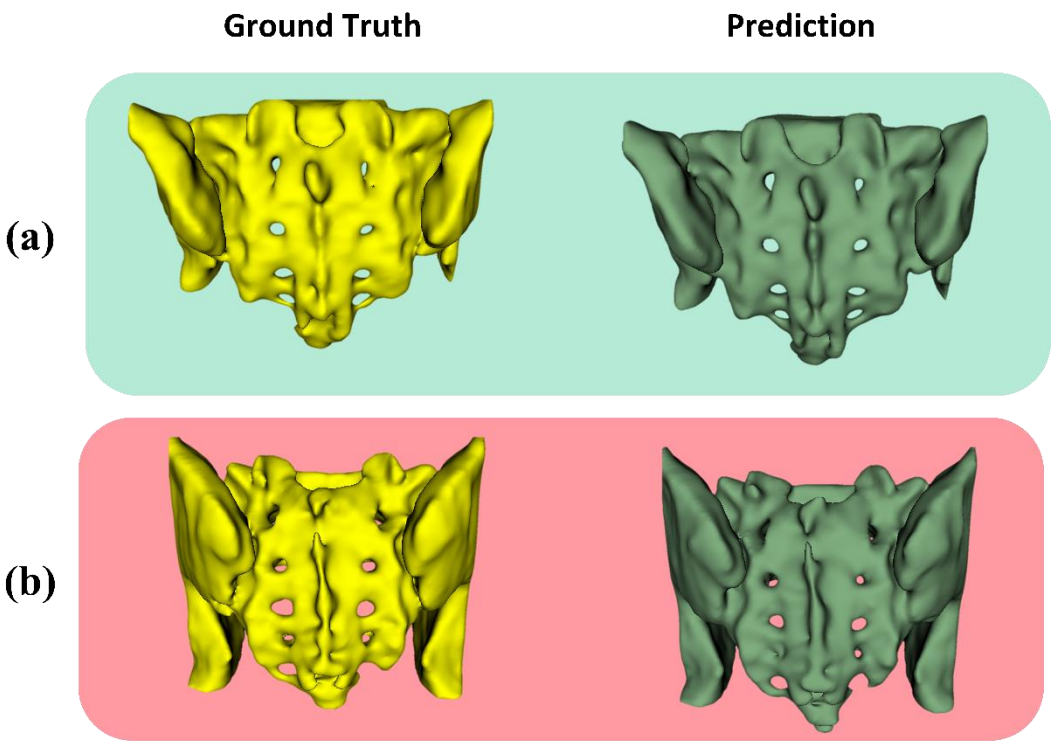

Figure 7.10. Virtual 3D model of the sacrum of two different cases. (**a**) Case with the highest dice score of the testing data set. (**b**) Case with the worst dice score of the test data set. The ground truth manual segmentations 3D models are represented on the left side and on the right side the predicted ones.

7.5.2. Evaluation results

According to the most experienced surgeons participating in the experiment, the needle insertion in the phantom was comparable to the clinical procedure. The silicone mimicking soft tissue offered a small initial resistance when trespassing the first layer, and then a smooth needle insertion until passing through the foramen. When the needle collides with the PLA of the bone, the sensation was similar to reaching bone in actual patients. The needle did not bend during the insertion in the silicone, avoiding the repetition of the pivot calibration between experiments. Due to the thick fat layer (present in the patient used to develop the phantom) and the material properties of the foam silicone, it was difficult for some physicians to localize bony landmarks on surface of the phantom. This step facilitates the orientation during the actual surgical procedure. However, it did not impede the operators from perceiving the sacrum position.

Table 7.3 represents the medians and interquartile range (IQR) obtained from the different experiments and metrics for the three evaluated methods. The median [IQR] time for the physicians was 106.64 [73.4 - 215.12] seconds with the clinical approach. In comparison, the navigation methods reduced the total time by 3 or 2 times using OTS (32.26 [24.12 - 56.71] s) and AR (53.29 [35.73 - 94.52] s) navigation systems, respectively. Moreover, with respect to the number of punctures needed to reach the target, the physicians needed 1 insertion in most cases to reach the foramen when using the OTS navigation, and 1 or 2 insertions when using the AR method. In contrast, performing the simulated clinical SNS procedure, users inserted the needle 2.0 [1.0 to 4.0] times to reach the foramen. Additionally, operators spend more time per puncture when inserting the needle with the AR system than with the OTS device. In all the metrics, there is a significant difference between all methods with a p-value <0.001.

Table 7.3. Median [interquartile range] for the evaluated metrics in all experiments grouped by guidance method.

Parameter	Clinical Method	OTS Method	AR Method	p-value
Total Time [s]	106.64 [73.40 - 215.12]	32.26 [24.12 - 56.71]	53.29 [35.73 - 94.52]	**< 0.001***
Number of Punctures	2.0 [1.0 - 4.0]	1.0 [1.0 - 1.0]	1.0 [1.0 - 2.0]	**< 0.001***
Time/Puncture [s/puncture]	51.82 [37.05 - 77.85]	30.65 [24.12 - 44.05]	41.67 [31.50 - 52.82]	**< 0.001***
Number of Stimulations	3.0 [1.0 - 7.0]	1.0 [1.0 - 1.0]	1.0 [1.0 - 2.0]	**< 0.001***

From **Table 7.3** we can also observe IQR range is larger in all metrics if we compare the data obtained when using the clinical with the navigation methods. For example, the IQR from the total time parameter is [73.40 - 215.12] s for the clinical method, and [24.12 - 56.71] s and [35.73 - 94.52] s from the OTS and AR methods, respectively. These results suggest that navigation methods may reduce subjectivity and provide similar results regardless of the previous user experience. Additionally, IQR for total time is larger for AR than with OTS.

Furthermore, for the traditional method, the participants asked for an average 10.71 (± 8.86) projections to complete the task. This value indicates that the radiation exposure to the patient would have been 6.4 (mSv) if we estimate that each projection radiates 0.6 mSv [224]. No x-ray projections would be needed when using the proposed navigation systems while navigating the needle.

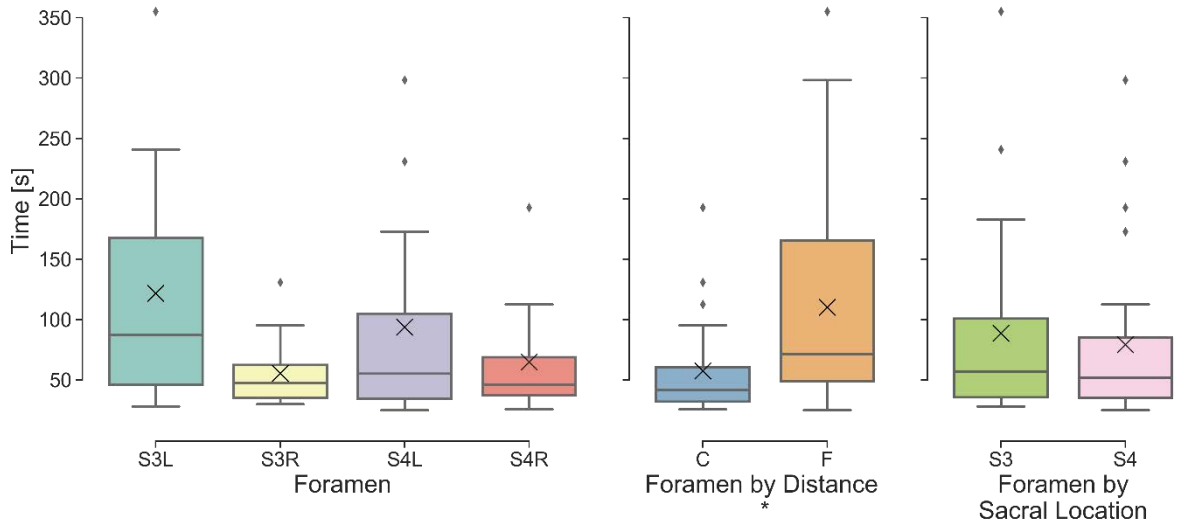

(**a**)

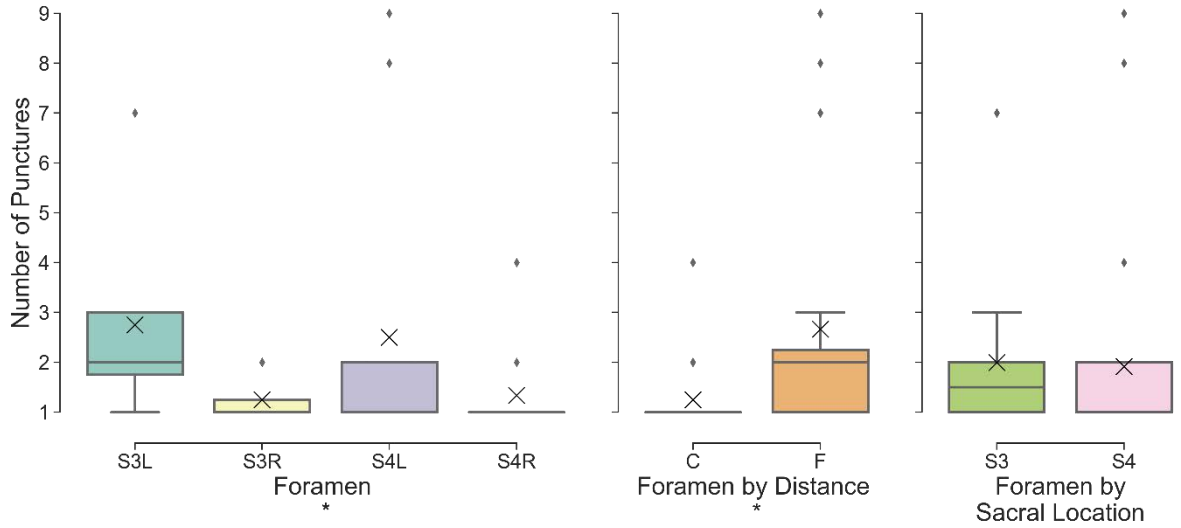

(**b**)

Figure 7.11. Boxplots from experiments when physicians performed the needle insertion while using the AR method as guidance. The results are grouped by target distance and target sacral location. (**a**) Distribution of the time needed to perform the task. (**b**) Distribution of the number of punctures needed to reach the target. The horizontal line inside the box represents the median and the cross the mean of each data set. (*) indicates significant ($p < 0.05$) statistical comparison.

When comparing metrics grouping the results by target, we did not see any significant difference, except when using the AR method. **Figure 7.11**a and **Figure 7.11**b show the distribution of the total time and number of punctures, respectively, when the operators performed the task with AR guidance. Each boxplot shows three different grouping criteria: on

the left, by target foramen (S3L, S3R, S4L, S4R), on the center, by distance from the operator (close, C; far, F) and on the right, by foramen sacral location (S3, S4). The distribution demonstrates that the physicians performed significantly worse (p-value <0.05) when the foramina are farther away in both metrics. Moreover, although no significant differences are found in all metrics when comparing the different targets, the plots show a tendency for a higher number of punctures and longer spent time in smaller foramina for all methods.

When comparing the different metrics grouped by the hierarchy of the physician (residents vs. attending physicians), we did not find any significant difference. However, we found different results between inexperienced and experienced users. **Table 7.4** presents the results separated by method and type of user (experienced and inexperienced). Focusing on the clinical method, we found that inexperienced users inserted the needle significantly fewer times (1.0, [1.0 - 2.0]) compared to experienced users (3.0, [1.0 - 5.25]). This probably means that experienced users prefer to repeat the insertion and not rummage in the patient while the needle is inserted. Looking at the OTS method, we found that experienced users took significantly longer times to perform the task ($p < 0.05$). This is an unexpected finding that may indicate that experienced users prefer to take their time to obtain a successful result, trying to avoid unnecessary harm to patients while performing the insertion.

Table 7.4. Median [interquartile range] for the evaluated metrics grouped by method (clinical and OTS navigation) and type of user (inexperienced and experienced).

Method	Parameter	Inexperienced	Experienced	p-value
Clinical	**Total Time [s]**	77.29 [68.47 - 154.00]	148.56 [80.51 - 234.19]	0.076
	Number of Punctures	1.0 [1.0 - 2.0]	3.0 [1.0 - 5.25]	**0.036***
	Time/puncture [s/puncture]	65.59 [44.16 - 85.59]	47.28 [27.86 - 77.07]	0.062
	Number of Stimulations	1.0 [1.0 - 4.0]	4.5 [2.0 - 7.5]	**0.029***
OTS Navigation	**Total Time [s]**	29.18 [19.92 - 34.95]	43.25 [27.53 - 67.37]	**0.021***
	Number of Punctures	1.0 [1.0 - 1.0]	1.0 [1.0 - 1.0]	0.226
	Time/puncture [s/puncture]	27.92 [19.92 - 33.03]	31.69 [27.53 - 49.84]	**0.033***
	Number of Stimulations	1.0 [1.0 - 1.0]	1.0 [1.0 - 1.0]	0.337

Survey results

All participants, twelve in total, answered the questionnaire. The barplot from **Figure 7.12** shows the answers for ten selected questions related to the experience and personal thoughts about each method. All the operators think that the actual procedure should be

improved to be easier (average score of 4.58). Furthermore, 91.7 % (11) of them assigned the highest score (total agreement, 5) when asked if more training is needed to practice the current procedure. The operators also think that the proposed x-ray software simulator and the manufactured phantom could be a useful training tool for current SNS procedures (mean score 4.83). Moreover, most of them (66.7 %) gave the maximum score to the usability of the OTS navigation system, responding with an average score of 4.67 that the information provided by the system was easy to interpret and with 4.75 that it was useful to know the needle position in real time. Regarding AR, 27.3 % (3) of the surgeons never heard of it before, 18.2% (3) heard about the technology but did not know what it was, 36.4 % (4) knew about the technology but had never used it, and just 18.2 % (2) have used this technology before. The operators believed that the information displayed on the smartphone was easy to interpret, with an average score of 4.08. Although the physicians think that smartphone use in a sterilized case could be feasible in the operating room (4.33), they prefer AR devices that let them have both hands available during surgery. 66.7% agreed that they would feel more confident in SNS procedures using any of the two navigation systems.

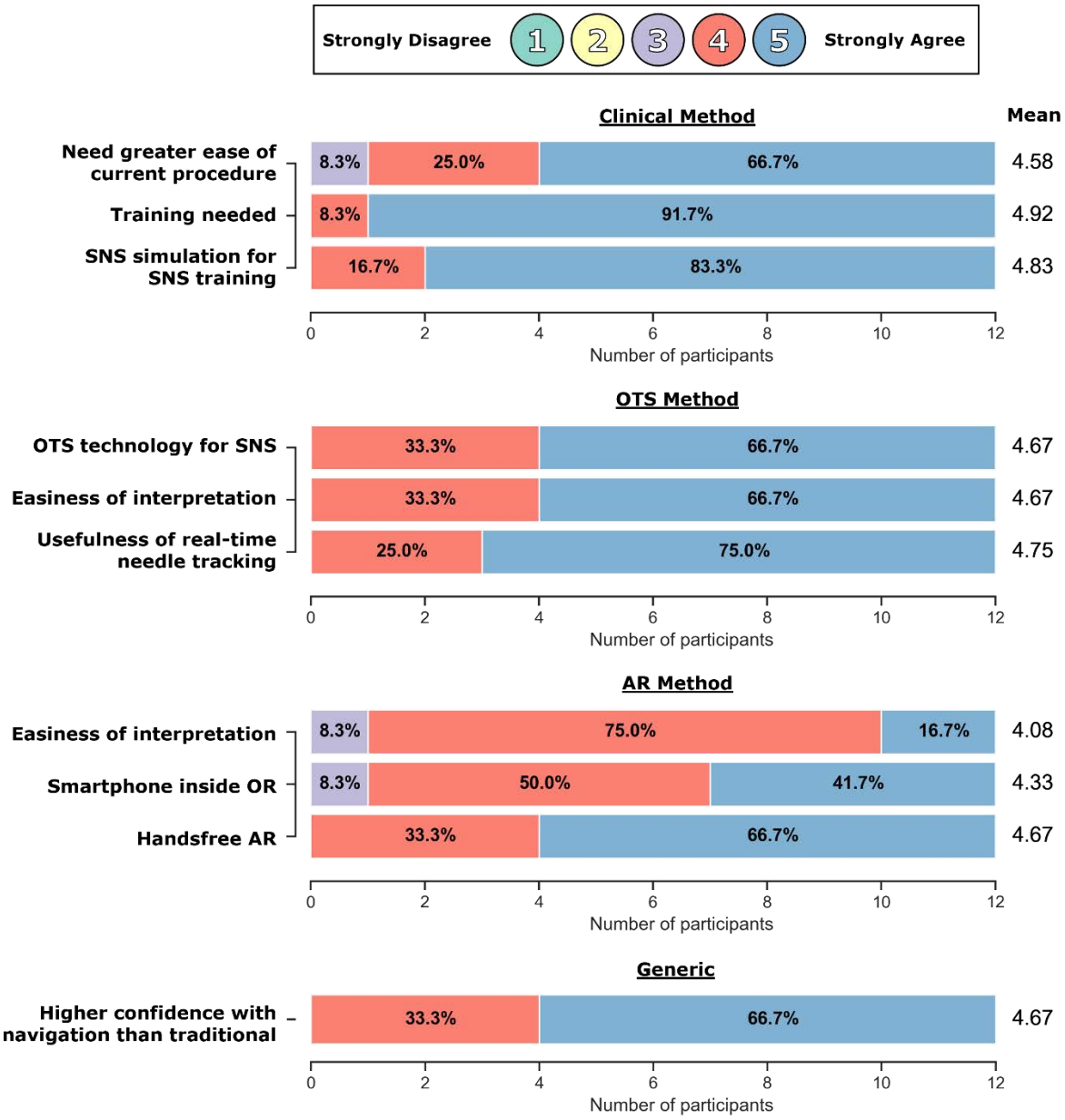

Figure 7.12. Distribution of scores obtained on ten selected questions from the whole questionnaire.

To conclude the survey, we asked the participants to compare all methods in terms of difficulty and training needed to use them in a clinical setting, providing an order of preference. They believed that the current SNS procedure is more complicated than the other two, being the OTS system the easiest. They also think that the clinical method would need more training than OTS and AR to become an expert on this technique. Additionally, 75.0 % (9) of the participants would choose OTS navigation as the first choice for SNS procedures, followed by AR, and almost all of them (11) would rather use any of the two proposed navigation methods than the actual procedure. All the results are represented in **Table 7.5**.

Table 7.5. Average (± standard deviation) scores obtained in questions comparing each method in terms of difficulty and training needed.

Question		Clinical Method	OTS Method	AR Method
General Difficulty		3.75 ± 0.75	2.25 ± 0.87	2.75 ± 1.06
Initial Difficulty		3.58 ± 0.67	1.83 ± 0.72	2.08 ± 0.9
Need Previous Training		4.92 ± 0.29	4.0 ± 1.21	3.92 ± 0.9
How Much Training		4.25 ± 0.87	2.33 ± 0.89	2.75 ± 1.06
Faster Insertion		-	4.67 ± 0.49	4.5 ± 0.67
More Precise Insertion		-	4.67 ± 0.49	4.5 ± 0.52
More Confidence		-	4.83 ± 0.39	4.58 ± 0.51
Would you use it?		-	4.75 ± 0.45	4.67 ± 0.49
Order of preference	**1st**	0.0 %	**75.0 %**	25.0 %
	2nd	8.3 %	25.0 %	**66.7 %**
	3rd	**91.7%**	0.0 %	8.3 %

7.6. Discussion

In this study, we have presented and evaluated two alternative surgical navigation systems to guide electrode placement in SNS procedures. The objectives were to reduce surgical time, minimize patient discomfort and improve surgical outcomes. The first proposal is based on optical tracking to guide needle insertion. In contrast, the second alternative presents a smartphone-based AR system to virtually superimpose the planned trajectory on the surface of the patient. Furthermore, we designed an automatic sacrum segmentation method to speed-up the definition of the virtual models, needed for trajectory definition, from the CT study. We have also developed an x-ray software tool simulator to compare our navigation solutions with the clinical method. The feasibility of the proposed systems has been evaluated by twelve physicians on a realistic anthropomorphic phantom.

Thanks to the developed machine learning algorithm, we can automatically segment the sacrum from the CT study in less than one second, eliminating one of the drawbacks from our previous work [213]. This method would reduce delays in the intervention, decreasing the stress experienced by the engineers involved in the process. The results achieved great accuracy with an average DSC of 0.906 for our method, calculated on the 17 subjects from the test set. This value is similar to the 0.92 DSC values for the sacrum reported by Wang et al. [215] on

the same database [216]. Moreover, we have created 3D virtual models from the segmented masks, observing that both S3 and S4 foramina are completely visible, allowing the needle trajectory definition before the surgical intervention.

During the evaluation, twelve physicians performed a total of 144 needle insertions. With this experiment we have compared both navigation alternatives with the clinical method in terms of number of punctures and time to complete the task. From these metrics we can observe that users performing any of the proposed navigation solutions took less time to complete each insertion, needed less punctures to reach the target, spent less time per puncture and needed a smaller number of stimulations, compared with the clinical method. Additionally, the results achieved from our navigation solutions in terms of average number of punctures (1.23 ± 0.59 and 1.96 ± 1.90 for the OTS and AR methods respectively) and mean puncture time (36.83 ± 20.40 s and 44.43 ± 17.53 s for the OTS and AR methods respectively) are comparable[1] with the ones found in the literature that used alternative navigation procedures in patients, obtaining similar values for number of punctures (1.5 ± 0.7) and mean puncture time (246 ± 132 s) [205]. Our solutions could improve surgical outcomes and reduce patient pain and discomfort during surgery.

The augmented reality alternative uses a smartphone to display virtual elements overlaid on the patient. However, the need to hold the device with one hand might not be the best option in a surgical scenario, since surgeons usually require the use of both hands continuously. Although this is a handicap, results from the experiment showed that AR improved the metrics compared to the clinical method. Nevertheless, depth perception and registration are limiting factors in AR. Participants needed significantly more punctures and total time to reach the farthest away target foramina. This can be explained by the difficulty in orienting the smartphone to correctly visualize the trajectory line perpendicular to the needle insertion point. This problem increases with the distance from the user, as can be observed in **Figure 7.9**, and produced a displacement of the needle trajectory when it was inserted. Additionally, marker-based registration is still a nuisance, as the marker always needs to be visible, frustrating users when the detection fails. As an alternative, surface recognition could be a solution to this problem, but accuracy results are still far from those obtained with marker-based registration [225].

[1] **Table 7.3** shows medians and interquartile range, but we calculated means and standard deviations from our original data for this comparison with previous literature.

Looking into the future, head-mounted displays, such as Microsoft HoloLens 2 [226], could be the perfect hands free AR alternative. This device recognizes hand gestures and voice commands to control the user interface. It can also superimpose virtual information on see-through holographic lenses with high accuracy. This device overcomes the main limitations of using the smartphone as AR device. Although recent studies have proposed HoloLens 2 as surgical guidance device [227], [228], registration, depth perception, and spatial awareness are still the main drawbacks that limit its use in everyday practice. Not to mention AR technology is still unknown for many physicians, as we could see in our survey results.

Although AR seems a promising alternative, participants obtained better results in all the metrics when using the more traditional optical navigation system. This solution had a better reception from the physicians, as it was more intuitive and easier to learn. Although the need to remove the attention from the phantom, looking away at an external display, could be the main drawback, they still performed better. Indeed, one of its best features is tracking the needle position in real time, which helped the surgeons to insert the needle more confidently as depth was continuously reported. This feature could be included in the AR navigation to improve depth perception by adding an extra marker to the needle holder [228], [229]. However, this reference needs to be large enough to be detected by the AR camera, adding extra weight that could limit the manipulation of the needle. The current state of the art in AR needs improvement, so traditional navigation is still the best solution in the near future.

Regarding insertion time, experienced users were significantly slower and performed a higher number of insertions in comparison with inexperienced participants. Experienced users know that performing shorter insertions involves less suffering for the patient, although it may take longer times or more punctures to reach the target foramen. Additionally, the metrics when using navigation show a lower interquartile range, indicating that the variability between surgeons is reduced, as they achieve similar results no matter the patient or the target.

Actual SNS training methodologies are just based on theoretical lectures combined with surgical procedures where trainee physicians participate as passive spectators. When practical lessons are offered, they are limited to performing the procedure in pigs. As shown in the results from our survey, all the participants, including experienced users, believed that more SNS training should be offered, including practical sessions. For that reason, we believe the proposed simulation software and the manufactured phantom could be easily adapted for low-

cost training, teaching professionals SNS needle insertion without involving animal experiments.

Tracking systems or AR technologies have been previously proposed as navigation solutions for needle insertion guidance in surgical procedures. However, these alternatives have only been implemented in phantoms, under controlled conditions [49], [230]. Although results suggests that they could be translated to clinical scenarios, they do not propose a feasible clinical workflow. Hetch et al. offered an AR navigation solution with a reference marker for registration in a phantom, but this registration method could not be easily implemented inside the OR [110]. For this reason, the following section presents our proposal of a feasible surgical workflow to introduce both proposed methodologies, including registration steps, in clinical scenarios.

7.7. Surgical workflow proposal

We evaluated the proposed systems on a phantom, but steps such as tool calibration or image-to-patient registration would not be feasible in an actual surgical scenario. Therefore, this section introduces a practical surgical workflow for each suggested navigation methodology that could be implemented in the operating room.

Figure 7.13 is a flowchart diagram that represents each step for both navigation systems. Both have the following steps in common:

1. Patient CT scan acquisition right before the surgical intervention in prone position.
2. CT scan transfer to the automatic segmentation workflow, obtaining a virtual 3D model of the sacrum.
3. Manual selection of the target foramina by using 3D Slicer and virtual navigation 3D models creation.
4. Image-to-patient intraoperative registration.
5. Needle guidance using the selected navigation system.

Steps 4 and 5 will be explained in detail for each method in the following subsections.

7.7.2. Optical tracking system workflow

The left side (in blue) of **Figure 7.13** represents the surgical workflow using the OTS navigation system. First, before the CT acquisition, skin fiducials are placed on the patient's skin surrounding the affected area. These fiducials are identified in the CT scan while defining the needle trajectory and transferred to the navigation software.

The patient should be lying in a prone position in the OR with the skin fiducials accessible and looking upwards. The optical tracking device is mounted on a tripod, ensuring that it covers the surgical area. A patient RB is fixed on the skin close to the affected area to compensate for patient's movements. The NDI probe is used to record points on the skin fiducials, and these coordinates enable patient-to-image registration with a point-based algorithm. Then, a customized sterilized needle adaptor is placed on the needle. The distance from the tip to the RB is calculated by performing pivot calibration on one side of the patient's bed without requiring any movement of the OTS cameras.

After registration, navigation could start. First, the support engineer initializes the software with the navigation models that have been automatically segmented. Then, the physician chooses which specific foramen to target. From an automatically predefined trajectory, the physician gives feedback to the engineer updating this path for correct needle insertion. Once the trajectory has been decided, the physician performs the insertion following the navigation software guidance. After the needle reaches the target point, the final position is verified with an x-ray projection. Finally, the customized cap is easily removed from the needle to proceed with the surgical procedure, ensuring that the needle position is not modified.

7.7.3. Smartphone augmented reality application workflow

The right side (in green) of **Figure 7.13** shows the surgical workflow steps for the AR navigation system. Once the patient is in prone position and the surgical asepsis has been ensured in the OR, the registration procedure is performed. First, a customized marker adaptor is fixed on the skin of the patient, right above the gluteus. This marker adapter is 3D printed in biocompatible resin material to be in contact with the patient. Then, the sterilized 3D printed cubic reference marker is placed on the adaptor. In order to obtain the exact position of the marker with respect to the patient's anatomy, a two-step registration is performed [112].

First, a mobile structured light scanner, Artec EVA® (Artec Group, Luxembourg), is used to acquire 3D photographs, including geometric and textural information, of the surgical field, encompassing the patient's visible skin surface and the black and white patterns of the cubic reference marker. With this information, we can apply a surface-to-surface registration algorithm to align the acquired 3D texture of the skin surface with the skin model obtained from the CT scan of the patient. Then, we identify seven landmarks from the marker patterns on the 3D textured images. These landmarks are used to compute the position of the marker with respect to the patient after a fiducial-based registration. Finally, the virtual models' position is calculated and uploaded to the AR smartphone application to ensure accurate visualization of the needle's trajectory during the intervention.

To start the navigation, the smartphone is introduced in a sterilized case (CleanCase, Steridev Inc., Lansing, MI, USA) to maintain the asepsis of the surgical field. Then, the surgeon opens the *SacralNSAR* application and selects the desired target foramen. After that, with the smartphone on one hand, and the needle on the other, the surgeon points to the marker reference with the camera. Once it is detected, the trajectory of the needle is displayed overlaid in the surgical field. The surgeon is guided by the AR app to finally insert the needle, rotating the smartphone at any orientation to better understand the optimum trajectory and the target insertion depth. Once the needle is inserted, the surgeon acquires an x-ray projection to verify the correct position of the needle. Once the lead is finally in the desired position, the navigation finishes.

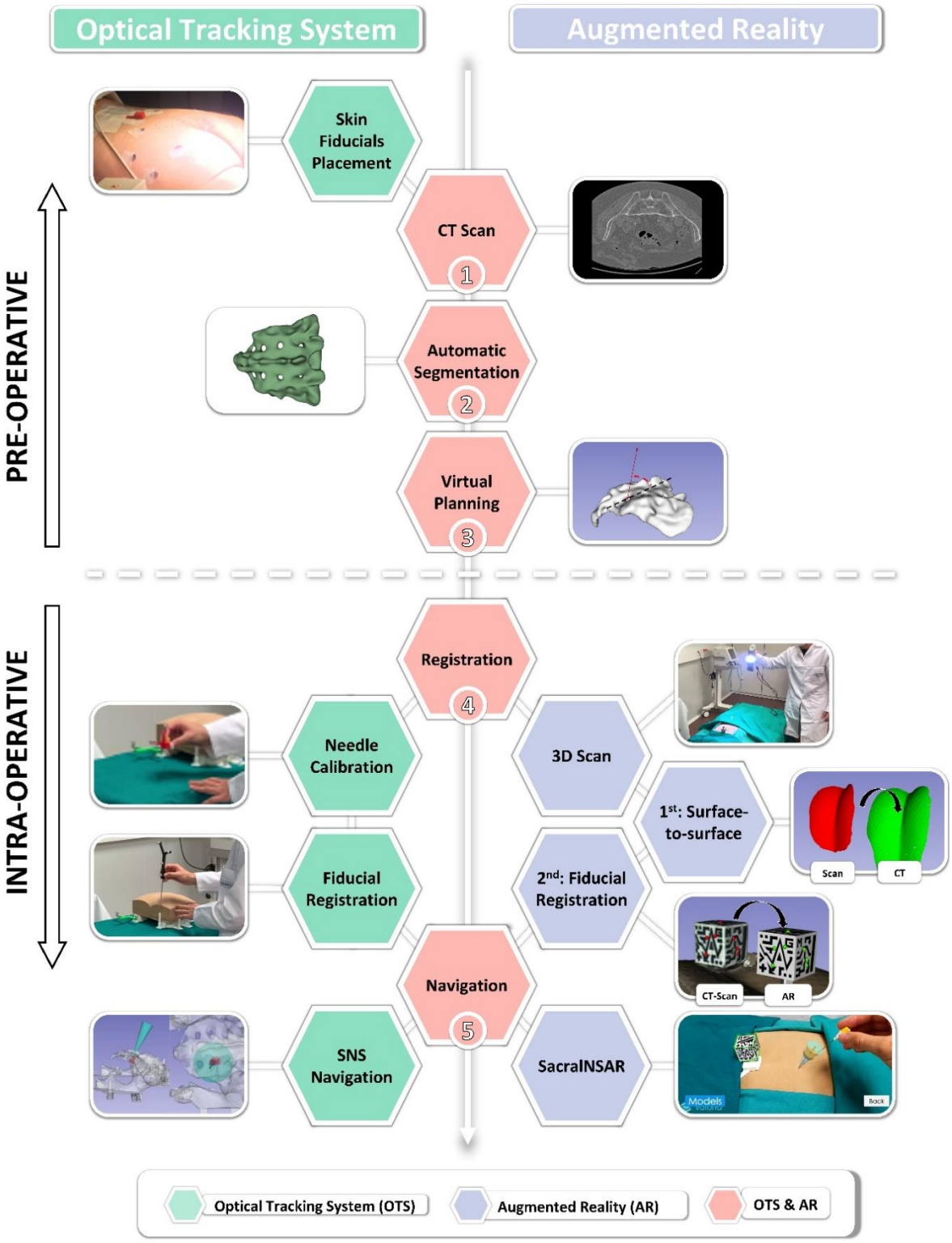

Figure 7.13. Proposed surgical workflow. Left side (blue) represents the proposed surgical workflow using optical tracking for the navigation system and the right side (green) shows the proposal for the augmented reality navigation system.

7.8. Conclusion

In conclusion, we have shown two navigation alternatives, one based on traditional tracking systems and the other one on AR technology, that could improve surgical outcome in by reducing surgical time and patients' pain, significantly reducing needle insertions in SNS procedures. The two alternatives have been evaluated by twelve physicians performing several needle insertions tasks in an anthropomorphic phantom with each navigation system and on a clinical procedure simulator. We believe that these solutions are feasible to replace current SNS clinical procedures, although AR technology still needs to be improved until it finally reaches a clinical scenario.

Part of the content of this chapter is currently under review for publication in the journal Computer Methods and Programs in Biomedicine:

R. Moreta-Martinez, I. Rubio-Pérez, M. García-Sevilla, L. García-Elcano, J. Pascau. "Novel framework for needle navigation in sacral nerve stimulation: traditional vs optical navigation vs augmented reality". Computer Methods and Programs in Biomedicine (2021) [submitted]

This chapter also contains parts from the work that was presented in the Computer Assisted Radiology and Surgery Proceedings of the 35th International Congress and Exhibition (CARS 2021):

R. Moreta-Martinez, M. García-Sevilla, D. García-Mato, A. Pose-Díez-de-la-Lastra, I. Rubio-Pérez, J. Pascau. "Smartphone-based augmented reality system for needle insertion guidance in sacral nerve stimulation". In: CARS 2021 - Computer Assisted Radiology and Surgery Proceedings of the 35th International Congress and Exhibition, Munich, Germany, June 21–25, 2021. Int J CARS 16, 1–119 (2021)

8

Discussion

In In the last twenty years, personalized medicine has changed the medical practice by focusing on the problems and needs of each patient as an individual, thanks to the significant advances in healthcare technology [2]. In surgical procedures, personalization has been possible thanks to key navigation technologies that allow physicians to provide individualized treatment adapting to patients' features and anatomy. Tracking systems, augmented reality (AR), 3D printing, and artificial intelligence (AI) have been part of this process [28], [46], [69], [102]. However, their independent contributions show several limitations in terms of patient-to-image registration, lack of flexibility to adapt to the requirements of each case, large preoperative planning times, and navigation complexity. In this context, we focused our research on combining all these technologies to introduce surgical navigation in more complex cases, create new patient registration methods, facilitate access to augmented reality by the medical community, and automate clinical procedures.

Surgical navigation has shown potential benefits in orthopedic oncologic surgery thanks to the development of commercial navigation systems that have been designed for specific procedures [119], [120]. However, commercial devices have a high cost and lack the flexibility to adapt to the requirements of every case, showing no clear benefits in procedures such as the resection of acral tumors (those located in distal extremities such as hands or feet). These extremities have a large number of joints with complex movements, so traditional registration methods do not provide sufficient accuracy. To overcome these limitations, we presented a surgical framework that combines open-source navigation software, optical tracking system (OTS) and desktop 3D printing to achieve accurate tumor resection.

Our solution used additive manufacturing to create a patient-specific mold that maintained the same pose for the distal extremity during preoperative imaging and image-guided surgery. We validated how low-temperature sterilization did not significantly deform the 3D printing polylactic acid (PLA) material. The combination of open-source navigation software and 3D printing allowed us to track surgical tools with specific adaptors on the instruments. The feasibility of the proposed workflow was evaluated in two clinical cases (soft-tissue sarcomas in hand and foot). First, we achieved an overall accuracy of the system of 1.88 mm evaluated on the patient-specific 3D printed phantoms. Then, surgical navigation was implemented on the surgical procedures showing that the proposed surgical workflow could be easily integrated into the operating room to ensure proper margin during acral tumor removal. Surgeons gave positive feedback, suggesting that our solution could benefit acral tumor resection by reducing errors and increasing surgeons' confidence.

Traditional navigation devices have been used in computer-assisted surgeries for the past thirty years with great success [30], [31]. Nevertheless, AR presents great potential to overcome some of their limitations, such as the display of navigation information, which requires the surgeon to divert his attention from the patient. Microsoft HoloLens head-mounted display could solve this issue by showing virtual information right in front of your eyes on a semitransparent screen. However, current registration solutions were manual and complex methods [107], [108], not practical for surgical applications in orthopedic oncology. To overcome this limitation, we introduced 3D printed patient-specific surgical guides with a tracking marker for automatic registration. This registration method was validated on a 3D printed patient-specific phantom, showing that the surgical guide position on the bone could be replicated with an accuracy of 2 mm and that AR visualization error was lower than 3 mm. The solution was then evaluated during the actual surgery, where surgeons obtained a fast automatic patient-to-image registration with the surgical guide. They could visualize the skin, affected bone, tumor and the medical images right on top of the patient during the intervention. Our results illustrated the feasibility of the proposed AR solution for surgical guidance in cases where rigid body structures such as bone are accessible.

Medical applications of AR have grown exponentially in recent years [39]. In the study presented in **Chapter 4**, we realized that devices such as Microsoft HoloLens can bring AR features to surgical treatments in ways that were not imaginable before. However, these gadgets are still in their early technological stages and their price limits the adoption by physicians. On the other hand, smartphones could be used as AR devices, accelerating the spread of this

technology in healthcare. Nevertheless, developing AR solutions requires advanced software engineering skills. To solve this issue, we have presented a step-by-step methodology that enables inexperienced users to create a smartphone app combining AR and 3D printing to visualize anatomical 3D models. The proposed protocol requires freely available software and provides access to a GitHub repository with a clinical example and the necessary materials to 3D print a cubic reference marker for AR visualization. Furthermore, we showed four clinical cases where the final AR application benefits surgical specialties such as maxillofacial, neuro, or orthopedics. We believe that our protocol contributes to accelerating the adoption of AR by medical professionals. In less than two years after the publication of the video article [157], we have reached more than 10.000 views, demonstrating an incredible interest in these technologies in the biomedical field.

The next step was to show the benefits of these technologies when implemented in a complete surgical workflow in orthopedic oncology, including preoperative planning, patient communication, and surgical intervention. First, we evaluated the approach in six 3D printed phantoms based on patients suffering from a large variety of tumors on different anatomical locations. We verified the uniqueness of the 3D printed surgical guide positioning on the bone, achieving slightly lower errors (1.75 mm) than those presented in **Chapter 4**. However, this time we used a biocompatible resin material that could withstand the high temperatures from more common sterilization techniques and contact the patient for more extended periods. The marker developed in **Chapter 4** was planar, but the cubic reference marker designed in **Chapter 5** allowed visualization of registered virtual data from different points of view. The measured AR tracking error was of 2.80 mm, a value similar to that obtained in **Chapter 4** using HoloLens. However, in some areas further from the marker, errors were larger. This must be considered when designing applications. Nonetheless, working volumes are limited around the surgical guide in orthopedic oncology, decreasing the importance of this error source.

After this phantom evaluation, the methodology was favorably tested during the complete medical workflow on two clinical cases. According to the surgeons' feedback, the AR 3D visualization allowed establishing a surgical strategy more confidently during preoperative planning. Both patients welcomed this technology to understand their situation better, and surgeons found it very useful to explain the pathology and surgical approach. During surgery, the AR system displayed the corresponding tumor position on top of the patient with virtual anatomical elements, boosting surgeons' confidence to verify that the tumor had been adequately resected.

As a final contribution, we have combined AR, 3D printing, and navigation to improve electrode placement accuracy in sacral neurostimulation (SNS) surgeries. Our research group proposed a surgical navigation system based on an electromagnetic tracking for these procedures [213]. However, it presented limited software functionalities, long preoperative planning times, and several distortions at the OR that could affect tracking accuracy. In **Chapter 7**, we gather all the experience acquired from previous works to propose new solutions to overcome the limitations mentioned above and improve needle placement in SNS procedures. We proposed and evaluated two different navigation systems to guide electrode placement in order to reduce surgical time, minimize patient discomfort and improve surgical outcomes in SNS. We compared three alternatives: optical tracking of the needle, smartphone-based AR application for virtual guidance and the standard clinical method.

Twelve physicians performed needle insertions through a specific target to validate the performance of all alternative SNS methods on a realistic anthropomorphic phantom. With each navigation solution, we observed that users took less average time to complete each insertion (36.83 seconds and 44.43 seconds for the OTS and AR methods respectively) and needed fewer average punctures to reach the target (1.23 and 1.96 for the OTS and AR methods respectively) than following the standard clinical method (189.28 seconds and 3.65 punctures). These results are comparable with those found in the literature that used alternative navigation procedures in patients [205].

Finally, we proposed a feasible clinical workflow to use both navigation methodologies during a clinical intervention. One step of the workflow included the segmentation of the sacral bone right after the CT acquisition. We developed an AI algorithm that can automatically segment the sacrum mask from the medical image to create the virtual 3D model used to define the needle trajectory before surgery. This automatic method could reduce delays in the intervention and decrease stress experienced by the staff involved in the procedure. The segmentation results were accurate compared with the values reported in the literature on the same database [215], [216]. Additionally, the proposed clinical workflow offers feasible intraoperative patient-to image registration, solving the major problem encountered in this kind of scenarios.

In this last study, we showed how AR technology could significantly improve the clinical procedure by displaying the needle trajectory directly over the patient. However, the need to hold the smartphone device with one hand limits surgeon's mobility. HoloLens is

currently the best alternative available for surgical interventions, since the surgeon visualizes guidance information in the OR hands-free. Nevertheless, both kinds of AR devices still have several limitations. Depth perception is deficient as shown in **Chapter 7**, where results were worse in cases where the smartphone was harder to position in the proper orientation, misleading the trajectory. This limitation may be reduced once AR technology improves. Our AR registration methodology also obstructs surgeon's movements during the intervention to ensure that the reference marker is constantly visible. The future of registration will be markerless, as new advances in sensors and cameras should improve detection inside the OR providing completely automatic patient registration without any extra tools. However, we are still far away from surface detection as a primary patient registration method.

Although AR seems a promising alternative to replace current surgical navigation technologies, more traditional navigation systems are still better in some cases. OTS, although requiring to divert the attention from the patient when looking at the navigation display, had a better response from the physicians, being more intuitive and easier to learn. AR is a promising alternative for teaching and training. However, more improvements are needed on AR to replace traditional navigation, which is still the best solution in the near future.

Right now, we are living a technological transition in surgical treatments. AI has shown a phenomenal capacity to automatize medical image analysis, accelerating personalization in many clinical treatments. Conventional navigation devices will probably disappear, letting the path to augmented reality systems once these devices provide substantial benefits. 3D printing is here to stay and, indeed, it will accelerate personalization in hospitals both for patients and physicians. Finally, patient-to-image registration and tool tracking will be marker-less thanks to the use of AI.

In this thesis we have demonstrated that the combination of technologies such as tracking systems, augmented reality, 3D printing, and artificial intelligence overcomes many limitations in surgical treatments. Our results encourage the medical community to combine these technologies to improve surgical workflows and outcomes in more clinical scenarios.

9

Conclusions

The main contributions and conclusions of this thesis are as follows:

- We proposed a novel framework for acral tumor resection combining desktop 3D printing and surgical navigation. We used 3D printing to create a patient-specific mold enabling automatic patient-to-image registration for surgical navigation. The simulation with 3D printed limbs and its application in two clinical cases demonstrated the feasibility of the solution for guiding acral tumor resection.

- We evaluated surgical guidance with augmented reality using 3D printed patient-specific surgical guides containing a tracking pattern for automatic patient-to-image registration in orthopedic oncology. The results show that the surgical guide can be placed precisely on the reference bone anatomy. During the surgical intervention, this solution allowed physicians to visualize bone, tumor and medical images overlaid on the patient using Microsoft HoloLens.

- We designed a step-by-step guide that enables inexperienced users to create a smartphone app combining augmented reality and 3D printing to visualize anatomical 3D models obtained from patient data. Our solution brings AR closer to the final clinical user, combining free and open-source software with an open-access protocol.

- We presented and evaluated a novel framework deployed in orthopedic oncology combining augmented reality on a smartphone and 3D printing to assist at different stages of the surgical workflow. 3D printed patient-specific surgical guides with a cubic reference marker were accurate for patient registration. Our method supports surgical planning, enhances patient communication, and provides guidance during surgical interventions.

- Two surgical navigation systems were developed and evaluated to guide electrode placement in sacral neurostimulation (SNS) procedures based on optical tracking and augmented reality. Our results show that both systems could minimize patient discomfort and improve surgical outcomes by reducing needle insertion time and number of punctures. Additionally, we proposed a feasible clinical workflow for guiding SNS interventions with both navigation methodologies, including automatically creating sacral virtual 3D models for trajectory definition using artificial intelligence and intraoperative patient-to-image registration.

10

Supplementary Material

10.1. Pectoralis muscles and subcutaneous fat segmentation

Body composition measurements are considered very valuable for patient treatment, as the distribution of fat and muscle in the body is critical in several conditions. In the case of chronic obstructive pulmonary disease (COPD), pectoralis mass area (PMA) and subcutaneous adipose tissue (SAT) measurements from one chest CT image slice have demonstrated to be more clinically relevant biomarkers than others, such as body mass index, which are more commonly used [231].

Regardless of the potential of body composition analysis, these measurements are still cumbersome to obtain, since manual or semi-automated segmentation methods are required, preventing their clinical use. Thus, better and more automated techniques for body composition quantification are needed [232]. In this work, we proposed a complete automated segmentation workflow based on convolutional neural networks (CNNs) to obtain clinically relevant PMA and SAT measurements from CT images. First, structures were detected with the method proposed by Onieva et al. [233], which uses CNNs to automatically identify a reproducible axial slice from a CT where pectorals and fat are visible. Second, body composition measurement is predicted on the selected slice by segmenting pectoralis muscles and subcutaneous fat with a U-Net based CNN architecture. **Figure 10.1** shows the anatomical structures that are automatically segmented through the trained neural network.

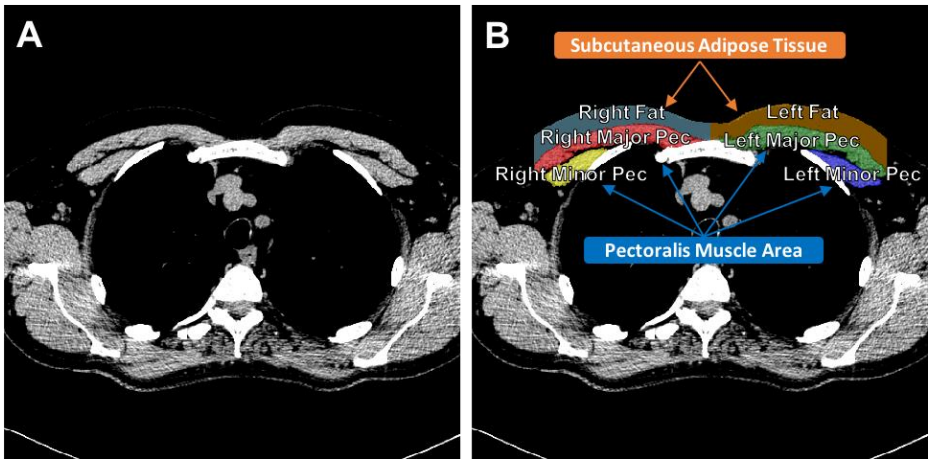

Figure 10.1. (**A**) Axial CT scan slice. (**B**) Segmented anatomical labels that contribute to the calculation of the pectoralis muscle area (PMA) and subcutaneous adipose tissue (SAT) measurements.

Our method showed a high correlation with clinically relevant outcomes in a large COPD database, matching the previously reported results obtained with manual segmentations. Best and worst segmentation results are illustrated in **Figure 10.2**. Additionally, the automatic body composition measurements from CT scans obtained through our automatic segmentation workflow have aided in finding the correlation between respiratory exacerbations and muscle loss in current and former smokers [234].

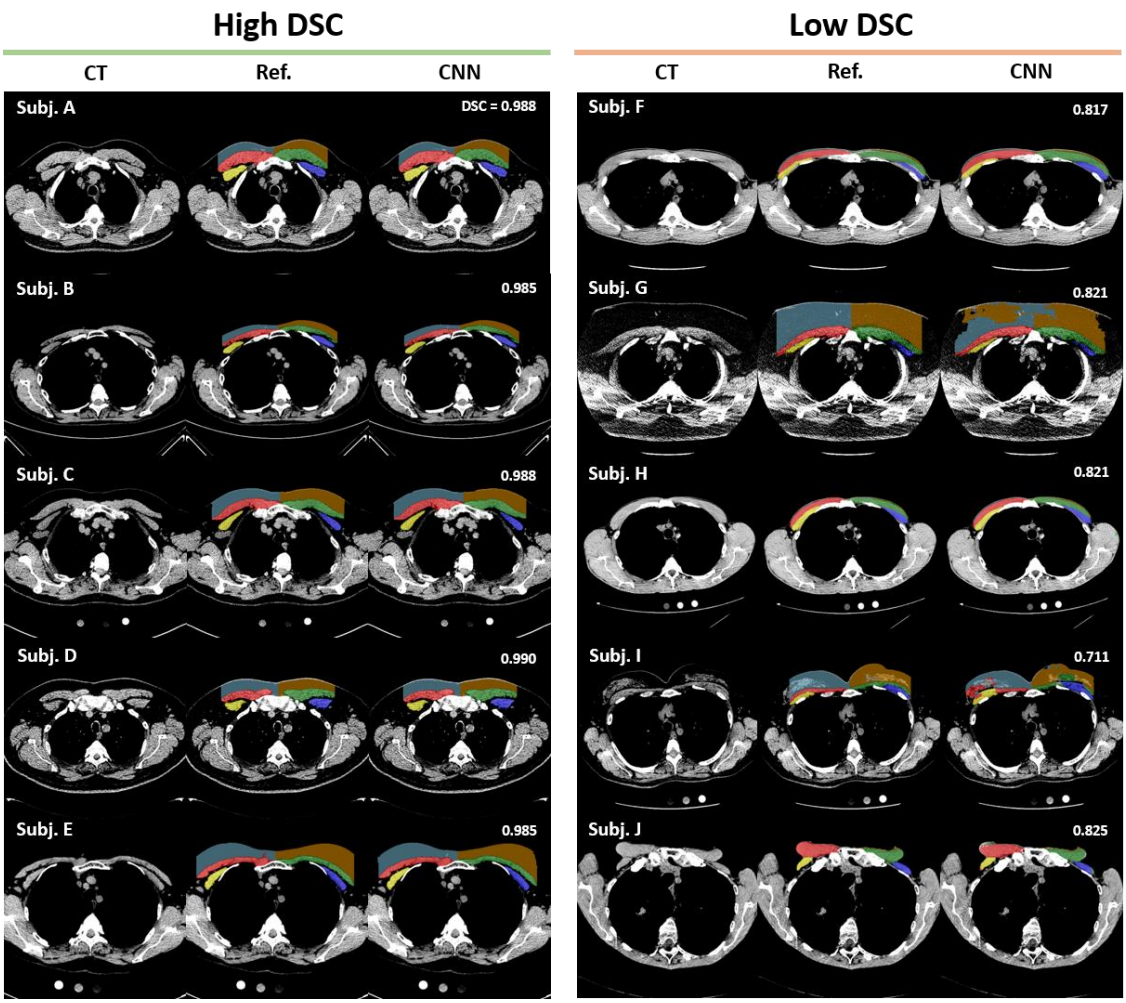

Figure 10.2. Segmentation results from the trained U-Net based architecture. Subject A to Subject E represent cases with the best accuracy scores. Subject F to Subject J shows some of the worst results cases. Color labels are defined in **Figure 10.1**.

The content from this section was presented in the Computer Assisted Radiology and Surgery Proceedings of the 31st International Congress and Exhibition (CARS 2017) and is in preparation to be submitted in the journal Radiology AI:

R. Moreta-Martínez, S. Mason, J. Onieva-Onieva, J.Pascau, R. San José Estepar, "End-to-End Body Composition Assessment in Thoracic CT scans with Deep Learning," Radiology AI. [in preparation]

10.2. Multi-cavity heart segmentation

The analysis of cardiac structure and function has proven to be a key element in the diagnosis and follow-up of patients suffering from cardiopulmonary diseases. Although echocardiography and cardiac MRI (cMRI) are commonly acquired to study cardiac structure and function, these are not systematically deployed in every thoracic exploration. In contrast, computed tomographic (CT) imaging of the chest is broadly used in clinical care and lung cancer screening in high-risk smokers [235]. For this reason, there is an increasing interest in the community in identifying patients at higher risk of developing cardiac dysfunction from CT scans. Delineating the structures of the heart in chest CT is a challenging task, especially when non-contrast-enhanced and non-gated acquisitions are available. A previous approach based on active shape models (ASMs) provided an estimation of the internal cavities (ventricles and atria) [236]. Although ASMs can produce a proper delineation of the pericardium, the complex shape of the cardiac chambers causes overlapping with other structures such as the aorta or the lungs. Additionally, the lack of internal references contributes to inconsistencies in the estimated chamber sizes.

In this work, we studied the potential of CNNs to learn the inter-relations of a multicavity active shape model to accurately estimate the internal cavities in non-gated and non-contrast CT scans. We proposed an innovative architecture (**Figure 10.3**) based on the most recent advances in semantic segmentation that learn the appearance model of the heart from an inaccurate training dataset (segmentation results from the ASM).

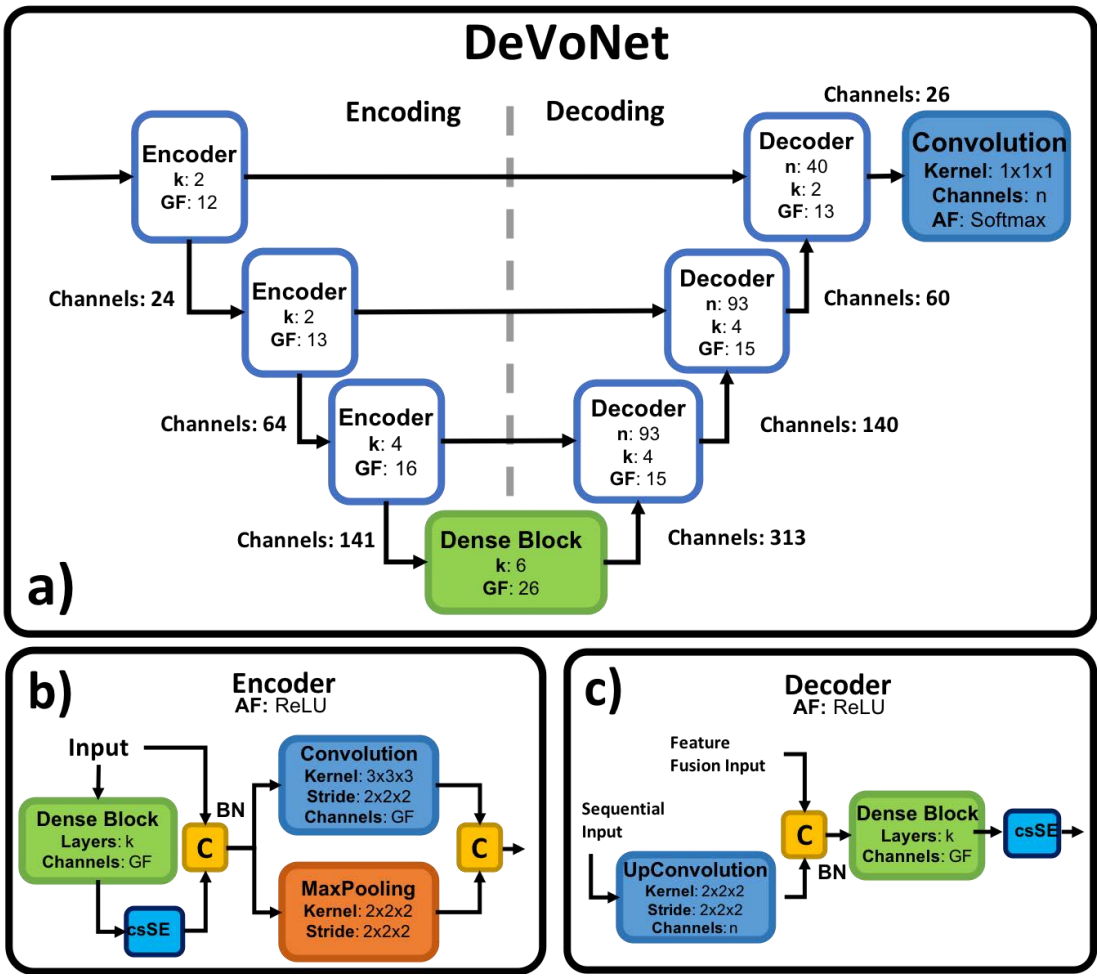

Figure 10.3. a) DeVoNet architecture design, where k is the number of layers defined as a batch normalization, convolution and activation. **b**) Design of the encoder. **c**) Design of the decoder. GF: Growth factor, i.e., number of filters per convolutional layer. n: number of filters in the UpConvolution layer. BN: batch normalization.

Results demonstrate that our CNN approach improves the achievements when compared to the reference standard by analyzing correlation with measures acquired in cMRI [237]. **Figure 10.4** shows an illustration of five subjects randomly selected from our testing set with an increasing degree of pulmonary impairment (defined by the GOLD guidelines). It is worth noting that the overall segmentation is robust for all the subjects despite the anatomical variation. The proposed automated method to quantify heart dysfunction given by abnormal ventricular volumes could serve as an invaluable screening tool during regular CT explorations, for example, within the lung cancer screening context.

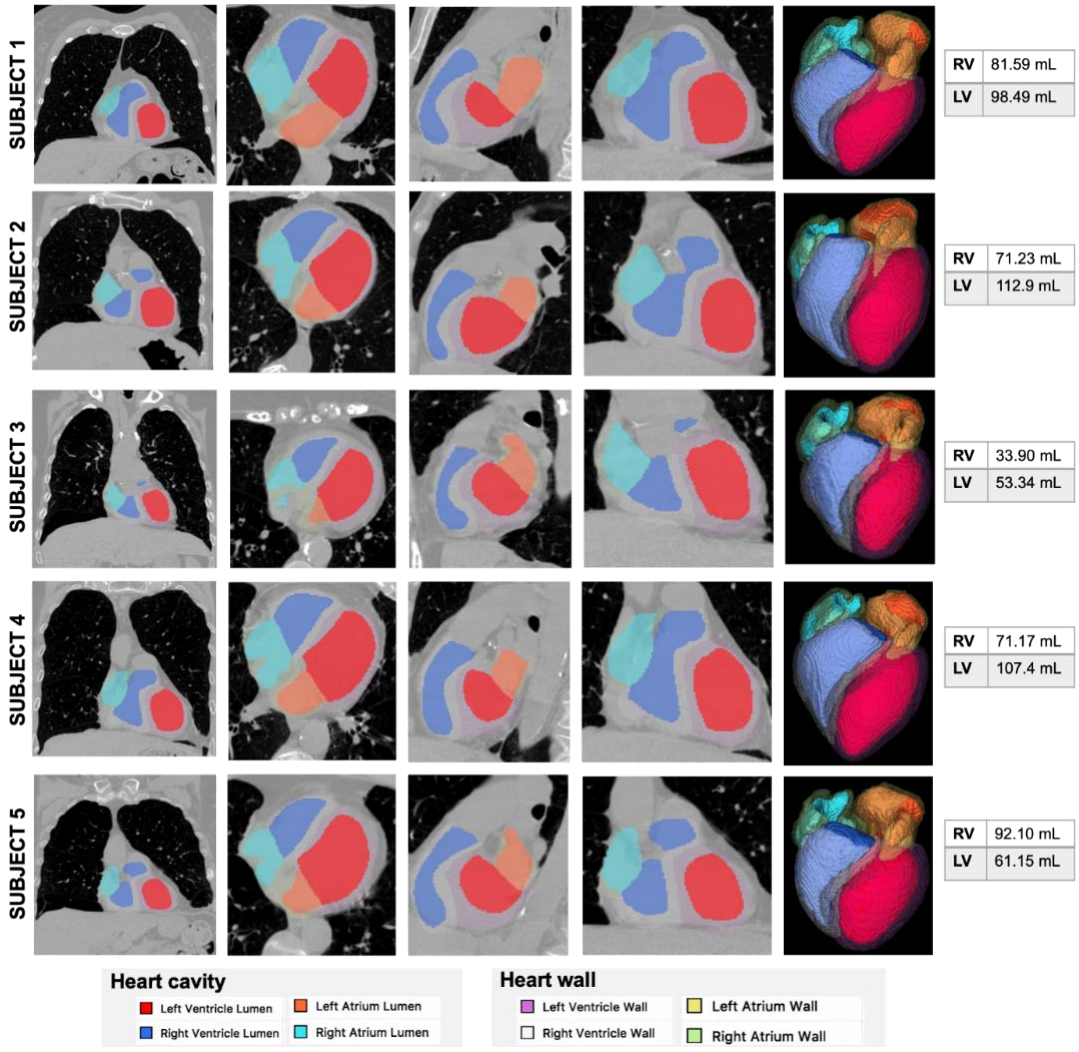

Figure 10.4. Heart cavities and walls segmentation overlays using proposed CNN architecture for five subjects from our testing set. From left to right, full coronal view from the CT at the ventricles' level, axial, sagittal, and coronal close-up views and 3D mesh rendering (walls semitransparent). For each subject, the estimated chamber ventricular volumes are also shown.

The content from this section was presented at the 23rd International Conference on Medical Image Computing & Computer Assisted Intervention (MICCAI) 2020, and published in the Thoracic Image Analysis (TIA 2020) as part of the Lecture Notes in Computer Science book series (LNCS, volume 12502):

R. Moreta-Martínez, G. Vegas Sánchez-Ferrero, L. Andresen, J. Qvortrup Holsting, and R. San José Estépar, "Multi-cavity Heart Segmentation in Non-contrast Non-ECG Gated CT Scans with F-CNN". Thoracic Image Analysis, 2020, pp. 14–23.

11

Publications

11.1. Related to this thesis

11.1.1. Articles in Peer Reviewed Journals

R. Moreta-Martinez, A. Pose-Díez-de-la-Lastra, J. A. Calvo-Haro, L. Mediavilla-Santos, R. Pérez-Mañanes, and J. Pascau. *Combining Augmented Reality and 3D Printing to Improve Surgical Workflows in Orthopedic Oncology: Smartphone Application and Clinical Evaluation*. Sensors, vol. 21, no. 4. 2021 [*https://doi.org/10.3390/s21041370*] – Impact Factor: 3.275 (Q1)

R. Moreta-Martinez, J. A. Calvo-Haro, R. Pérez-Mañanes, M. García-Sevilla, L. Mediavilla-Santos, and J. Pascau. *Desktop 3D Printing: Key for Surgical Navigation in Acral Tumors?* Appl. Sci., vol. 10, no. 24, p. 8984, Dec. 2020 [*https://doi.org/10.3390/app10248984*] – Impact Factor: 2.474 (Q2)

R. Moreta-Martinez, D. García-Mato, M. García-Sevilla, R. Pérez-Mañanes, J. A. Calvo-Haro, and J. Pascau. *Combining Augmented Reality and 3D Printing to Display Patient Models on a Smartphone*. J. Vis. Exp., no. 155, 2020 [*https://doi.org/10.3791/60618*] – Impact factor: 1.163 (Q3)

R. Moreta-Martinez, D. García-Mato, M. García-Sevilla, R. Pérez-Mañanes, J. A. Calvo, J. Pascau. *Augmented reality in computer-assisted interventions based on patient-specific 3D printed reference.* Healthc. Technol. Lett., vol. 5, no. 5, pp. 162–166, 2018 [*https://doi.org/10.1049/htl.2018.5072*]

R. Moreta-Martínez, I. Rubio-Pérez, M. García-Sevilla, L. García-Elcano, and J. Pascau. *Proposal and comparison of two alternatives for needle navigation in sacral nerve stimulation*. Computer Methods and Programs in Biomedicine [*submitted*] – Impact factor: 5.428 (Q1)

R. Moreta-Martínez, G. Vegas Sánchez-Ferrero, L. Andresen, J. Qvortrup Holsting, and R. San José Estépar. *Multi-cavity Heart Segmentation in Non-contrast Non-ECG Gated CT Scans with F-CNN.* Thoracic Image Analysis, 2020, pp. 14–23 [*https://doi.org/10.1007/978-3-030-62469-9_2*]

R. Moreta-Martínez, S. Mason, J. Onieva-Onieva, J. Pascau, R. San José Estepar. *End-to-End Body Composition Assessment in Thoracic CT scans with Deep Learning*. Radiology AI. [*in preparation*]

M. García-Sevilla, L. Mediavilla-Santos, **Rafael Moreta-Martinez**, D. García-Mato, R. Pérez-Mañanes, J. Antonio Calvo-Haro, J. Pascau. *Combining Surgical Navigation and 3D Printing for Less Invasive Pelvic Tumor Resections*. IEEE Access (2021) [*https://doi.org/10.1109/ACCESS.2021.3115984*] Impact factor: 3.367 (Q2)

S. Mason, **R. Moreta-Martinez**, W. W. Labaki, M. Strand, D. Baraghoshi, E. A. Regan, J. Bon, R. San Jose Estepar, R. Casaburi, M.-L. N. McDonald, H. Rossiter, B. J. Make, M. T. Dransfield, M. K. Han, K. A. Young, G. Kinney, J. E. Hokanson, R. San Jose Estepar, and G. R. Washko. *Respiratory exacerbations are associated with muscle loss in current and former smokers*. Thorax (2021) [*https://doi.org/10.1136/thoraxjnl-2020-215999*] Impact factor: 9.139 (Q1)

D. García-Mato, **R. Moreta-Martinez**, M. García-Sevilla, S. Ochandiano, R. García-Leal, R. Pérez-Mañanes, J. A. Calvo-Haro, J.I. Salmerón, and J. Pascau. *Augmented reality visualization for craniosynostosis surgery*. Comput. Methods Biomech. Biomed. Eng. Imaging Vis., vol. 0, no. 0, pp. 1–8, 2020. [*https://doi.org/10.1080/21681163.2020.1834876*] – Impact factor: 1.502 (Q3)

11.1.2. International Conferences

R. Moreta-Martinez, M. García-Sevilla, D. García-Mato, A. Pose-Díez-de-la-Lastra, I. Rubio-Pérez, and J. Pascau. *Smartphone-based augmented reality system for needle insertion guidance in sacral nerve stimulation*. In: CARS 2021 - Computer Assisted Radiology and

Surgery Proceedings of the 35th International Congress and Exhibition, Munich, Germany, June 21–25, 2021. Int J CARS 15, 1–214 (2021)

R. Moreta-Martinez, G. Vegas Sanchez-Ferrero, L. Andresen, J. Q. Holsting, and R. San Jose Estepar. Multi-cavity heart segmentation in non-contrast non-ECG gated CT scans with F-CNN. The Second International Workshop on Thoracic Image Analysis, 23rd International Conference on Medical Image Computing & Computer Assisted Intervention (MICCAI), Lima, Peru (2020)

R. Moreta-Martinez, D. García-Mato, M. García-Sevilla, R. Pérez-Mañanes, J. A. Calvo, and J. Pascau. *AR in computer-assisted interventions based on patient-specific 3D printed reference*. Augmented Environments for Computer-Assisted Interventions Workshop (AECAI), 21st International Conference on Medical Image Computing & Computer Assisted Intervention (MICCAI), Granada, Spain (2018)

R. Moreta-Martinez, J. Onieva-Onieva, J. Pascau, and R. San Jose Estepar. *Pectoralis muscle and subcutaneous adipose tissue segmentation on CT images based on convolutional networks*. In: CARS 2017 - Computer Assisted Radiology and Surgery Proceedings of the 31st International Congress and Exhibition, Barcelona, Spain, June 20-24, 2017. Int J CARS 12, 1–286 (2017)

R. Moreta-Martinez, D. García-Mato, M. García-Sevilla, S. Ochandiano, R. García-Leal, R. Pérez-Mañanes, J. A. Calvo-Haro, J. I. Salmerón, and J. Pascau. *Augmented reality for bone fragment positioning during craniosynostosis reconstruction surgery*. In: CARS 2020 - Computer Assisted Radiology and Surgery Proceedings of the 34th International Congress and Exhibition, Munich, Germany, June 23–27, 2020. Int J CARS 15, 1–214 (2020)

M. García-Sevilla, **R. Moreta-Martinez**, D. García-Mato, A. Pose-Díez-de-la-Lastra, R. Pérez-Mañanes, J. Calvo-Haro, and J. Pascau. *Augmented reality for improved PSI placement in pelvic tumor resections*. In: CARS 2021 - Computer Assisted Radiology and Surgery Proceedings of the 35th International Congress and Exhibition, Munich, Germany, June 21–25, 2021. Int J CARS 15, 1–214 (2021)

A. Pose-Díez-de-la-Lastra, **R. Moreta-Martinez**, J. A. Calvo-Haro, L. Mediavilla Santo, R. Pérez-Mañanes, and J. Pascau. *Combining augmented reality and 3D printing to improve orthopedic oncological surgeries*. In: CARS 2021 - Computer Assisted Radiology and

Surgery Proceedings of the 35th International Congress and Exhibition, Munich, Germany, June 21–25, 2021. Int J CARS 15, 1–214 (2021)

D. García-Mato, **R. Moreta-Martinez**, M. García-Sevilla, S. Ochandiano, R. García-Leal, R. Pérez-Mañanes, J. A. Calvo-Haro, J. I. Salmerón, and J. Pascau. *Augmented Reality Visualization for Craniosynostosis Surgery*. 23rd International Conference on Medical Image Computing & Computer Assisted Intervention (MICCAI), Lima, Peru (2020)

V. García-Vázquez, G. Rodríguez-Lozano, R. Pérez-Mañanes, J.A. Calvo, **R. Moreta-Martínez**, J.M. Asencio, M. Desco, and J. Pascau. *Surgical navigation and 3D printing in hemipelvic osteotomy*. In: CARS 2017 - Computer Assisted Radiology and Surgery Proceedings of the 31st International Congress and Exhibition, Barcelona, Spain, June 20-24, 2017. Int J CARS 12, 1–286 (2017)

11.1.3. National Conferences

A. Pose-Díez-de-la-Lastra, **R. Moreta Martínez**, J. A. Calvo-Haro, L. Mediavilla-Santos, R. Pérez-Mañanes, and J. Pascau. *ARHealth: App que combina Realidad Aumentada e Impresión 3D para Mejorar el Flujo Quirúrgico*. Congreso Anual de la Sociedad Española de Ingeniería Biomédica (CASEIB), November 2020, Valladolid, Spain (2020)

A. Moreno, M. A. Iparraguirre, J. A. Lopez, M. Gomez, R. Perez, **R. Moreta-Martinez**, G. Parrilla, and J. M. Asencio. *Aplicación de la reconstrucción 3D y navegación en un procedimiento de cirugía pélvica extrema*. XXXI Congreso Nacional de Cirugía 2016. Madrid, Spain (2016)

11.2. Other publications

11.2.1. Articles in Peer Reviewed Journals

M. García-Sevilla, J. De León-Luis, R. Moreta-Martínez, **D. García-Mato**, R. Pérez-Mañanes, J. A. Calvo-Haro, and J. Pascau. *Performance Evaluation to Improve Training in Forceps-Assisted Delivery.* OR 2.0 Context-Aware Operating Theaters, Computer Assisted Robotic Endoscopy, Clinical Image-Based Procedures, and Skin Image Analysis, pp. 69-77 (2018)

11.2.2. International Conferences

M. García-Sevilla, D. García-Mato, **R. Moreta-Martinez**, S. Ochandiano, M. Tousidonis, C. Navarro-Cuéllar, and J. Pascau. *Surgical navigation for palate carcinoma resection using a non-invasive 3D-printed reference frame*. In: CARS 2020 - Computer Assisted Radiology and Surgery Proceedings of the 34th International Congress and Exhibition, Munich, Germany, June 23–27, 2020. Int J CARS 15, 1–214 (2020)

S. Mason, R. San Jose Estepar, **R. Moreta-Martinez**, M.T. Dransfield, E.A. Regan, M.J. Strand, and G.R. Washko. *Acute Respiratory Exacerbations Are Associated with Skeletal Muscle Loss in Chronic Obstructive Pulmonary Disease*. A94. EXPANDING OUR HORIZONS; LEADING RESEARCH IN PULMONARY REHABILITATION: 2020. Am J Respir Crit Care Med 2020;201:A2509. (2020)

M. Concepción-Brito, **R. Moreta-Martinez**, J. Serrano, D. García-Mato, M. García-Sevilla, and J. Pascau. *Segmentation of Organs at Risk in Head and Neck Radiation Therapy with 3D Convolutional Networks*. In: CARS 2019 - Computer Assisted Radiology and Surgery Proceedings of the 33rd International Congress and Exhibition, Rennes, France, June 18–21, 2019. Int J CARS 14, 1–194 (2019)

M. García-Sevilla, J. De León-Luis, **R. Moreta-Martínez**, D. García-Mato, R. Pérez-Mañanes, J. A. Calvo-Haro, and J. Pascau. *Performance Evaluation to Improve Training in Forceps-Assisted Delivery*. OR 2.0 Context-Aware Operating Theaters Workshop, 21st International Conference on Medical Image Computing & Computer Assisted Intervention (MICCAI), Granada, Spain (2018)

D. García-Mato, M. García-Sevilla, S. Ochandiano, **R. Moreta-Martinez**, J. V. Darriba-Allés, R. García-Leal, J. I. Salmerón, and J. Pascau. *Intraoperative Outcome Evaluation in Craniosynostosis Reconstruction Surgery using 3D Photography*. In: CARS 2020 - Computer Assisted Radiology and Surgery Proceedings of the 34th International Congress and Exhibition, Munich, Germany, June 23–27, 2020. Int J CARS 15, 1–214 (2020)

D. García-Mato, S. Ochandiano, S. Espías-Alonso, M. García-Sevilla, **R. Moreta-Martinez**, J. A. Calvo-Haro, R. Pérez-Mañanes, and J. Pascau. *Non-invasive computer-assisted dental implant surgery based on optical tracking and 3D printing*. In: CARS 2019 - Computer Assisted Radiology and Surgery Proceedings of the 33rd International Congress and Exhibition, Rennes, France, June 18–21, 2019. Int J CARS 14, 1–194 (2019)

D. García-Mato, S. Ochandiano, M. Tousidonis, **R. Moreta-Martínez**, M. García-Sevilla, M. Desco, and J. Pascau. *Orbital Floor Reconstruction Workflow based on 3D Printing and Surgical Navigation*. In: CARS 2018 - Computer Assisted Radiology and Surgery Proceedings of the 32nd International Congress and Exhibition, Berlin, Germany, June 20–23, 2018. Int J CARS 13, 1–273 (2018)

12

References

[1] I. F. Dragan, D. Dalessandri, L. A. Johnson, A. Tucker, and A. D. Walmsley, “Impact of scientific and technological advances,” *Eur. J. Dent. Educ.*, vol. 22, no. S1, pp. 17–20, Mar. 2018, doi: https://doi.org/10.1111/eje.12342.

[2] L. Hood, R. Balling, and C. Auffray, “Revolutionizing medicine in the 21st century through systems approaches.,” *Biotechnol. J.*, vol. 7, no. 8, pp. 992–1001, Aug. 2012, doi: 10.1002/biot.201100306.

[3] A. D. Weston and L. Hood, “Systems Biology, Proteomics, and the Future of Health Care: Toward Predictive, Preventative, and Personalized Medicine,” *J. Proteome Res.*, vol. 3, no. 2, pp. 179–196, Apr. 2004, doi: 10.1021/pr0499693.

[4] L. Hood, J. R. Heath, M. E. Phelps, and B. Lin, “Systems Biology and New Technologies Enable Predictive and Preventative Medicine,” *Science (80-.).*, vol. 306, no. 5696, pp. 640 LP – 643, Oct. 2004, doi: 10.1126/science.1104635.

[5] *A New Biology for the 21st Century: Ensuring the United States Leads the Coming Biology Revolution*. Washington (DC), 2009.

[6] B. F. C. Wu J. X. , Burke Z., “Personalized Medicine and Surgery,” *CellR4*, vol. 2, no. 2, p. e856, 2014.

[7] N. Egalite, I. J. Groisman, and B. Godard, “Personalized medicine in oncology: ethical implications for the delivery of healthcare,” *Per. Med.*, vol. 11, no. 7, pp. 659–668, Sep. 2014, doi: 10.2217/pme.14.53.

[8] M. Gerlinger *et al.*, “Intratumor Heterogeneity and Branched Evolution Revealed by

Multiregion Sequencing," *N. Engl. J. Med.*, vol. 366, no. 10, pp. 883–892, Mar. 2012, doi: 10.1056/NEJMoa1113205.

[9] A. Goldhirsch *et al.*, "Personalizing the treatment of women with early breast cancer: highlights of the St Gallen International Expert Consensus on the Primary Therapy of Early Breast Cancer 2013.," *Ann. Oncol. Off. J. Eur. Soc. Med. Oncol.*, vol. 24, no. 9, pp. 2206–2223, Sep. 2013, doi: 10.1093/annonc/mdt303.

[10] E. Roncali, A. Taebi, C. Foster, and C. T. Vu, "Personalized Dosimetry for Liver Cancer Y-90 Radioembolization Using Computational Fluid Dynamics and Monte Carlo Simulation," *Ann. Biomed. Eng.*, vol. 48, no. 5, pp. 1499–1510, May 2020, doi: 10.1007/s10439-020-02469-1.

[11] O. Golubnitschaja *et al.*, "Medicine in the early twenty-first century: paradigm and anticipation - EPMA position paper 2016," *EPMA J.*, vol. 7, no. 1, p. 23, 2016, doi: 10.1186/s13167-016-0072-4.

[12] U. Mezger, C. Jendrewski, and M. Bartels, "Navigation in surgery.," *Langenbeck's Arch. Surg.*, vol. 398, no. 4, pp. 501–514, Apr. 2013, doi: 10.1007/s00423-013-1059-4.

[13] Y. Enchev, "Neuronavigation: geneology, reality, and prospects," *Neurosurg. Focus FOC*, vol. 27, no. 3, p. E11, 2009, doi: 10.3171/2009.6.FOCUS09109.

[14] E. M. Friets, J. W. Strohbehn, J. F. Hatch, and D. W. Roberts, "A frameless stereotaxic operating microscope for neurosurgery.," *IEEE Trans. Biomed. Eng.*, vol. 36, no. 6, pp. 608–617, Jun. 1989, doi: 10.1109/10.29455.

[15] D. W. Roberts, J. W. Strohbehn, J. F. Hatch, W. Murray, and H. Kettenberger, "A frameless stereotaxic integration of computerized tomographic imaging and the operating microscope.," *J. Neurosurg.*, vol. 65, no. 4, pp. 545–549, Oct. 1986, doi: 10.3171/jns.1986.65.4.0545.

[16] A. D. Wiles, D. G. Thompson, and D. D. Frantz, "Accuracy assessment and interpretation for optical tracking systems," in *Proc.SPIE*, 2004, vol. 5367.

[17] R. L. J. Galloway, R. J. Maciunas, and C. A. 2nd Edwards, "Interactive image-guided neurosurgery.," *IEEE Trans. Biomed. Eng.*, vol. 39, no. 12, pp. 1226–1231, Dec. 1992, doi: 10.1109/10.184698.

[18] K. Cleary, V. Watson, D. Lindisch, A. Patriciu, D. Mazilu, and D. Stoianovici,

"Robotically Assisted Interventions: Clinical Trial for Spinal Blocks BT - Medical Image Computing and Computer-Assisted Intervention - MICCAI 2003," 2003, pp. 963–964.

[19] L. Joskowicz, "Computer-aided surgery meets predictive, preventive, and personalized medicine," *EPMA Journal*, vol. 8, no. 1. 2017, doi: 10.1007/s13167-017-0084-8.

[20] P. Liverneaux, E. Nectoux, and C. Taleb, "The future of robotics in hand surgery," *Chir. Main*, vol. 28, no. 5, pp. 278–285, 2009, doi: 10.1016/j.main.2009.08.002.

[21] M. Heller *et al.*, "Applications of patient-specific 3D printing in medicine," *Int. J. Comput. Dent.*, vol. 19, no. 4, pp. 323–339, 2016.

[22] K. C. Wong, "3D-printed patient-specific applications in orthopedics," *Orthop. Res. Rev.*, vol. 8, pp. 57–66, Oct. 2016, doi: 10.2147/ORR.S99614.

[23] W. Yang *et al.*, "Three-dimensional printing of patient-specific surgical plates in head and neck reconstruction: A prospective pilot study," *Oral Oncol.*, vol. 78, pp. 31–36, 2018, doi: https://doi.org/10.1016/j.oraloncology.2018.01.005.

[24] A. C. Colchester *et al.*, "Development and preliminary evaluation of VISLAN, a surgical planning and guidance system using intra-operative video imaging.," *Med. Image Anal.*, vol. 1, no. 1, pp. 73–90, Mar. 1996, doi: 10.1016/s1361-8415(01)80006-2.

[25] K.-H. Yu, A. L. Beam, and I. S. Kohane, "Artificial intelligence in healthcare," *Nat. Biomed. Eng.*, vol. 2, no. 10, pp. 719–731, 2018, doi: 10.1038/s41551-018-0305-z.

[26] W. E. Grimson, R. Kikinis, F. A. Jolesz, and P. M. Black, "Image-guided surgery.," *Sci. Am.*, vol. 280, no. 6, pp. 62–69, Jun. 1999, doi: 10.1038/scientificamerican0699-62.

[27] T. M. Peters and K. R. Cleary, *Image-guided interventions: technology and applications*. Springer, 2008.

[28] D. Guha and V. X. D. Yang, "Perspective review on applications of optics in spinal surgery.," *J. Biomed. Opt.*, vol. 23, no. 6, pp. 1–8, Jun. 2018, doi: 10.1117/1.JBO.23.6.060601.

[29] C. H. Ewurum, Y. Guo, S. Pagnha, Z. Feng, and X. Luo, "Surgical Navigation in Orthopedics: Workflow and System Review BT - Intelligent Orthopaedics: Artificial Intelligence and Smart Image-guided Technology for Orthopaedics," G. Zheng, W.

Tian, and X. Zhuang, Eds. Singapore: Springer Singapore, 2018, pp. 47–63.

[30] R. Bucholz and L. McDurmont, “The History, Current Status, and Future of the StealthStation Treatment Guidance System BT - Textbook of Stereotactic and Functional Neurosurgery,” A. M. Lozano, P. L. Gildenberg, and R. R. Tasker, Eds. Berlin, Heidelberg: Springer Berlin Heidelberg, 2009, pp. 543–565.

[31] M. Schulder, *Handbook of Stereotactic and Functional Neurosurgery*, 1st Editio. Boca Raton: CRC Press, 2003.

[32] P. Catala-Lehnen, J. V Nüchtern, D. Briem, T. Klink, J. M. Rueger, and W. Lehmann, “Comparison of 2D and 3D navigation techniques for percutaneous screw insertion into the scaphoid: results of an experimental cadaver study.,” *Comput. Aided Surg.*, vol. 16, no. 6, pp. 280–287, 2011, doi: 10.3109/10929088.2011.621092.

[33] A. Lasso, T. Heffter, A. Rankin, C. Pinter, T. Ungi, and G. Fichtinger, “PLUS: open-source toolkit for ultrasound-guided intervention systems.,” *IEEE Trans. Biomed. Eng.*, vol. 61, no. 10, pp. 2527–2537, Oct. 2014, doi: 10.1109/TBME.2014.2322864.

[34] S. Pieper, M. Halle, and R. Kikinis, “3D Slicer,” in *2004 2nd IEEE International Symposium on Biomedical Imaging: Nano to Macro (IEEE Cat No. 04EX821)*, 2004, pp. 632-635 Vol. 1, doi: 10.1109/ISBI.2004.1398617.

[35] D. García-Mato *et al.*, “Craniosynostosis surgery: workflow based on virtual surgical planning, intraoperative navigation and 3D printed patient-specific guides and templates,” *Sci. Rep.*, vol. 9, no. 1, p. 17691, 2019, doi: 10.1038/s41598-019-54148-4.

[36] T. Ungi *et al.*, “Navigated Breast Tumor Excision Using Electromagnetically Tracked Ultrasound and Surgical Instruments,” *IEEE Trans. Biomed. Eng.*, vol. 63, no. 3, pp. 600–606, 2016, doi: 10.1109/TBME.2015.2466591.

[37] A. Sternheim *et al.*, “Navigated Pelvic Osteotomy and Tumor Resection,” *J. Bone Jt. Surg.*, vol. 97-A, no. 1, pp. 40–46, 2015.

[38] L. Jeys, G. S. Matharu, R. S. Nandra, and R. J. Grimer, “Can computer navigation-assisted surgery reduce the risk of an intralesional margin and reduce the rate of local recurrence in patients with a tumour of the pelvis or sacrum?,” *Bone Joint J.*, vol. 95-B, no. 10, pp. 1417–1424, Oct. 2013, doi: 10.1302/0301-620X.95B10.31734.

[39] L. Chen, T. Day, W. Tang, and N. W. John, “Recent Developments and Future

Challenges in Medical Mixed Reality," pp. 123–135, 2017, doi: 10.1109/ISMAR.2017.29.

[40] R. Gierwiało, M. Witkowski, M. Kosieradzki, W. Lisik, Ł. Groszkowski, and R. Sitnik, "Medical Augmented-Reality Visualizer for Surgical Training and Education in Medicine," *Applied Sciences* , vol. 9, no. 13. 2019, doi: 10.3390/app9132732.

[41] P. E. Pelargos *et al.*, "Utilizing virtual and augmented reality for educational and clinical enhancements in neurosurgery," *J. Clin. Neurosci.*, vol. 35, pp. 1–4, 2017.

[42] C. Papakostas, C. Troussas, A. Krouska, and C. Sgouropoulou, "Measuring User Experience, Usability and Interactivity of a Personalized Mobile Augmented Reality Training System," *Sensors* , vol. 21, no. 11. 2021, doi: 10.3390/s21113888.

[43] D. Amiras *et al.*, "Augmented reality simulator for CT-guided interventions," *Eur. Radiol.*, 2021, doi: 10.1007/s00330-021-08043-0.

[44] M. C. Davis, D. D. Can, J. Pindrik, B. G. Rocque, and J. M. Johnston, "Virtual Interactive Presence in Global Surgical Education: International Collaboration Through Augmented Reality," *World Neurosurg.*, vol. 86, pp. 103–111, 2016, doi: https://doi.org/10.1016/j.wneu.2015.08.053.

[45] A. S. Rose, H. Kim, H. Fuchs, and J.-M. Frahm, "Development of augmented-reality applications in otolaryngology-head and neck surgery," *Laryngoscope*, 2019.

[46] C. Zhou *et al.*, "Robot-Assisted Surgery for Mandibular Angle Split Osteotomy Using Augmented Reality: Preliminary Results on Clinical Animal Experiment," *Aesthetic Plast. Surg.*, vol. 41, no. 5, pp. 1228–1236, 2017.

[47] J. Fotouhi *et al.*, "Plan in 2-D, execute in 3-D: an augmented reality solution for cup placement in total hip arthroplasty.," *J. Med. imaging (Bellingham, Wash.)*, vol. 5, no. 2, p. 21205, Apr. 2018, doi: 10.1117/1.JMI.5.2.021205.

[48] W. Deng, F. Li, M. Wang, and Z. Song, "Easy-to-Use Augmented Reality Neuronavigation Using a Wireless Tablet PC," *Stereotact. Funct. Neurosurg.*, vol. 92, no. 1, pp. 17–24, 2014.

[49] F. Heinrich, L. Schwenderling, M. Becker, M. Skalej, and C. Hansen, "HoloInjection: augmented reality support for CT-guided spinal needle injections.," *Healthc. Technol. Lett.*, vol. 6, no. 6, pp. 165–171, Dec. 2019, doi: 10.1049/htl.2019.0062.

[50] S. Al-Nimer *et al.*, *3D Holographic Guidance and Navigation for Percutaneous Ablation of Solid Tumor.*, vol. 31, no. 3. United States, 2020, pp. 526–528.

[51] M. H. Michalski and J. S. Ross, "The Shape of Things to Come: 3D Printing in Medicine," *JAMA*, vol. 312, no. 21, pp. 2213–2214, Dec. 2014, doi: 10.1001/jama.2014.9542.

[52] P. Tack, J. Victor, P. Gemmel, and L. Annemans, "3D-printing techniques in a medical setting: a systematic literature review," *Biomed. Eng. Online*, vol. 15, no. 1, p. 115, 2016, doi: 10.1186/s12938-016-0236-4.

[53] A. Armillotta *et al.*, "Use of rapid prototyping models in the planning of percutaneous pulmonary valved stent implantation.," *Proc. Inst. Mech. Eng. Part H, J. Eng. Med.*, vol. 221, no. 4, pp. 407–416, May 2007, doi: 10.1243/09544119JEIM83.

[54] M. Colaco, D. A. Igel, and A. Atala, "The potential of 3D printing in urological research and patient care," *Nat. Rev. Urol.*, vol. 15, no. 4, pp. 213–221, 2018, doi: 10.1038/nrurol.2018.6.

[55] A. Marro, T. Bandukwala, and W. Mak, "Three-Dimensional Printing and Medical Imaging: A Review of the Methods and Applications," *Curr. Probl. Diagn. Radiol.*, vol. 45, no. 1, pp. 2–9, 2015, doi: 10.1067/j.cpradiol.2015.07.009.

[56] S. Derakhshanfar, R. Mbeleck, K. Xu, X. Zhang, W. Zhong, and M. Xing, "3D bioprinting for biomedical devices and tissue engineering: A review of recent trends and advances," *Bioact. Mater.*, vol. 3, no. 2, pp. 144–156, 2018, doi: https://doi.org/10.1016/j.bioactmat.2017.11.008.

[57] B. Leukers *et al.*, "Hydroxyapatite scaffolds for bone tissue engineering made by 3D printing," *J. Mater. Sci. Mater. Med.*, vol. 16, no. 12, pp. 1121–1124, 2005, doi: 10.1007/s10856-005-4716-5.

[58] S.-J. Yoo *et al.*, "3D printing in medicine of congenital heart diseases," *3D Print. Med.*, vol. 2, no. 1, p. 3, 2016, doi: 10.1186/s41205-016-0004-x.

[59] E. G. Milano *et al.*, "Current and future applications of 3D printing in congenital cardiology and cardiac surgery," *Br. J. Radiol.*, vol. 92, no. 1094, p. 20180389, Nov. 2018, doi: 10.1259/bjr.20180389.

[60] I. Rubio-Pérez and A. Díaz Lantada, "Surgical Planning of Sacral Nerve Stimulation

Procedure in Presence of Sacral Anomalies by Using Personalized Polymeric Prototypes Obtained with Additive Manufacturing Techniques.," *Polymers (Basel).*, vol. 12, no. 3, Mar. 2020, doi: 10.3390/polym12030581.

[61] M. Y. Chen *et al.*, "Current applications of three-dimensional printing in urology," *BJU Int.*, vol. 125, no. 1, pp. 17–27, Jan. 2020, doi: https://doi.org/10.1111/bju.14928.

[62] J. Hakim, A. Oluyemisi, C. Buskmiller, R. Krishnamurthy, W. Cohn, and J. E. Dietrich, "Innovative Use of 3D Printers in Gynecology," *J. Pediatr. Adolesc. Gynecol.*, vol. 28, no. 2, p. e67, 2015, doi: https://doi.org/10.1016/j.jpag.2015.02.089.

[63] J. Chen, H. He, T. Song, C. Su, and D. Chen, "Utilizing 3D Printing Model of Placenta Percreta to Guide Obstetric Operation [3D]," *Obstet. Gynecol.*, vol. 129, no. 5, 2017.

[64] M. George, K. R. Aroom, H. G. Hawes, B. S. Gill, and J. Love, "3D Printed Surgical Instruments: The Design and Fabrication Process," *World J. Surg.*, vol. 41, no. 1, pp. 314–319, 2017, doi: 10.1007/s00268-016-3814-5.

[65] H.-S. Yang and J.-Y. Park, "3D Printer Application for Endoscope-Assisted Spine Surgery Instrument Development: From Prototype Instruments to Patient-Specific 3D Models," *Yonsei Med J*, vol. 61, no. 1, pp. 94–99, Jan. 2020.

[66] J. Minto, X. Zhou, J. Osborn, L. G. Zhang, K. Sarkar, and R. D. Rao, "Three-Dimensional Printing: A Catalyst for a Changing Orthopaedic Landscape," *JBJS Rev.*, vol. 8, no. 2, 2020, doi: 10.2106/JBJS.RVW.19.00076.

[67] H. Lal and M. K. Patralekh, "3D printing and its applications in orthopaedic trauma: A technological marvel," *J. Clin. Orthop. Trauma*, vol. 9, no. 3, pp. 260–268, 2018, doi: https://doi.org/10.1016/j.jcot.2018.07.022.

[68] R. Vaishya, M. K. Patralekh, A. Vaish, A. K. Agarwal, and V. Vijay, "Publication trends and knowledge mapping in 3D printing in orthopaedics," *J. Clin. Orthop. Trauma*, vol. 9, no. 3, pp. 194–201, 2018, doi: https://doi.org/10.1016/j.jcot.2018.07.006.

[69] R. Pérez-Mañanes, J. A. Burró, J. R. Manaute, F. C. Rodriguez, and J. V. Martín, "3D Surgical Printing Cutting Guides for Open-Wedge High Tibial Osteotomy: Do It Yourself.," *J. Knee Surg.*, vol. 29, no. 8, pp. 690–695, Nov. 2016, doi: 10.1055/s-0036-1572412.

[70] F. Chana-Rodríguez, R. P. Mañanes, J. Rojo-Manaute, P. Gil, J. M. Martínez-Gómiz,

and J. Vaquero-Martín, “3D surgical printing and pre contoured plates for acetabular fractures.,” *Injury*, vol. 47, no. 11, pp. 2507–2511, Nov. 2016, doi: 10.1016/j.injury.2016.08.027.

[71] H. C. Gemalmaz, K. Sarıyılmaz, O. Ozkunt, M. Sungur, İ. Kaya, and F. Dikici, “A new osteotomy for the prevention of prominent lateral condyle after cubitus varus correctional surgery-made possible by a 3D printed patient specific osteotomy guide: A case report,” *Int. J. Surg. Case Rep.*, vol. 41, pp. 438–442, 2017, doi: https://doi.org/10.1016/j.ijscr.2017.10.048.

[72] B. Otsuki *et al.*, “Developing a novel custom cutting guide for curved peri-acetabular osteotomy,” *Int. Orthop.*, vol. 37, no. 6, pp. 1033–1038, 2013, doi: 10.1007/s00264-013-1873-x.

[73] P.-F. Zheng, J. Chen, X. P. Xux, B. Jiang, Q.-Q. Yao, and L.-M. Wang, “Accurate osteotomy assisted by individualized navigation templates for the treatment of children cubitus varus,” *Zhongguo Gu Shang*, vol. 30, no. 4, pp. 377–382, 2017, doi: 10.3969/j.issn.1003-0034.2017.04.020.

[74] Y. Z. Zhang, S. Lu, B. Chen, J. M. Zhao, R. Liu, and G. X. Pei, “Application of computer-aided design osteotomy template for treatment of cubitus varus deformity in teenagers: A pilot study,” *J. Shoulder Elb. Surg.*, vol. 20, no. 1, pp. 51–56, 2011, doi: https://doi.org/10.1016/j.jse.2010.08.029.

[75] E. M. Taylor and M. L. Iorio, “Surgeon-Based 3D Printing for Microvascular Bone Flaps.,” *J. Reconstr. Microsurg.*, vol. 33, no. 6, pp. 441–445, Jul. 2017, doi: 10.1055/s-0037-1600133.

[76] Y. Sha *et al.*, “A novel patient-specific navigational template for anatomical reconstruction of the lateral ankle ligaments,” *Int. Orthop.*, vol. 40, no. 1, pp. 59–64, 2016, doi: 10.1007/s00264-015-2817-4.

[77] S. L. Sing, J. An, W. Y. Yeong, and F. E. Wiria, “Laser and electron-beam powder-bed additive manufacturing of metallic implants: A review on processes, materials and designs.,” *J. Orthop. Res. Off. Publ. Orthop. Res. Soc.*, vol. 34, no. 3, pp. 369–385, Mar. 2016, doi: 10.1002/jor.23075.

[78] K. C. Wong, S. M. Kumta, N. V Geel, and J. Demol, “One-step reconstruction with a

3D-printed, biomechanically evaluated custom implant after complex pelvic tumor resection," *Comput. Aided Surg.*, vol. 20, no. 1, pp. 14–23, Jan. 2015, doi: 10.3109/10929088.2015.1076039.

[79] R. Pérez-Mañanes, J. Calvo-Haro, J. Arnal-Burró, F. Chana-Rodríguez, P. Sanz-Ruiz, and J. Vaquero-Martín, "Nuestra experiencia con impresión 3D doméstica en Cirugía Ortopédica y Traumatología. Hazlo tú mismo," *Rev. Latinoam. Cirugía Ortopédica*, vol. 1, no. 2, pp. 47–53, 2016, doi: 10.1016/j.rslaot.2016.06.004.

[80] J. A. Calvo-Haro *et al.*, "Point-of-care manufacturing: a single university hospital's initial experience.," *3D Print. Med.*, vol. 7, no. 1, p. 11, Apr. 2021, doi: 10.1186/s41205-021-00101-z.

[81] D. S. Watson *et al.*, "Clinical applications of machine learning algorithms: beyond the black box," *BMJ*, vol. 364, p. l886, Mar. 2019, doi: 10.1136/bmj.l886.

[82] M. J. Iqbal *et al.*, "Clinical applications of artificial intelligence and machine learning in cancer diagnosis: looking into the future," *Cancer Cell Int.*, vol. 21, no. 1, p. 270, 2021, doi: 10.1186/s12935-021-01981-1.

[83] A. Kleppe, O.-J. Skrede, S. De Raedt, K. Liestøl, D. J. Kerr, and H. E. Danielsen, "Designing deep learning studies in cancer diagnostics," *Nat. Rev. Cancer*, vol. 21, no. 3, pp. 199–211, 2021, doi: 10.1038/s41568-020-00327-9.

[84] W. Zhu, L. Xie, J. Han, and X. Guo, "The Application of Deep Learning in Cancer Prognosis Prediction," *Cancers* , vol. 12, no. 3. 2020, doi: 10.3390/cancers12030603.

[85] P. Nardelli, J. C. Ross, and R. San José Estépar, "Generative-based airway and vessel morphology quantification on chest CT images," *Med. Image Anal.*, vol. 63, p. 101691, 2020, doi: https://doi.org/10.1016/j.media.2020.101691.

[86] M. I. Campo, J. Pascau, and R. S. J. Estépar, "Emphysema quantification on simulated X-rays through deep learning techniques," in *2018 IEEE 15th International Symposium on Biomedical Imaging (ISBI 2018)*, 2018, pp. 273–276, doi: 10.1109/ISBI.2018.8363572.

[87] G. Altan, Y. Kutlu, and N. Allahverdi, "Deep Learning on Computerized Analysis of Chronic Obstructive Pulmonary Disease," *IEEE J. Biomed. Heal. Informatics*, vol. 24, no. 5, pp. 1344–1350, 2020, doi: 10.1109/JBHI.2019.2931395.

[88] R. Gargeya and T. Leng, “Automated Identification of Diabetic Retinopathy Using Deep Learning,” *Ophthalmology*, vol. 124, no. 7, pp. 962–969, 2017, doi: https://doi.org/10.1016/j.ophtha.2017.02.008.

[89] T. D. Shanafelt *et al.*, “Burnout and medical errors among American surgeons.,” *Ann. Surg.*, vol. 251, no. 6, pp. 995–1000, Jun. 2010, doi: 10.1097/SLA.0b013e3181bfdab3.

[90] B. L. Raymond *et al.*, “Use of the American College of Surgeons National Surgical Quality Improvement Program Surgical Risk Calculator During Preoperative Risk Discussion: The Patient Perspective.,” *Anesth. Analg.*, vol. 128, no. 4, pp. 643–650, Apr. 2019, doi: 10.1213/ANE.0000000000003718.

[91] B. Shickel, T. J. Loftus, L. Adhikari, T. Ozrazgat-Baslanti, A. Bihorac, and P. Rashidi, “DeepSOFA: A Continuous Acuity Score for Critically Ill Patients using Clinically Interpretable Deep Learning,” *Sci. Rep.*, vol. 9, no. 1, p. 1879, 2019, doi: 10.1038/s41598-019-38491-0.

[92] T. J. Loftus *et al.*, “Artificial Intelligence and Surgical Decision-making,” *JAMA Surg.*, vol. 155, no. 2, pp. 148–158, Feb. 2020, doi: 10.1001/jamasurg.2019.4917.

[93] T. M. Ward *et al.*, “Computer vision in surgery,” *Surgery*, vol. 169, no. 5, pp. 1253–1256, 2021, doi: https://doi.org/10.1016/j.surg.2020.10.039.

[94] D. A. Hashimoto, G. Rosman, D. Rus, and O. R. Meireles, “Artificial Intelligence in Surgery: Promises and Perils.,” *Ann. Surg.*, vol. 268, no. 1, pp. 70–76, Jul. 2018, doi: 10.1097/SLA.0000000000002693.

[95] A. Pose Díez de la Lastra, L. García-Duarte Sáenz, D. García-Mato, L. Hernández-Álvarez, S. Ochandiano, and J. Pascau, “Real-Time Tool Detection for Workflow Identification in Open Cranial Vault Remodeling,” *Entropy* , vol. 23, no. 7. 2021, doi: 10.3390/e23070817.

[96] M. Pfeiffer, C. Riediger, J. Weitz, and S. Speidel, “Learning soft tissue behavior of organs for surgical navigation with convolutional neural networks,” *Int. J. Comput. Assist. Radiol. Surg.*, vol. 14, no. 7, pp. 1147–1155, 2019, doi: 10.1007/s11548-019-01965-7.

[97] “NVIDIA Clara.” [Online]. Available: https://developer.nvidia.com/clara. [Accessed: 07-Jul-2021].

[98] O. Ronneberger, P. Fischer, and T. Brox, “U-Net: Convolutional Networks for Biomedical Image Segmentation,” *Miccai*, pp. 234–241, 2015, doi: 10.1007/978-3-319-24574-4_28.

[99] V. Badrinarayanan, A. Kendall, and R. Cipolla, “SegNet: A Deep Convolutional Encoder-Decoder Architecture for Image Segmentation,” *IEEE Trans. Pattern Anal. Mach. Intell.*, vol. 39, no. 12, pp. 2481–2495, 2017, doi: 10.1109/TPAMI.2016.2644615.

[100] A. Qayyum *et al.*, “Hybrid 3D-ResNet Deep Learning Model for Automatic Segmentation of Thoracic Organs at Risk in CT Images,” in *2020 International Conference on Industrial Engineering, Applications and Manufacturing (ICIEAM)*, 2020, pp. 1–5, doi: 10.1109/ICIEAM48468.2020.9111950.

[101] A. T. Grainger *et al.*, “Deep Learning-based Quantification of Abdominal Subcutaneous and Visceral Fat Volume on CT Images,” *Acad. Radiol.*, 2020, doi: https://doi.org/10.1016/j.acra.2020.07.010.

[102] J. W. Chan *et al.*, “A convolutional neural network algorithm for automatic segmentation of head and neck organs at risk using deep lifelong learning,” *Med. Phys.*, vol. 46, no. 5, pp. 2204–2213, May 2019, doi: https://doi.org/10.1002/mp.13495.

[103] Y. Jonmohamadi *et al.*, “Automatic Segmentation of Multiple Structures in Knee Arthroscopy Using Deep Learning,” *IEEE Access*, vol. 8, pp. 51853–51861, 2020, doi: 10.1109/ACCESS.2020.2980025.

[104] P. S. Young, S. W. Bell, and A. Mahendra, “The evolving role of computer-assisted navigation in musculoskeletal oncology,” *Bone Jt. J.*, vol. 97-B, no. 2, pp. 258–264, 2015, doi: 10.1302/0301-620X.97B2.34461.

[105] M. Schulze *et al.*, “Complex Bone Tumors of the Trunk—The Role of 3D Printing and Navigation in Tumor Orthopedics: A Case Series and Review of the Literature,” *Journal of Personalized Medicine* , vol. 11, no. 6. 2021, doi: 10.3390/jpm11060517.

[106] L. Chen, T. W. Day, W. Tang, and N. W. John, “Recent Developments and Future Challenges in Medical Mixed Reality,” in *2017 IEEE International Symposium on Mixed and Augmented Reality (ISMAR)*, 2017, pp. 123–135, doi: 10.1109/ISMAR.2017.29.

[107] P. Pratt *et al.*, “Through the HoloLens™ looking glass: augmented reality for extremity reconstruction surgery using 3D vascular models with perforating vessels,” *Eur. Radiol. Exp.*, vol. 2, no. 1, p. 2, 2018, doi: 10.1186/s41747-017-0033-2.

[108] I. Kuhlemann, M. Kleemann, P. Jauer, A. Schweikard, and F. Ernst, “Towards X-ray free endovascular interventions – using HoloLens for on-line holographic visualisation,” *Healthc. Technol. Lett.*, vol. 4, no. 5, pp. 184–187, Oct. 2017, doi: 10.1049/htl.2017.0061.

[109] R. Tang *et al.*, “Augmented reality navigation in open surgery for hilar cholangiocarcinoma resection with hemihepatectomy using video-based in situ three-dimensional anatomical modeling: A case report,” *Medicine (Baltimore).*, vol. 96, no. 37, p. e8083, Sep. 2017, doi: 10.1097/MD.0000000000008083.

[110] R. Hecht *et al.*, “Smartphone Augmented Reality CT-Based Platform for Needle Insertion Guidance: A Phantom Study.,” *Cardiovasc. Intervent. Radiol.*, vol. 43, no. 5, pp. 756–764, May 2020, doi: 10.1007/s00270-019-02403-6.

[111] S. Abdel Al, M. K. A. Chaar, A. Mustafa, M. Al-Hussaini, F. Barakat, and W. Asha, “Innovative Surgical Planning in Resecting Soft Tissue Sarcoma of the Foot Using Augmented Reality With a Smartphone,” *J. Foot Ankle Surg.*, vol. 59, no. 5, pp. 1092–1097, Sep. 2020, doi: 10.1053/j.jfas.2020.03.011.

[112] D. García-Mato *et al.*, “Augmented reality visualization for craniosynostosis surgery,” *Comput. Methods Biomech. Biomed. Eng. Imaging Vis.*, pp. 1–8, Oct. 2020, doi: 10.1080/21681163.2020.1834876.

[113] “CARS 2019—Computer Assisted Radiology and Surgery Proceedings of the 33rd International Congress and Exhibition, Rennes, France, June 18–21, 2019,” *Int. J. Comput. Assist. Radiol. Surg.*, vol. 14, no. 1, pp. 1–194, 2019, doi: 10.1007/s11548-019-01969-3.

[114] N. Wake *et al.*, “Patient-specific 3D printed and augmented reality kidney and prostate cancer models: impact on patient education,” *3D Print. Med.*, vol. 5, no. 1, pp. 1–8, 2019.

[115] S. R. Barber *et al.*, “Augmented Reality, Surgical Navigation, and 3D Printing for Transcanal Endoscopic Approach to the Petrous Apex,” *OTO Open Off. Open Access J.*

Am. Acad. Otolaryngol. Neck Surg. Found., vol. 2, no. 4, 2018.

[116] J. Witowski *et al.*, "Augmented reality and three-dimensional printing in percutaneous interventions on pulmonary arteries," *Quant. Imaging Med. Surg.*, vol. 9, no. 1, 2019.

[117] S. González Izard, R. Sánchez Torres, Ó. Alonso Plaza, J. A. Juanes Méndez, and F. J. García-Peñalvo, "Nextmed: Automatic Imaging Segmentation, 3D Reconstruction, and 3D Model Visualization Platform Using Augmented and Virtual Reality," *Sensors* , vol. 20, no. 10. 2020, doi: 10.3390/s20102962.

[118] E. N. D. Kok *et al.*, "Accurate surgical navigation with real-time tumor tracking in cancer surgery," *NPJ Precis. Oncol.*, vol. 4, p. 8, Apr. 2020, doi: 10.1038/s41698-020-0115-0.

[119] L. A. Aponte-Tinao, L. E. Ritacco, F. E. Milano, M. A. Ayerza, and G. F. Farfalli, "Techniques in surgical navigation of extremity tumors: state of the art," *Curr. Rev. Musculoskelet. Med.*, vol. 8, no. 4, pp. 319–323, 2015, doi: 10.1007/s12178-015-9305-8.

[120] S. E. Bosma, A. H. G. Cleven, and P. D. S. Dijkstra, "Can Navigation Improve the Ability to Achieve Tumor-free Margins in Pelvic and Sacral Primary Bone Sarcoma Resections? A Historically Controlled Study.," *Clin. Orthop. Relat. Res.*, vol. 477, no. 7, pp. 1548–1559, Jul. 2019, doi: 10.1097/CORR.0000000000000766.

[121] K. Ando *et al.*, "Computed tomography-based navigation system-assisted surgery for primary spine tumor.," *J. Clin. Neurosci.*, vol. 63, pp. 22–26, May 2019, doi: 10.1016/j.jocn.2019.02.015.

[122] Y. Zhang *et al.*, "New perspectives on surgical accuracy analysis of image-guided bone tumour resection surgery.," *Int. Orthop.*, vol. 44, no. 5, pp. 987–994, May 2020, doi: 10.1007/s00264-020-04539-4.

[123] L. Aponte-Tinao, L. E. Ritacco, M. A. Ayerza, D. Luis Muscolo, J. I. Albergo, and G. L. Farfall, "Does Intraoperative Navigation Assistance Improve Bone Tumor Resection and Allograft Reconstruction Results?," *Clin. Orthop. Relat. Res.*, vol. 473, no. 3, pp. 796–804, 2015, doi: 10.1007/s11999-014-3604-z.

[124] G. Gauvin *et al.*, "Real-time electromagnetic navigation for breast-conserving surgery using NaviKnife technology: A matched case-control study," *Breast J.*, vol. 26, no. 3,

pp. 399–405, Mar. 2020, doi: 10.1111/tbj.13480.

[125] C. Askeland *et al.*, “CustusX: an open-source research platform for image-guided therapy,” *Int. J. Comput. Assist. Radiol. Surg.*, vol. 11, no. 4, pp. 505–519, 2016, doi: 10.1007/s11548-015-1292-0.

[126] D. Fan *et al.*, “Progressive 3D Printing Technology and Its Application in Medical Materials,” *Front. Pharmacol.*, vol. 11, p. 122, 2020, doi: 10.3389/fphar.2020.00122.

[127] H. H. Malik *et al.*, “Three-dimensional printing in surgery: a review of current surgical applications,” *J. Surg. Res.*, vol. 199, no. 2, pp. 512–522, 2015, doi: 10.1016/j.jss.2015.06.051.

[128] P. Marti, F. Lampus, D. Benevento, and C. Setacci, “Trends in use of 3D printing in vascular surgery: a survey.,” *Int. Angiol.*, vol. 38, no. 5, pp. 418–424, Oct. 2019, doi: 10.23736/S0392-9590.19.04148-8.

[129] Y. Tong, D. J. Kaplan, J. M. Spivak, and J. A. Bendo, “Three-dimensional printing in spine surgery: a review of current applications,” *Spine J.*, vol. 20, no. 6, pp. 833–846, 2020, doi: https://doi.org/10.1016/j.spinee.2019.11.004.

[130] D. Chang *et al.*, “Three-Dimensional Printing for Procedure Rehearsal/Simulation/Planning in Interventional Radiology,” *Tech. Vasc. Interv. Radiol.*, vol. 22, no. 1, pp. 14–20, 2019, doi: https://doi.org/10.1053/j.tvir.2018.10.004.

[131] X. Chen, L. Xu, Y. Wang, Y. Hao, and L. Wang, “Image-guided installation of 3D-printed patient-specific implant and its application in pelvic tumor resection and reconstruction surgery,” *Comput. Methods Programs Biomed.*, vol. 125, pp. 66–78, 2016, doi: 10.1016/j.cmpb.2015.10.020.

[132] T. Zislis, S. A. Martin, E. Cerbas, J. R. Heath, J. L. Mansfield, and J. O. Hollinger, “A scanning electron microscopic study of in vitro toxicity of ethylene-oxide-sterilized bone repair materials.,” *J. Oral Implantol.*, vol. 15, no. 1, pp. 41–6, Feb. 1989.

[133] T. Ungi, A. Lasso, and G. Fichtinger, “Open-source platforms for navigated image-guided interventions.,” *Medical image analysis*, vol. 33. Netherlands, pp. 181–186, Oct-2016, doi: 10.1016/j.media.2016.06.011.

[134] E. Marinetto, D. García-Mato, A. GarcíA, S. Martínez, M. Desco, and J. Pascau, “Multicamera Optical Tracker Assessment for Computer Aided Surgery Applications,”

IEEE Access, vol. 6, pp. 64359–64370, 2018, doi: 10.1109/ACCESS.2018.2878323.

[135] J. Tokuda *et al.*, "OpenIGTLink: an open network protocol for image-guided therapy environment," *Int. J. Med. Robot.*, vol. 5, no. 4, pp. 423–434, Dec. 2009, doi: 10.1002/rcs.274.

[136] K. S. Arun, T. S. Huang, and S. D. Blostein, "Least-Squares Fitting of Two 3-D Point Sets," *IEEE Trans. Pattern Anal. Mach. Intell.*, vol. PAMI-9, no. 5, pp. 698–700, 1987, doi: 10.1109/TPAMI.1987.4767965.

[137] N. Sharma *et al.*, "Effects of Steam Sterilization on 3D Printed Biocompatible Resin Materials for Surgical Guides-An Accuracy Assessment Study," *J. Clin. Med.*, vol. 9, no. 5, p. 1506, May 2020, doi: 10.3390/jcm9051506.

[138] V. García-Vázquez, E. Marinetto, J. A. Santos-Miranda, F. A. Calvo, M. Desco, and J. Pascau, "Feasibility of integrating a multi-camera optical tracking system in intra-operative electron radiation therapy scenarios.," *Phys. Med. Biol.*, vol. 58, no. 24, pp. 8769–8782, Dec. 2013, doi: 10.1088/0031-9155/58/24/8769.

[139] D. Inoue *et al.*, "Preliminary Study on the Clinical Application of Augmented Reality Neuronavigation," *J. Neurol. Surg. A. Cent. Eur. Neurosurg.*, vol. 74, pp. 71–76, Mar. 2013, doi: 10.1055/s-0032-1333415.

[140] T. R. Coles, N. W. John, D. Gould, and D. G. Caldwell, "Integrating Haptics with Augmented Reality in a Femoral Palpation and Needle Insertion Training Simulation," *IEEE Trans. Haptics*, vol. 4, no. 3, pp. 199–209, 2011, doi: 10.1109/TOH.2011.32.

[141] K. Abhari *et al.*, "Training for Planning Tumour Resection: Augmented Reality and Human Factors," *IEEE Trans. Biomed. Eng.*, vol. 62, no. 6, pp. 1466–1477, 2015, doi: 10.1109/TBME.2014.2385874.

[142] R. Van Krevelen and R. Poelman, "A Survey of Augmented Reality Technologies, Applications and Limitations," *Int. J. Virtual Real.*, vol. 9, p. 1, Jun. 2010.

[143] DAQRI, "Artoolkit.org: Open source augmented reality sdk." [Online]. Available: http://artoolkit.org/. [Accessed: 25-Feb-2018].

[144] R. Plantefève, I. Peterlik, N. Haouchine, and S. Cotin, "Patient-Specific Biomechanical Modeling for Guidance During Minimally-Invasive Hepatic Surgery," *Ann. Biomed. Eng.*, vol. 44, no. 1, pp. 139–153, 2016, doi: 10.1007/s10439-015-1419-z.

[145] J. Vaquero, J. Arnal, R. Perez-Mañanes, J. Calvo-Haro, and F. Chana, "3D patient-specific surgical printing cutting blocks guides and spacers for open- wedge high tibial osteotomy (HTO) - do it yourself," *Rev. Chir. Orthopédique Traumatol.*, vol. 102, no. 7, Supplement, p. S131, 2016, doi: https://doi.org/10.1016/j.rcot.2016.08.136.

[146] J. Arnal-Burró, R. Pérez-Mañanes, E. Gallo-del-Valle, C. Igualada-Blazquez, M. Cuervas-Mons, and J. Vaquero-Martín, "Three dimensional-printed patient-specific cutting guides for femoral varization osteotomy: Do it yourself," *Knee*, vol. 24, no. 6, pp. 1359–1368, Dec. 2017, doi: 10.1016/j.knee.2017.04.016.

[147] M. Zhu *et al.*, "A novel augmented reality system for displaying inferior alveolar nerve bundles in maxillofacial surgery," *Sci. Rep.*, vol. 7, p. 42365, Feb. 2017, doi: 10.1038/srep42365.

[148] PTC Inc., "Vuforia." [Online]. Available: http://www.vuforia.com/. [Accessed: 15-Feb-2018].

[149] T. Zislis, D. E. Mark, S. A. Martin, E. L. Cerbas, and J. R. Heath, "Scanning Electron Microscopic Study of In Vitro Toxicity of Ethylene Oxide Sterilized Bone Repair Materials.," 1988.

[150] R. Uppot *et al.*, "Implementing Virtual and Augmented Reality Tools for Radiology Education and Training, Communication, and Clinical Care," *Radiology*, vol. 291, p. 182210, 2019, doi: 10.1148/radiol.2019182210.

[151] F. Heinrich, F. Joeres, K. Lawonn, and C. Hansen, "Comparison of Projective Augmented Reality Concepts to Support Medical Needle Insertion," *IEEE Trans. Vis. Comput. Graph.*, vol. 25, no. 6, p. 1, 2019.

[152] Z. Fan, Y. Weng, G. Chen, and H. Liao, "3D interactive surgical visualization system using mobile spatial information acquisition and autostereoscopic display," *J. Biomed. Inform.*, vol. 71, pp. 154–164, 2017, doi: 10.1016/j.jbi.2017.05.014.

[153] A. De La Peña, J. De La Peña-Brambila, J. Pérez-De La Torre, M. Ochoa, and G. Gallardo, "Low-cost customized cranioplasty using a 3D digital printing model: a case report," *3D Print. Med.*, vol. 4, no. 1, pp. 1–9, 2018.

[154] T. Kamio *et al.*, "Utilizing a low-cost desktop 3D printer to develop a 'one-stop 3D printing lab' for oral and maxillofacial surgery and dentistry fields," *3D Print. Med.*,

vol. 4, no. 1, pp. 1–7, 2018.

[155] T. Punyaratabandhu, P. Liacouras, and S. Pairojboriboon, “Using 3D models in orthopedic oncology: presenting personalized advantages in surgical planning and intraoperative outcomes,” *3D Print. Med.*, vol. 4, no. 1, pp. 1–13, 2018.

[156] R. Moreta-Martínez, D. García-Mato, M. García-Sevilla, R. Pérez-Mañanes, J. Calvo-Haro, and J. Pascau, “Augmented reality in computer-assisted interventions based on patient-specific 3D printed reference,” *Healthc. Technol. Lett.*, 2018.

[157] R. Moreta-Martinez, D. García-Mato, M. García-Sevilla, R. Pérez-Mañanes, J. A. Calvo-Haro, and J. Pascau, “Combining Augmented Reality and 3D Printing to Display Patient Models on a Smartphone,” *JoVE*, no. 155, 2020, doi: doi:10.3791/60618.

[158] C. D. Fletcher, K. Unni, and F. Mertens, “Pathology and genetics of tumours of soft tissue and bone,” 2002.

[159] J. Y. C. Hui, “Epidemiology and Etiology of Sarcomas,” *Surg. Clin. North Am.*, vol. 96, no. 5, pp. 901–914, 2016, doi: https://doi.org/10.1016/j.suc.2016.05.005.

[160] M. A. Clark, C. Fisher, I. Judson, and J. M. Thomas, “Soft-Tissue Sarcomas in Adults,” *N. Engl. J. Med.*, vol. 353, no. 7, pp. 701–711, Aug. 2005, doi: 10.1056/NEJMra041866.

[161] P. G. Casali, L. Jost, S. Sleijfer, J. Verweij, and J.-Y. Blay, “Soft tissue sarcomas: ESMO clinical recommendations for diagnosis, treatment and follow-up.,” *Ann. Oncol. Off. J. Eur. Soc. Med. Oncol.*, vol. 19 Suppl 2, pp. ii89-93, May 2008, doi: 10.1093/annonc/mdn101.

[162] “Bone sarcomas: ESMO Clinical Practice Guidelines for diagnosis, treatment and follow-up.,” *Ann. Oncol. Off. J. Eur. Soc. Med. Oncol.*, vol. 25 Suppl 3, pp. iii113-23, Sep. 2014, doi: 10.1093/annonc/mdu256.

[163] L. Jeys, R. Grimer, S. Carter, R. Tillman, and S. Abudu, “OUTCOMES OF PRIMARY BONE TUMOURS OF THE PELVIS – THE ROH EXPERIENCE,” *Orthop. Proc.*, vol. 94-B, no. SUPP_XIV, p. 39, Apr. 2012, doi: 10.1302/1358-992X.94BSUPP_XIV.EMSOS2010-039.

[164] N. Kawaguchi, A. R. Ahmed, S. Matsumoto, J. Manabe, and Y. Matsushita, “The Concept of Curative Margin in Surgery for Bone and Soft Tissue Sarcoma,” *Clin. Orthop. Relat. Res.*, vol. 419, 2004.

[165] K. R. Gundle *et al.*, "Analysis of Margin Classification Systems for Assessing the Risk of Local Recurrence After Soft Tissue Sarcoma Resection," *J. Clin. Oncol.*, vol. 36, no. 7, pp. 704–709, Jan. 2018, doi: 10.1200/JCO.2017.74.6941.

[166] Y. A. Qureshi, J. R. Huddy, J. D. Miller, D. C. Strauss, J. M. Thomas, and A. J. Hayes, "Unplanned excision of soft tissue sarcoma results in increased rates of local recurrence despite full further oncological treatment.," *Ann. Surg. Oncol.*, vol. 19, no. 3, pp. 871–877, Mar. 2012, doi: 10.1245/s10434-011-1876-z.

[167] M. A. Smolle, D. Andreou, P.-U. Tunn, J. Szkandera, B. Liegl-Atzwanger, and A. Leithner, "Diagnosis and treatment of soft-tissue sarcomas of the extremities and trunk," *EFORT Open Rev.*, vol. 2, no. 10, pp. 421–431, Oct. 2017, doi: 10.1302/2058-5241.2.170005.

[168] K. Atesok, D. Galos, L. M. Jazrawi, and K. A. Egol, "Preoperative Planning in Orthopaedic Surgery. Current Practice and Evolving Applications.," *Bull. Hosp. Jt. Dis.*, vol. 73, no. 4, pp. 257–268, Dec. 2015.

[169] O. Cartiaux *et al.*, "Surgical inaccuracy of tumor resection and reconstruction within the pelvis: An experimental study," *Acta Orthop.*, vol. 79, no. 5, pp. 695–702, Jan. 2008, doi: 10.1080/17453670810016731.

[170] H. S. Cho, J. H. Oh, I. Han, and H.-S. Kim, "The outcomes of navigation-assisted bone tumour surgery," *J. Bone Joint Surg. Br.*, vol. 94-B, no. 10, pp. 1414–1420, Oct. 2012, doi: 10.1302/0301-620X.94B10.28638.

[171] C. L. Ventola, "Medical Applications for 3D Printing: Current and Projected Uses.," *P T*, vol. 39, no. 10, pp. 704–711, Oct. 2014.

[172] J. H. Shuhaiber, "Augmented Reality in Surgery," *Arch. Surg.*, vol. 139, no. 2, pp. 170–174, Feb. 2004, doi: 10.1001/archsurg.139.2.170.

[173] K. Wee Sim, B. Baker, K. Amin, A. Chan, K. Patel, and J. Wong, "Augmented and virtual reality in surgery—the digital surgical environment: applications, limitations and legal pitfalls," *Ann. Transl. Med. Vol 4, No 23 (December 2016) Ann. Transl. Med. (Focus "Innovations Technol. Surgery")*, 2016.

[174] T. Punyaratabandhu, P. C. Liacouras, and S. Pairojboriboon, "Using 3D models in orthopedic oncology: presenting personalized advantages in surgical planning and

intraoperative outcomes," *3D Print. Med.*, vol. 4, no. 1, p. 12, 2018, doi: 10.1186/s41205-018-0035-6.

[175] M. Jiang, G. Chen, J. Coles-Black, J. Chuen, and A. Hardidge, "Three-dimensional printing in orthopaedic preoperative planning improves intraoperative metrics: a systematic review," *ANZ J. Surg.*, vol. 90, no. 3, pp. 243–250, Mar. 2020, doi: https://doi.org/10.1111/ans.15549.

[176] J. Arnal-Burró, R. Pérez-Mañanes, E. Gallo-del-Valle, C. Igualada-Blazquez, M. Cuervas-Mons, and J. Vaquero-Martín, "Three dimensional-printed patient-specific cutting guides for femoral varization osteotomy: Do it yourself," *Knee*, vol. 24, no. 6, pp. 1359–1368, 2017, doi: https://doi.org/10.1016/j.knee.2017.04.016.

[177] A. Sternheim, Y. Gortzak, Y. Kolander, and S. Dadia, "Chapter 15 - 3D Printing in Orthopedic Oncology," M. Dipaola and F. M. B. T.-3D P. in O. S. Wodajo, Eds. Elsevier, 2019, pp. 179–194.

[178] R. Souzaki *et al.*, "An augmented reality navigation system for pediatric oncologic surgery based on preoperative CT and MRI images.," *J. Pediatr. Surg.*, vol. 48, no. 12, pp. 2479–2483, Dec. 2013, doi: 10.1016/j.jpedsurg.2013.08.025.

[179] R. Tang *et al.*, "Augmented reality navigation in open surgery for hilar cholangiocarcinoma resection with hemihepatectomy using video-based in situ three-dimensional anatomical modeling: A case report.," *Medicine (Baltimore).*, vol. 96, no. 37, p. e8083, Sep. 2017, doi: 10.1097/MD.0000000000008083.

[180] *The United States pharmacopeia*, National f., vol. 1. Rockville (MD): United States Pharmacopeial Convention, 2012.

[181] R. Moreta-Martinez, J. A. Calvo-Haro, R. Pérez-Mañanes, M. García-Sevilla, L. Mediavilla-Santos, and J. Pascau, "Desktop 3D Printing: Key for Surgical Navigation in Acral Tumors?," *Appl. Sci.*, vol. 10, no. 24, p. 8984, Dec. 2020, doi: 10.3390/app10248984.

[182] M. Wayne, J. Ryan, and S. Stephen, "Virtual and Augmented Reality Applications in Medicine and Surgery The Fantastic Voyage is here," *Anat. Physiol. Curr. Res.*, vol. 9, no. 1, pp. 1–6, 2019, doi: 10.4172/2161-0940.1000313.

[183] R. Wen, C. B. Chng, and C. K. Chui, "Augmented reality guidance with multimodality

imaging data and depth-perceived interaction for robot-assisted surgery," *Robotics*, vol. 6, no. 2, 2017, doi: 10.3390/robotics6020013.

[184] J. M. Fitzpatrick, J. B. West, and C. R. Maurer, "Predicting Error in Rigid-body, Point-based Registration."

[185] L. Kerkeni *et al.*, "We are IntechOpen , the world ' s leading publisher of Open Access books Built by scientists , for scientists TOP 1 %," *Intech*, no. tourism, p. 13, 2016.

[186] D. Kaiser *et al.*, "The influence of different patient positions on the preoperative 3D planning for surgical resection of soft tissue sarcoma in the lower limb-a cadaver pilot study," *Surg. Oncol.*, vol. 35, pp. 478–483, 2020, doi: 10.1016/j.suronc.2020.10.008.

[187] D. Fett, R. Küsters, and G. Schmitz, "A Comprehensive Formal Security Analysis of OAuth 2.0," in *Proceedings of the 2016 ACM SIGSAC Conference on Computer and Communications Security*, 2016, pp. 1204–1215, doi: 10.1145/2976749.2978385.

[188] D. E. Irwin *et al.*, "Population-Based Survey of Urinary Incontinence, Overactive Bladder, and Other Lower Urinary Tract Symptoms in Five Countries: Results of the EPIC Study," *Eur. Urol.*, vol. 50, no. 6, pp. 1306–1315, 2006, doi: https://doi.org/10.1016/j.eururo.2006.09.019.

[189] I. Milsom, P. Abrams, L. Cardozo, R. G. Roberts, J. Thüroff, and A. J. Wein, "How widespread are the symptoms of an overactive bladder and how are they managed? A population-based prevalence study.," *BJU Int.*, vol. 87, no. 9, pp. 760–766, Jun. 2001, doi: 10.1046/j.1464-410x.2001.02228.x.

[190] E. R. Williams and S. W. Siegel, "Procedural techniques in sacral nerve modulation," *Int. Urogynecol. J.*, vol. 21, no. 2, pp. 453–460, 2010, doi: 10.1007/s00192-010-1280-4.

[191] H. B. Goldman *et al.*, "International Continence Society best practice statement for use of sacral neuromodulation.," *Neurourol. Urodyn.*, vol. 37, no. 5, pp. 1823–1848, Jun. 2018, doi: 10.1002/nau.23515.

[192] E. Ganio, A. R. Luc, G. Clerico, and M. Trompetto, "Sacral nerve stimulation for treatment of fecal incontinence: a novel approach for intractable fecal incontinence.," *Dis. Colon Rectum*, vol. 44, no. 5, pp. 619–631, May 2001, doi: 10.1007/BF02234555.

[193] M. A. Banakhar, T. Al-Shaiji, and M. Hassouna, "Sacral neuromodulation and refractory

overactive bladder: an emerging tool for an old problem," *Ther. Adv. Urol.*, vol. 4, no. 4, pp. 179–185, Aug. 2012, doi: 10.1177/1756287212445179.

[194] U. Jonas *et al.*, "Efficacy of sacral nerve stimulation for urinary retention: results 18 months after implantation.," *J. Urol.*, vol. 165, no. 1, pp. 15–19, Jan. 2001, doi: 10.1097/00005392-200101000-00004.

[195] S. A. Pilkington *et al.*, "Surgery for constipation: systematic review and practice recommendations," *Color. Dis.*, vol. 19, no. S3, pp. 92–100, Sep. 2017, doi: https://doi.org/10.1111/codi.13780.

[196] C. Arman *et al.*, "The human sacrum and safe approaches for screw placement.," *J. Clin. Neurosci. Off. J. Neurosurg. Soc. Australas.*, vol. 16, no. 8, pp. 1046–1049, Aug. 2009, doi: 10.1016/j.jocn.2008.07.081.

[197] T. C. Chai and G. J. Mamo, "Modified techniques of S3 foramen localization and lead implantation in S3 neuromodulation.," *Urology*, vol. 58, no. 5, pp. 786–790, Nov. 2001, doi: 10.1016/s0090-4295(01)01326-7.

[198] K. E. Husk, L. D. Norris, M. G. Willis-Gray, K. M. Borawski, and E. J. Geller, "Variation in bony landmarks and predictors of success with sacral neuromodulation.," *Int. Urogynecol. J.*, vol. 30, no. 11, pp. 1973–1979, Nov. 2019, doi: 10.1007/s00192-019-03883-3.

[199] K. E. Matzel *et al.*, "Sacral Neuromodulation: Standardized Electrode Placement Technique," *Neuromodulation Technol. Neural Interface*, vol. 20, no. 8, pp. 816–824, Dec. 2017, doi: 10.1111/ner.12695.

[200] C. P. Chung, P. A. Neese, H. K. Le, and E. T. Bird, "Computed tomography-guided S3 lead placement for sacral neuromodulation.," *Int. Urogynecol. J.*, vol. 24, no. 2, pp. 349–351, Feb. 2013, doi: 10.1007/s00192-012-1816-x.

[201] T. Meissnitzer, S. Trubel, R. Posch-Zimmermann, and M. W. Meissnitzer, "CT-Guided Lead Placement for Selective Sacral Neuromodulation to Treat Lower Urinary Tract Dysfunctions," *Am. J. Roentgenol.*, vol. 205, no. 5, pp. 1139–1142, Oct. 2015, doi: 10.2214/AJR.14.14270.

[202] P. A. Hellström, J. Katisko, P. Finnilä, and M. H. Vaarala, "Sacral nerve stimulation lead implantation using the o-arm," *BMC Urol.*, vol. 13, no. 1, p. 48, 2013, doi:

10.1186/1471-2490-13-48.

[203] J. Castillo *et al.*, "Sacral nerve stimulation lead implantation in partial sacral agenesis using intra-operative computerized tomography," *Color. Dis.*, vol. 18, no. 9, pp. O330–O333, Sep. 2016, doi: 10.1111/codi.13437.

[204] D. Mendelsohn *et al.*, "Patient and surgeon radiation exposure during spinal instrumentation using intraoperative computed tomography-based navigation.," *Spine J.*, vol. 16, no. 3, pp. 343–354, Mar. 2016, doi: 10.1016/j.spinee.2015.11.020.

[205] J. Zhang *et al.*, "Application of an individualized and reassemblable 3D printing navigation template for accurate puncture during sacral neuromodulation," *Neurourol. Urodyn.*, vol. 37, no. 8, pp. 2776–2781, Nov. 2018, doi: 10.1002/nau.23769.

[206] Z. Cui, Z. Wang, G. Ye, C. Zhang, G. Wu, and J. Lv, "A novel three-dimensional printed guiding device for electrode implantation of sacral neuromodulation.," *Color. Dis. Off. J. Assoc. Coloproctology Gt. Britain Irel.*, vol. 20, no. 1, pp. O26–O29, Jan. 2018, doi: 10.1111/codi.13958.

[207] J. Krücker *et al.*, "Electromagnetic tracking for thermal ablation and biopsy guidance: clinical evaluation of spatial accuracy.," *J. Vasc. Interv. Radiol.*, vol. 18, no. 9, pp. 1141–1150, Sep. 2007, doi: 10.1016/j.jvir.2007.06.014.

[208] G. Turtulici *et al.*, "Ultrasound-guided transvaginal radiofrequency ablation of uterine fibroids assisted by virtual needle tracking system: a preliminary study," *Int. J. Hyperth.*, vol. 35, no. 1, pp. 97–104, Dec. 2018, doi: 10.1080/02656736.2018.1479778.

[209] S. W. Wong, A. U. Niazi, K. J. Chin, and V. W. Chan, "Real-time ultrasound-guided spinal anesthesia using the SonixGPS® needle tracking system: a case report.," *Can. J. Anaesth.*, vol. 60, no. 1, pp. 50–53, Jan. 2013, doi: 10.1007/s12630-012-9809-2.

[210] B. J. Park, S. J. Hunt, C. 3rd Martin, G. J. Nadolski, B. J. Wood, and T. P. Gade, "Augmented and Mixed Reality: Technologies for Enhancing the Future of IR.," *J. Vasc. Interv. Radiol.*, vol. 31, no. 7, pp. 1074–1082, Jul. 2020, doi: 10.1016/j.jvir.2019.09.020.

[211] R. Rahman, M. E. Wood, L. Qian, C. L. Price, A. A. Johnson, and G. M. Osgood, "Head-Mounted Display Use in Surgery: A Systematic Review.," *Surg. Innov.*, vol. 27, no. 1, pp. 88–100, Feb. 2020, doi: 10.1177/1553350619871787.

[212] T. Kuzhagaliyev *et al.*, "Augmented reality needle ablation guidance tool for irreversible

electroporation in the pancreas," in *Proc.SPIE*, 2018, vol. 10576, doi: 10.1117/12.2293671.

[213] R. López-Velazco *et al.*, "Image Guidance for Sacral Neuromodulation," in *Computer Assisted Radiology and Surgery Proceedings of the 31st International Congress and Exhibition Barcelona, Spain, June 20–24*, 2017, pp. 105–106, doi: 10.1007/s11548-017-1588-3.

[214] O. Ronneberger, P. Fischer, and T. Brox, "U-Net: Convolutional Networks for Biomedical Image Segmentation," pp. 1–8, 2015, doi: 10.1007/978-3-319-24574-4_28.

[215] C. Wang, B. Connolly, P. F. de Oliveira Lopes, A. F. Frangi, and Ö. Smedby, "Pelvis Segmentation Using Multi-pass U-Net and Iterative Shape Estimation BT - Computational Methods and Clinical Applications in Musculoskeletal Imaging," 2019, pp. 49–57.

[216] B. Connolly and C. Wang, "Segmented CT pelvis scans with annotated anatomical landmarks." 2019, doi: 10.23698/aida/ctpel.

[217] S. Weidert *et al.*, "3D printing method for next-day acetabular fracture surgery using a surface filtering pipeline: feasibility and 1-year clinical results.," *Int. J. Comput. Assist. Radiol. Surg.*, vol. 15, no. 3, pp. 565–575, Mar. 2020, doi: 10.1007/s11548-019-02110-0.

[218] Ö. Çiçek, A. Abdulkadir, S. S. Lienkamp, T. Brox, and O. Ronneberger, "3D U-Net: Learning Dense Volumetric Segmentation from Sparse Annotation," *Lect. Notes Comput. Sci. (including Subser. Lect. Notes Artif. Intell. Lect. Notes Bioinformatics)*, vol. 9901 LNCS, pp. 424–432, Jun. 2016.

[219] K. Kamnitsas *et al.*, "Ensembles of Multiple Models and Architectures for Robust Brain Tumour Segmentation BT - Brainlesion: Glioma, Multiple Sclerosis, Stroke and Traumatic Brain Injuries," 2018, pp. 450–462.

[220] D. P. Kingma and J. Ba, "Adam: A Method for Stochastic Optimization," Dec. 2014.

[221] K. He, X. Zhang, S. Ren, and J. Sun, "Delving Deep into Rectifiers: Surpassing Human-Level Performance on ImageNet Classification," in *2015 IEEE International Conference on Computer Vision (ICCV)*, 2015, pp. 1026–1034, doi: 10.1109/ICCV.2015.123.

[222] L. Levine and M. Levine, “DRRGenerator: A Three-dimensional Slicer Extension for the Rapid and Easy Development of Digitally Reconstructed Radiographs,” *J. Clin. Imaging Sci.*, vol. 10, p. 69, 2020, doi: 10.25259/JCIS_105_2020.

[223] P. Virtanen *et al.*, “SciPy 1.0: fundamental algorithms for scientific computing in Python,” *Nat. Methods*, vol. 17, no. 3, pp. 261–272, 2020, doi: 10.1038/s41592-019-0686-2.

[224] F. A. Mettler, W. Huda, T. T. Yoshizumi, and M. Mahesh, “Effective doses in radiology and diagnostic nuclear medicine: a catalog.,” *Radiology*, vol. 248 1, pp. 254–263, 2008.

[225] C. M. Andrews, A. B. Henry, I. M. Soriano, M. K. Southworth, and J. R. Silva, “Registration Techniques for Clinical Applications of Three-Dimensional Augmented Reality Devices,” *IEEE J. Transl. Eng. Heal. Med.*, vol. 9, p. 4900214, Dec. 2020, doi: 10.1109/JTEHM.2020.3045642.

[226] “Microsoft HoloLens 2.” [Online]. Available: https://www.microsoft.com/en-us/hololens. [Accessed: 21-Sep-2021].

[227] B. J. Park, S. J. Hunt, G. J. Nadolski, and T. P. Gade, “Augmented reality improves procedural efficiency and reduces radiation dose for CT-guided lesion targeting: a phantom study using HoloLens 2,” *Sci. Rep.*, vol. 10, no. 1, p. 18620, 2020, doi: 10.1038/s41598-020-75676-4.

[228] M. Farshad, P. Fürnstahl, and J. M. Spirig, “First in man in-situ augmented reality pedicle screw navigation,” *North Am. Spine Soc. J.*, vol. 6, p. 100065, 2021, doi: https://doi.org/10.1016/j.xnsj.2021.100065.

[229] T. Song, C. Yang, O. Dianat, and E. Azimi, “Endodontic guided treatment using augmented reality on a head-mounted display system,” *Healthc. Technol. Lett.*, vol. 5, no. 5, pp. 201–207, Oct. 2018, doi: https://doi.org/10.1049/htl.2018.5062.

[230] M. Solbiati *et al.*, “Augmented reality for interventional oncology: proof-of-concept study of a novel high-end guidance system platform,” *Eur. Radiol. Exp.*, vol. 2, p. 18, Jul. 2018, doi: 10.1186/s41747-018-0054-5.

[231] A. A. Diaz *et al.*, “Pectoralis muscle area and mortality in smokers without airflow obstruction,” *Respir. Res.*, vol. 19, no. 1, p. 62, Apr. 2018, doi: 10.1186/s12931-018-0771-6.

[232] B. Wang and M. Torriani, “Artificial Intelligence in the Evaluation of Body Composition,” *Semin Musculoskelet Radiol*, vol. 24, no. 01, pp. 30–37, 2020, doi: 10.1055/s-0039-3400267.

[233] J. O. Onieva, G. G. Serrano, T. P. Young, G. R. Washko, M. J. L. Carbayo, and R. S. J. Estépar, “Multiorgan structures detection using deep convolutional neural networks,” in *Proc.SPIE*, 2018, vol. 10574, doi: 10.1117/12.2293761.

[234] S. E. Mason *et al.*, “Respiratory exacerbations are associated with muscle loss in current and former smokers,” *Thorax*, p. thoraxjnl-2020-215999, Feb. 2021, doi: 10.1136/thoraxjnl-2020-215999.

[235] A. Jemal and S. A. Fedewa, “Lung Cancer Screening With Low-Dose Computed Tomography in the United States—2010 to 2015,” *JAMA Oncol.*, vol. 3, no. 9, pp. 1278–1281, Sep. 2017, doi: 10.1001/jamaoncol.2016.6416.

[236] F. N. Rahaghi *et al.*, “Ventricular Geometry From Non-contrast Non-ECG-gated CT Scans: An Imaging Marker of Cardiopulmonary Disease in Smokers,” *Acad. Radiol.*, vol. 24, no. 5, pp. 594–602, May 2017, doi: 10.1016/j.acra.2016.12.007.

[237] R. Moreta-Martínez, G. Vegas Sánchez-Ferrero, L. Andresen, J. Qvortrup Holsting, and R. San José Estépar, “Multi-cavity Heart Segmentation in Non-contrast Non-ECG Gated CT Scans with F-CNN BT - Thoracic Image Analysis,” 2020, pp. 14–23, doi: https://doi.org/10.1007/978-3-030-62469-9_2.